SAN-1604-1

SOLAR CENTRAL RECEIVER PROTOTYPE HELIOSTATS

Volume I: Final Technical Report

Work Performed Under Contract No. EG-77-C-03-1604

Boeing Engineering and Construction
Seattle, Washington

U.S. Department of Energy

Solar Energy

DISCLAIMER

NOTICE

SAN-1604-1
Distribution Category UC-62

VOLUME I

SOLAR CENTRAL RECEIVER PROTOTYPE HELIOSTAT

Final Technical Report

1 June, 1979

Prepared For

United States

Department of Energy

Under

Contract EG-77-C-03-1604

By

Boeing Engineering and Construction
a Division of The Boeing Company
Seattle, Washington

FOREWORD

This document (Vol I) is the Final Technical Report of work performed under DOE Contract EG-77-C-03-1604, "Solar Central Receiver Prototype Heliostats." Companion documents describe Phase II Planning (Vol II) and Commercial Plant Cost Estimates (Vol III). The primary objective of this study was to develop a preliminary design of heliostats which is consistent with production quantities and rates projected for future commercial utilization of solar energy. Work under this Phase I contract was initiated on October 1, 1977, and is scheduled for completion on June 30, 1978. Program management was performed by the DOE office in Oakland, California and technical performance was monitored by Sandia Laboratories in Livermore, California.

VOLUME I

TABLE OF CONTENTS

TABLE OF CONTENTS (CONTINUED)

1.0 INTRODUCTION

Boeing Engineering and Construction (BEC) submits herein the Final Technical Report of work performed under DOE Contract EG-77-C-03-1604. The objective of this project was to support the Solar Central Receiver Power Plant research, development and demonstration effort by:

Establishment of a heliostat design, with associated manufacturing, assembly, installation and maintenance approaches, that, in quantity production will yield significant reductions in capital and operating costs over an assumed 30 year plant lifetime as compared with existing designs.

Identification of needs for near term and future research and development in heliostat concept, materials, manufacture, installation, maintenance, and other areas, where successful accomplishment and application would offer significant payoffs in the further reduction of the cost of electrical energy from solar central receiver power plants.

Definition of a Phase II program which will:

1) Provide detail design, fabrication and testing of one or more prototype heliostats.
2) Provide preliminary design of processes, tooling and equipment for commercial level production and utilization of heliostats.
3) Provide a refined estimation of heliostat life cycle cost.

The Phase I study has defined a heliostat preliminary design which can be manufactured and installed for a capital cost which is less than $\$50/m^2$. Details of cost information are given in Volume III of this report.

Figures 1.0-1 and 1.0-2 show the heliostat configuration selected to achieve low cost when produced at high production rates required for commercial utilization of solar power. The primary features of the design are summarized below:

Enclosure - A 9.7m (31.8 ft.) diameter air-supported spherical enclosure which protects the reflector assembly from the environment. Weatherized polyester film (0.07mm, 3 mils thick) was selected on the basis of its low cost, long-life (on greenhouse application), high specular transmittance (0.88) and superior strength. Enclosures will be fabricated using a high production thermoforming process wherein a flat-sheet preform is free-blown into spherical shape. This process was selected on the basis of recommendation from plastics manufacturers, and encouraging results of thermoforming experiments performed with Boeing research funds.

Reflector - A 9.3m (30.5 ft.) diameter reflector consisting of a 0.05mm (2 mil) thick aluminized polyester membrane which is tensioned and bonded to a tubular aluminum structure. The polyester membrane is specially selected for high specular reflectance (0.91), and contains an ultraviolet stabilizer for long-life. The reflector is gravity focused by pre-setting membrane tension during manufacture to a value of 8.0 MN/m^2 (1,150 psi). A reflector/gimbal interface design has been provided which places the reflector center-of-gravity on the gimbal elevation axis, eliminating the need for a counterweight and minimizing torque. Automated production planning for reflector includes ram-forming of tubing, electromagnetic swaging of tubing joints, and a high speed press for tensioning and bonding the reflective membrane onto the structure.

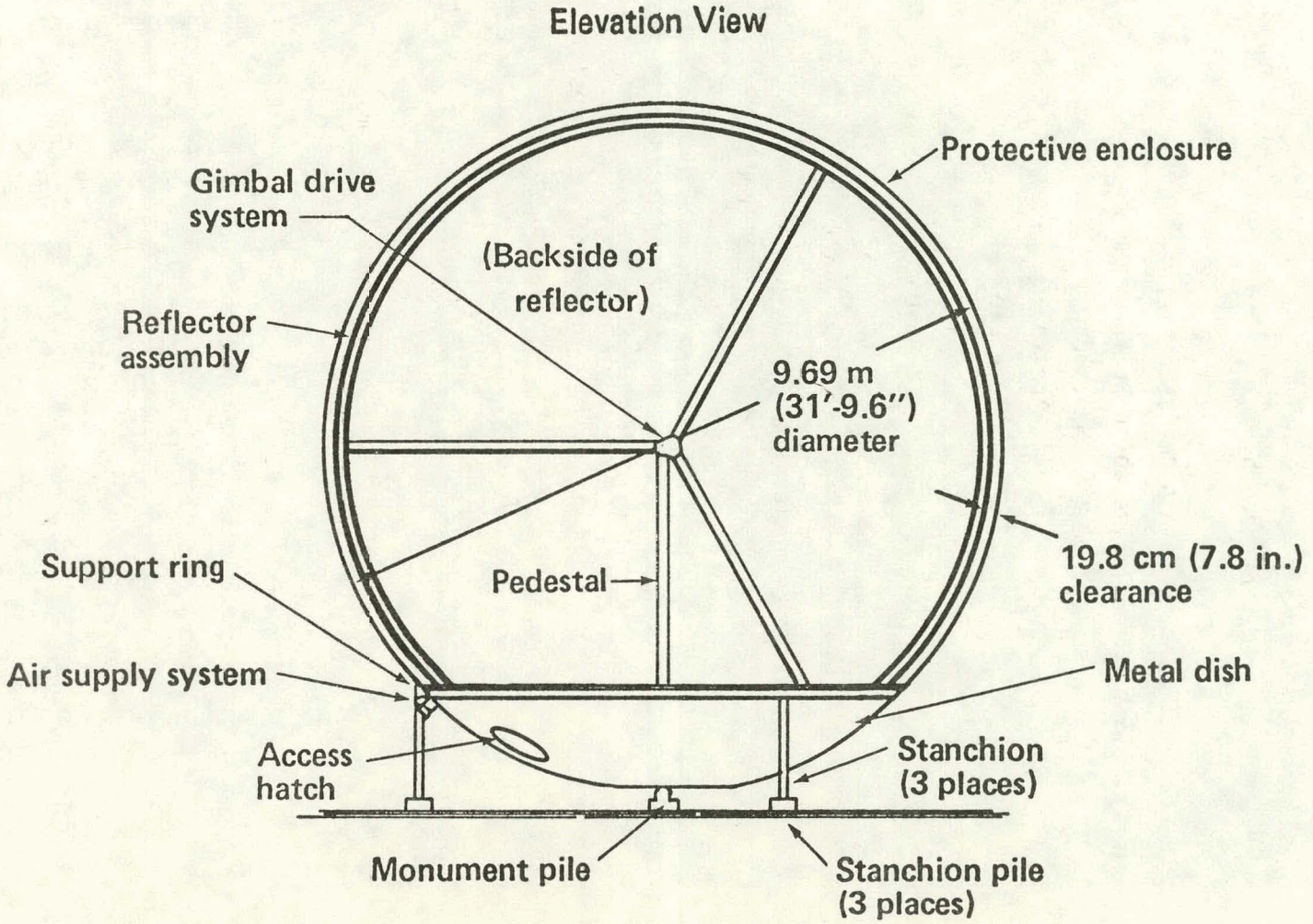

Figure 1.0-1. Heliostat Configuration

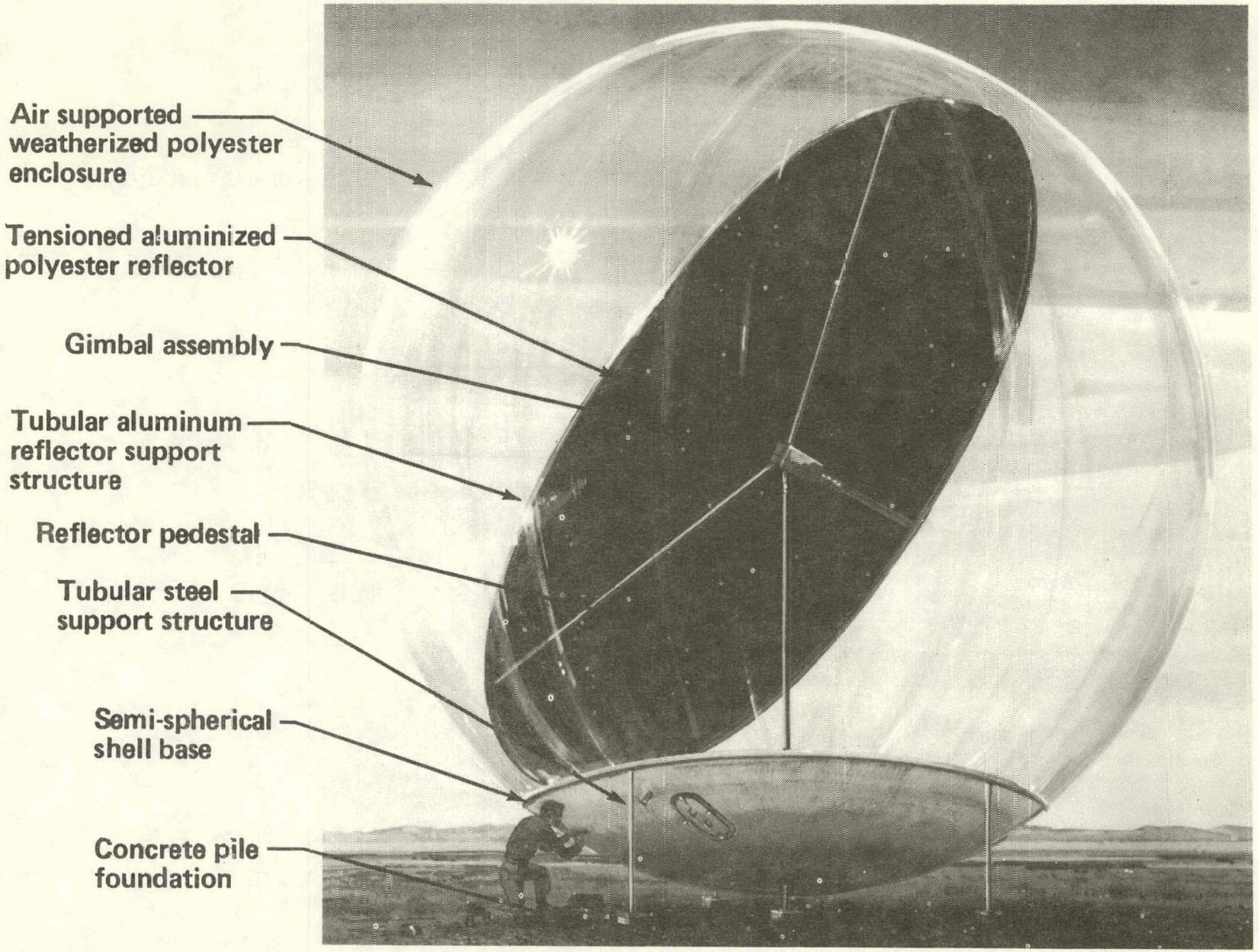

Figure 1.0-2. Selected Configuration

Base/Foundation - A base/foundation support for the protective enclosure and reflector consisting of a tubular steel frame, a spherical-segment preformed steel dish, concrete piling, and an air supply package. The design provides simplicity, minimum use of materials, and factory assembly of the entire heliostat adjacent to plant sites. The latter results in minimum use of field labor to install heliostats; thus, minimizing overall costs. The reflector is supported by a 12.7cm (5 in.) diameter steel pipe pedestal which passes through the steel dish, and is attached to a concrete piling.

The 6.85m (22.5 ft.) diameter base ring structure formed with 10.16cm (4 in.) diameter steel pipe, provides the interface (retention) to the enclosure and supports the steel dish. Lift and drag wind loads are transmitted through three pipe stanchions to reinforced concrete pilings. Stanchions are welded to steel plates on the pilings during installation. Conceptual automated processes have been designed for steel pipe and dish fabrication, and concrete piling installation.

The air supply system is designed to maintain internal enclosure pressure at 6.9 KN/m^2 (0.1 psig) with highly filtered air. Filters and the enclosure/base leak rate (0.006 m^3/min, 0.2 cfm) were selected to eliminate the need for cleaning the reflector over a 15 year interval. Filter maintenance has been reduced to replacement of first-stage filters on 5 year intervals.

Control System - An open-loop computer based control system providing tracking and mode control inputs to stepper motors on an az./el. gimbal. Design of the control system has been refined and simplified for high volume/low cost production ease of installation, and ease of maintenance. An alignment procedure has been defined, which through the use of control system software, eliminates the need for accurate reflector pedestal installation. An optical sensor array on the central receiver tower is used to detect the position of the reflected solar beam at several different times. Comparing the expected beam position to actual position on the array, the gimbal azimuth axis orientation is computed.

For ease of maintenance and weather protection, heliostat controller electronics are located on the inside of the base access hatch. To eliminate need for entering the heliostat for gimbal maintenance, synchro shaft position indicators have been selected, and all associated electronics have been placed on the access hatch. Additionally, high reliability components have been used in the control system wherever cost trades have indicated life-cycle cost savings.

Performance - A system-engineered heliostat design which meets or exceeds all specification 001 requirements. Optical performance analyses have predicted a reflected-energy capture efficiency (for the vertical cylinder receiver option) which exceeds 98% for all heliostat positions and times. A beam pointing accuracy of 2mr on a 1σ basis has been selected as a design goal.

Low heliostat weight is an indication of ability to achieve production cost goals. Table 1.0-1 shows a weight breakdown by major subassembly, resulting in a total of 36.4 Lb/m^2 (excluding concrete and embedments).

TABLE 1.0-1

WEIGHT BREAKDOWN

	LB	LB/M^2
Base Structure	1655	25.2
Pedestal	270	4.1
Gimbal & Drives	65	1.0
Reflector	301	4.6
Enclosure	54	0.8
Electronics	30	0.5
Pressurization	15	0.2
subtotal	2390	36.4
Concrete and Embeds	4370	66.5
TOTAL	6760	102.9

2.0 HELIOSTAT PRELIMINARY DESIGN

2.1 KEY DESIGN REQUIREMENTS/SPECIFICATIONS

The design requirements of Specification 001 together with the design response indicating design compliance is summarized in Table 2.1-1.

TABLE 2.1-1 SPECIFICATION COMPLIANCE

SPEC. PARA.	SUBJECT	REQUIREMENT SUMMARY	DESIGN RESPONSE
3.1.1.1	Availability	Maximize for daylight hours	High reliability - off operating hours maintenance
3.1.1.2	Interchange-ability	Major components shall be interchangeable	All components interchangeable throughout field.
3.1.1.3	Electrical Transients	Equipment shall not be adversely affected by specified transients. Normal operating - voltage $\pm$ 10% - frequency $\pm$ 0.1% Startup or shutdown - voltage +10% -25% with recovery within 5 cycles at 60 Hz Emergency - momentary total loss of power	Momentary power loss may necessitate reloading heliostat controller RAM memories.
		Lightning - Effective protection on a cost-risk basis.	Lightning protection prevents damage propogating to adjacent heliostats.
3.1.2.1.2	Wind - Operational limit	Max operation wind speed consistent with min. cost of electricity production.	Operate to 90 mph (40 m/s)
3.1.2.1.3	Wind - Stowage initiation	Stow wind speed selected on tradeoff between loss of direct beam insolation and heliostat cost.	Reflector protected by enclosure. Stowage not required. Enclosure survives 40 m/s wind.
3.1.2.1.4	Wind Rise Rate	Rise rate = .01 m/s^2. Withstand 25 m/s wind at any reflector orientation.	Reflector protected by enclosure. Withstands 40 m/s wind.
3.1.2.1.5	Survival Wind	Survive 40 m/s (90 mph) without damage.	Enclosure survives 90 mph and enclosure deflection does not interfere with mirror at any orientation. 15% margin yield at 132°F.
3.1.2.1.6	Wind Profile	Varies exponentially with height to 0.15 power. Reference height is 10 m.	Profile used for enclosure load/deflection analysis. Wind tunnel verification of loads.

SPEC. PARA.	SUBJECT	REQUIREMENT SUMMARY	DESIGN RESPONSE
3.1.2.1.7	Dust Devils	Dust devils with wind speed to 17 m/s survived without damage	No apparent structural or optical damage. (Criteria not definitive)
3.1.2.2	Temperature	Operate in ambient range from - 30°C to 50°C	No problems at 50°C. **Electronics heat dissipation assures operation at -30°C.**
3.1.2.3	Earthquake	Survive seismic zone 3. Realignment allowed.	Design for g loads.
3.1.2.4	Snow Environment	Survive 250 pascals (5 lb/sq. ft.)	Enclosure internal pressure is 14 lb/sq. ft. Orient reflector if deflections interfere.
3.1.2.5	Rain Environment	Average annual = 30 inches Max. 24 hour = 3 inches	No detrimental effects.
3.1.2.6	Ice Environment	Survive deposited ice layer 2 inches thick	Approximately 55% margin if ice deposited in cosine distribution over upper hemisphere of enclosure. (No ice on reflector)

SPEC. PARA.	SUBJECT	REQUIREMENTS SUMMARY	DESIGN RESPONSE
3.1.2.7	Hail	25 mm (1in.) dia. at 23 m/s (75 fps) Specific gravity = 0.9	Hailstone tests verify no structural failure. Negligible optical degradation over 15 yr. period.
3.1.2.8	Sandstorm	Survive tests per Mil. Std. 810B Method 510	Critical components protected by enclosure. Possible degradation of enclosure optical properties should be quantitatively assessed.
3.1.2.9	Lightning	Protection optimized on cost-risk basis	Lightning protection prevents damage from propogating to adjacent heliostats or to field controllers.
3.2	Performance	Optimize to achieve highest level of cost effectiveness,	Designed with reflector size, contour accuracy, pointing accuracy, focusing, and material properties to achieve cost effectiveness.
3.2.1	Operational Periods	Performance rated for specified hours of four specified days.	Calculated power intercept at the receiver is integrated average for each specified period based on 950 w/m^2 insolation times all efficiency factors.

SPEC. PARA.	SUBJECT	REQUIREMENTS SUMMARY	DESIGN RESPONSE
3.2.2	Targets	Performance assessment for one of 3 specified target options	Design for surface receiver specified by para. 3.2.2.1
3.2.2.1	Target	Vertical cylinder 17m diameter by 25 m high. Center elevation 250 m above ground level.	Used for heliostat design and performance analysis.
3.2.3.1	Field Positions	Performance satisfied from 3 field positions: Position: A — N of Tower: 1200 m — E of Tower: 430 m B — 800 m — 860 m C — -400 m — 430 m	Used for heliostat design and performance analysis.
3.2.4	Reflectivity	Maximum consistent with cost-optimized production of power.	**Selected materials with highest reflectance/ transmittance cost ratio.**
3.2.5	Reflective Area	Area selected consistent with cost-optimized production of power.	**Cost optimized within** constraints of enclosure material strength

SPEC. PARA.	SUBJECT	REQUIREMENTS SUMMARY	DESIGN RESPONSE
3.3	Drive & Control	See following requirements:	
3.3.1	General	See following requirements:	
3.3.1.1	Availability	Fail-safe operation during power outage and electrical transients	Momentary power loss may necessitate reloading heliostat controller RAM memories.
3.3.1.2	Power Input	TBD	Minimize power usage during operational and non-operational periods.
3.3.1.3	Limit Controls	Provide as necessary to protect equipment or personnel.	Electro-mechanical travel limit switches.
3.3.2	Normal Operations	See following requirements:	
3.3.2.1	Tracking	Control tracking accuracy	Open loop control system with pointing accuracy of 2mr(1σ) design goal. (See text Section 2.3.6)
3.3.2.2	Acquisition (beam-on)	Beam-on of groups of heliostats (less than 10% of field) on command from central control within 180 seccnds	Individual heliostats can be directed to receiver within 40 secs from standby.

SPEC. PARA.	SUBJECT	REQUIREMENTS SUMMARY	DESIGN RESPONSE
3.3.2.3	Synthetic Tracking	Continuous tracking during cloudy periods	Software controlled tracking. **based on ephemeris data.**
3.3.2.4	Offset Pointing	Capability to orient portions of array towards different locations on target to control flux levels and distribution	**Multiple targets can be incorporated in software.**
3.3.2.5	Normal Shutdown	Orient groups of heliostats to safe stowage on command from central control within T3D minutes.	Programmed in software. Time will be established based on system considerations.
3.3.2.6a	Receiver/Stowage -Traverse	Reflected energy shall not impinge on tower during startup and shutdown.	Programmed to **point reflected beam to standby position prior to start-up or shutdown.**
3.3.2.6b		All beams E of tower move one direction and all beams W of tower move in opposite direction when moved on or off receiver.	See 3.3.2.6c Can be accommodated by software if requirement is valid. Requires further study.
3.3.2.6c		Beams shall move in a controlled manner to avoid unsafe flux concentrations in the airspace.	Software controlled such that beams move first to standby, forming a toroid about the receiver. Then groups of beams moved in a controlled manner to stowage.
3.3.2.6d		Provide safe stowage to minimize environmental degradation.	All beams parallel and contained within field.

SPEC. PARA.	SUBJECT	REQUIREMENTS SUMMARY	DESIGN RESPONSE
3.3.3	Maintenance	Control features provided for maintenance convenience.	See subparagraphs
3.3.3.1	Manual Control	Provide (at heliostat) for maintenance and checkout purposes.	Manual control capability at each heliostat locks out central control and provides AZ and EL step or slew commands.
3.3.3.2	Calibration and Checkout	Provide orientation accuracy check from Central Control	Software programmed such that individual heliostat reflected beam can be directed to alignment array with position feedback to central control.
3.3.4	Abnormal Operations	Procedures shall be provided for abnormal conditions in any individual heliostat.	See subparagraphs
3.3.4.1	Failure Indication	Indication provided by local control to plant central control	Failure to correctly respond to programmed commands is communicated to central control. Individual heliostat controller automatically orients heliostat to stow. Other failure modes such as change in pressure could be communicated to central control.

SPEC. PARA.	SUBJECT	REQUIREMENTS SUMMARY	DESIGN RESPONSE
3.3.4.2	Emergency Shutdown	On command from central control, individual heliostat radiation on receiver reduced to 3% of initial value within TED seconds.	Central control can command individual heliostat to standby. **Slew rate is 0.135 deg. per second.**
3.4	Foundation	Maintain heliostat performance while operating in **specified environments.**	Foundation resists overturn from wind loads, and protects reflector components from environment.
3.4.1	Site Characteristics	Angle of internal friction is 30° $E = \beta (h + z)$ $\beta = 18.1$ MPa/m	Foundation design parameters
3.5	Physical Characteristics	See following requirements	
3.5a		Heliostat configuration and field spacing must permit access by service vehicles, and maintenance personnel.	Heliostat design and field spacing permits access. **Portable airlock provides maintenance access to inside of enclosure when required.**

SPEC. PARA.	SUBJECT	REQUIREMENTS SUMMARY	DESIGN RESPONSE
3.5.b		Provide for safe stow positions during maintenance, storms, or emergency shutdown.	Individual heliostats, groups or total field can be commanded to stow either from central control or from manual controllers at heliostat or field controllers.
3.5 c		Subsystems and components easily removed to facilitate maintenance.	All internal components requiring maintenance can be easily removed thru airlock. Enclosure and reflector easily replaced with mobile maintenance vehicle.
3.5d		Lifetime = 30 years with maintenance and replacement where necessary.	Selected components for lifetime consistent with minimizing cost of electric power production.
3.6	Reliability	Achieve high reliability	Use high reliability components consistent with minimizing life-cycle cost. Safety is prime consideration. Evaluate FMEA.

SPEC. PARA.	SUBJECT	REQUIREMENTS SUMMARY	DESIGN RESPONSE
3.7	Maintenance		
3.7a		Provide easy cleaning without excessive performance degradation	Eliminate requirement to clean reflector and inside of enclosure for 15 year period (estimated dome replacement interval). Provided for water spray cleaning of dome exterior.
3.7b		Components subject to wear or damage, shall be capable of being inspected, serviced or replaced.	Designed for minimum life-cycle cost. Requirements for periodic inspection, repair or replacement have been defined. Spares requirements defined.
3.7c		Components serviceable by personnel of normal skills. Special equipment for servicing shall be identified.	Special design consideration to simplify electronics trouble shooting and repair. Simple patching procedure to repair damage to enclosures. Identified field repair versus depot repair.

SPEC. PARA.	SUBJECT	REQUIREMENTS SUMMARY	DESIGN RESPONSE
3.8	Materials, Processes and Parts	Use standard materials and processes.	Utilized common materials, known processes and off-the-shelf components where cost effective.
3.9	Electrical Transients	See 3.1.1.3 and 3.1.2.9	
3.10	Workmanship	Use best modern practices consistent with cost and performance requirements.	Component manufacturing is highly automated. Maximized factory assembly. Installation by crews trained for single repetitive functions.
3.11	Interchange-ability	Permit interchangeability	Designed with tolerances such that all parts are interchangeable for every heliostat. Only software address is unique per heliostat.

SPEC. PARA.	SUBJECT	REQUIREMENTS SUMMARY	DESIGN RESPONSE
3.12	Safety		See paragraphs 3.3, 3.5 and 3.6
a			
b			
c			
d			
e			
f			
3.13	Documentation	For planning purposes only during Phase I study	
4.0	Quality Assurance Provisions	For planning purposes only during Phase I study	

2.2 INTERFACE REQUIREMENTS

Heliostat component/component interface requirements are defined in pertinent sections of this document. The interface definitions below are those between the heliostat and other related elements of the Solar Central Receiver Power Plant.

Interface	Requirement Definition
Receiver	. Cylindrical surface receiver as specified in paragraph 3.2.2.1 of specification 001
Control System	
Data Bus	. Transmission Line Serial Digital Data Bi-Phase Manchester Code 10V P to P (optional)
Data Transfer	. Information to Heliostat Controller . 49 BIT word . Update Rate - 5 sec . Heliostat address or master address . Heliostat mode . Shutdown . Standby . Track . Align . Data request . Current position . Time . Alignment position . Heliostat status . Power status . Data identifier . Position commands . Reference time . Cycle time . Position data: Align, shutdown . Power modes: On/Off . Data variable format-defined by data identifier field . Other functions . Time sync (single or master) . Motor power (single or master) . Idle . Data load . Manual control . Error in received message

- Information From Heliostat Controller
  - 49 BIT word
  - Update Rate - 5 sec
  - Heliostat Controller Address
  - Heliostat Mode Response
    - Shutdown
    - Standby
    - Track
    - Align
  - Data identifier
    - Current position
    - Time
    - Alignment positions
    - Power Status
    - Heliostat detailed status
  - Data variable format-defined by data identifier field
  - Received parity error
  - Other functions
    - Time sync
    - Motor power
    - Idle
    - Data load
    - Manual control
    - Error in received message

Field Cabling

- Signal wiring, pigtail out of conduit into each heliostat.
- Power wiring stubbed to J Box at each heliostat.

Alignment System

- Provision for attachment of array hardware to tower.
- 115V single phase power at tower interface point.
- Data transmission cabling from tower interface to central control.
- Surveyed directional monuments in field.

Site

- Rough graded and compacted
- Vegetation removed.
- Survey for heliostat locations
- 14 foot chain link fence at perimeter of plant with 50% porosity.
- Site security
- Area and layout TBD

Plant Utility Power	. Control system - each heliostat operation 34 watts 115VAC 60 shutdown 4.5 watts 115VAC 60 . Blower 10 watts (maximum) 115VAC 60
Plant Utility Water	. TBD gallons per day.
Manufacture/Assembly Facility	. 6 acres adjacent to "power park" required for production rate of 25,000 and 250,000/year. (12 acres for 1,000,000 heliostats per year.)
Transportation Facilities	. Access roads from public highway to manufacturing/assembly facility. . Rail spur to manufacture/assembly. . Inter-plant roads within the "power park". . 3 acres for parking required for production rated of 25,000 and 250,000/year.
Other Utilities	. Water and sewer to support 300 man factory and field work force for 25,000 and 250,000/year. (600 men for 1,000,000 heliostats per year) . Location for field controllers in or near central control facility. . Location for emergency generator and associated equipment. . Provision for spares and support equipment storage. . Maintenance equipment repair shop. . Office space for operations/ maintenance personnel.

2.3 PROTOTYPE HELIOSTAT CONFIGURATION

2.3.1 Optical Performance Analysis

2.3.1.1 Ground rules and Methodology

The optical performance was calculated for each of the three specified heliostat locations for each of the four specified periods. The specified heliostat locations and the specified periods are as provided in Table 2.3.1.1-1. The performance was calculated using the Boeing HACSM optical ray trace program. The optical performance is defined as the thermal energy received within the target geometry as specified in Table 2.3.1.1-2. The average daily direct insolation was 950 watts per meter squared. The reflectivity and the enclosure transmissivity as a function of the incidence angle is as shown in Figures 2.3.1.1-1 and 2.3.1.1-2.

A further performance parameter affecting image size at the receiver is the diffusion effects due to both the mirror surface quality and the enclosure material. These scattering effects are input to the HACSM computer program as a one sigma conical angle spreading of each ray. To estimate the proper scattering angle input to the computer program, image power density maps from actual tests at Livermore, California were correlated with the HACSM program data. Results of this correlation are shown in Figure 2.3.1.1-3 for a vacuum focused reflector. The scattering angle in the range of 0.05 to 0.10 degrees correlates with the actual test data. This correlation is for a 4 mil Tedlar enclosure. The particular batch of Tedlar used in the Livermore enclosure exhibited a relatively high scattering up to a cone angle of 0.6 degrees, as shown in Figure 2.3.1.1-4. Other candidate materials such as Melinex "O" and Celanar 4000 exhibit no significant scattering down to the instrument limit of about 0.08 degrees as illustrated in

TABLE 2.3.1.1-1

SPECIFIED HELIOSTATS AND PERFORMANCE PERIODS

HELIOSTAT	LOCATION		SLANT RANGE
	NORTH	EAST	
A	1200 M	430 M	1300 M
B	800 M	860 M	1200 M
C	-400 M	430 M	640 M

PERIOD	DAY	HOURS
Spring Equinox	March 21	8:00 A.M to 4:00 P.M.
Summer Solstice	June 22	6:00 A.M. to 6:00 P.M.
Fall Equinox	September 23	8:00 A.M. to 4:00 P.M.
Winter Solstice	December 22	9:00 A.M. to 3:00 P.M.

TABLE 2.3.1.1-2

SPECIFIED TARGET RECEIVER

Type	Cylindrical Surface
Diameter	17 meter
Height	25 meter
Elevation	250 meter (to center

Figure 2.3.1.1-1. Mirror Optical Characteristics

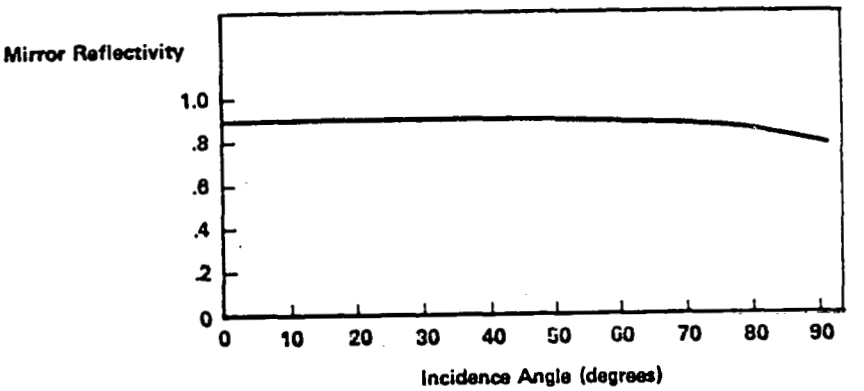

.910	.910	.910	.910	.906	.900	.897	.885	.861	.813
0	10	20	30	40	50	60	70	80	90

Figure 2.3.1.1-2. Enclosure Optical Characteristics

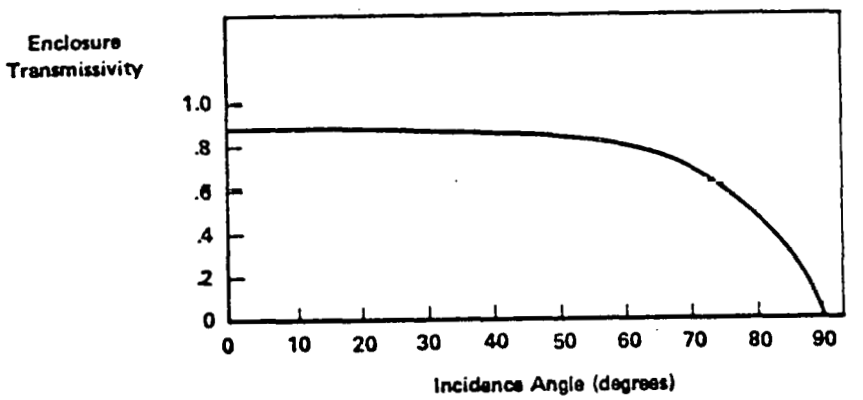

.884	.881	.879	.874	.864	.84	.812	.708	.515	0
0	10	20	30	40	50	60	70	80	90

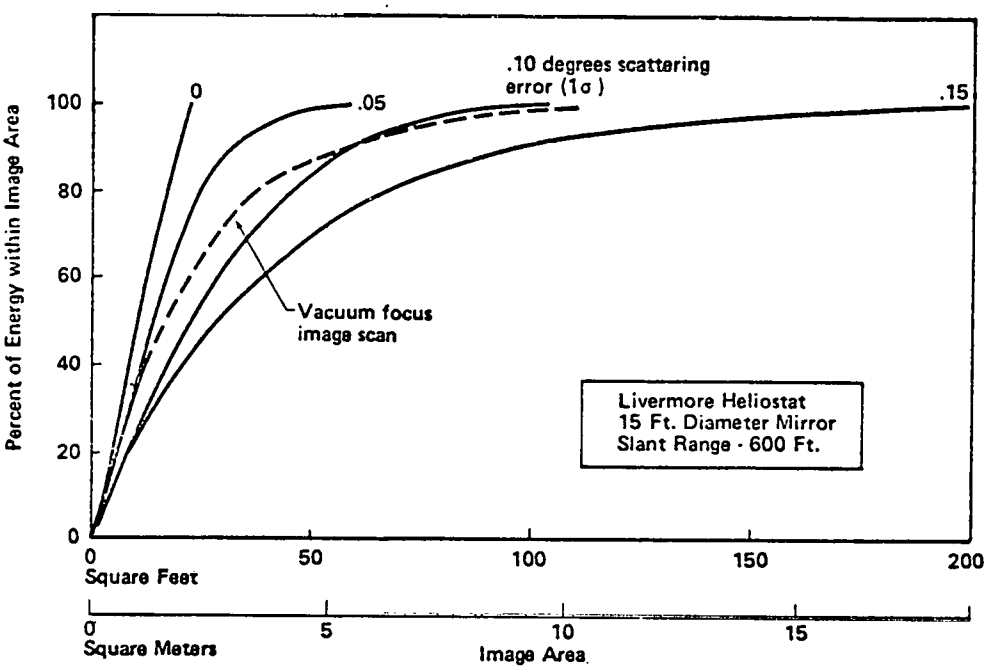

Figure 2.3.1.1-3. Correlation of Image Scan Data with with Calculated Energy Distribution

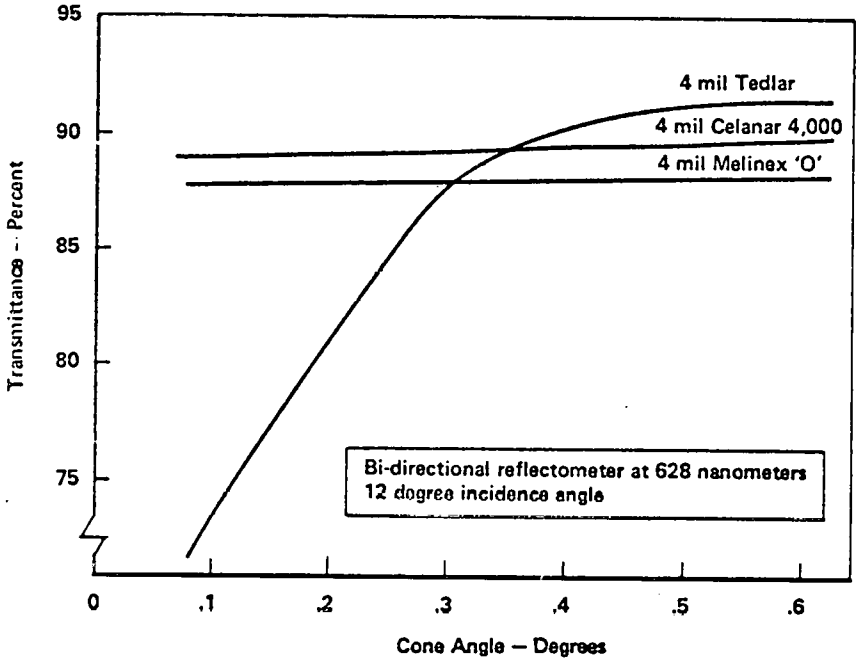

Figure 2.3.1.1-4. Enclosure Optical Transmittance

the figure. It can therefore be assumed that a polyester material would cause less image scattering in a heliostat.

The preliminary optical performance analysis for design optimization assumed a scattering error effect of 0.12 degrees, however, 0.05 degrees was used in the final performance analysis (Section 2.3.1.3). Figure 2.3.1.1-5 illustrates this effect of scattering error on capture efficiency for an arbitrary set of conditions (not values used in final performance analysis).

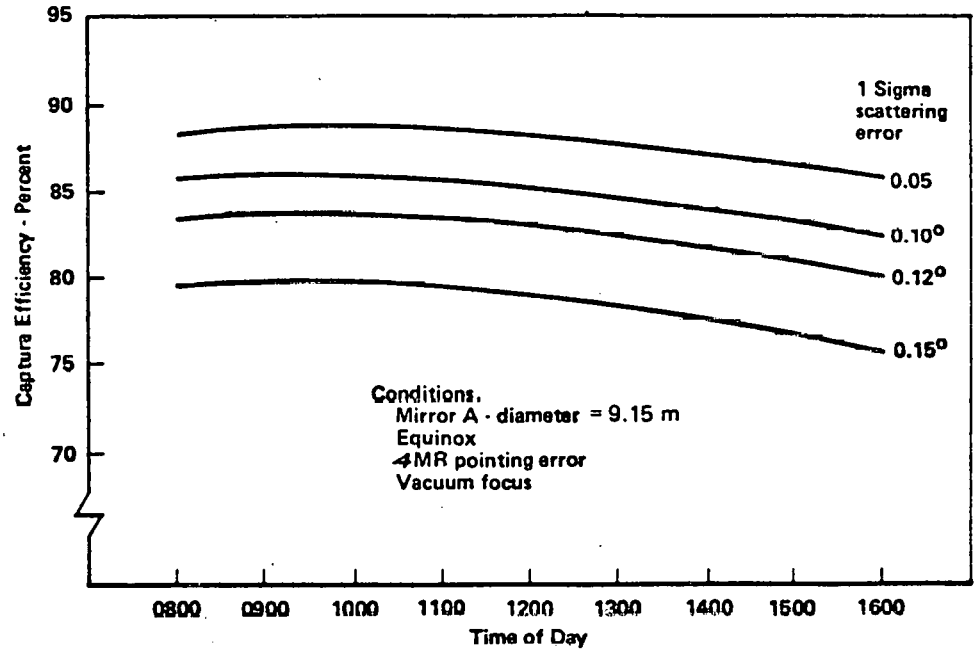

Figure 2.3.1.1-5. Effect of Scattering Error on Capture Efficiency

2.3.1.2 Performance Optimization

The preliminary optical performance analysis was combined with design and cost analyses in developing the selected configuration. The following discusses results of parametric studies which included the matrix of focusing concepts, beam pointing accuracy, and reflector size. The HACSM optical ray trace program was used for analyses.

The first issue in the trades was to evaluate and select the focusing concept for the recommended configuration. The membrane reflector has an inherent ability to provide some focusing due to gravity sag of the membrane. Control of sag (gravity focusing) can be achieved by varying membrane tension applied during manufacture. For this study, the optimum tension was established for the far field heliostat (position A) and not varied for heliostats in other zones. The membrane reflector can also be focused by mechanically pulling the center of the mirror or by applying a reflector back surface membrane and pulling a slight vacuum (vacuum focus). This concept is further enhanced by controlling the vacuum through the electronics and software to provide best focus for each mirror at all times. This is termed "active smart" focusing. A schematic of vacuum focusing and control is shown in Figure 2.3.1.2-1.

Focusing capabilities have been demonstrated with the heliostat installed at Sandia Laboratories, Livermore, California. A schematic of the test setup is shown in Figure 2.3.1.2-2. Figure 2.3.1.2-3 shows the heliostat directing energy to the target board. Figure 2.3.1.2-4 shows that vacuum focusing significantly reduces the image size compared to the partial gravity focused image.* These images were mapped and the

* The Livermore reflector was fabricated with 1,000 psi tension. For the reflector tilt angle involved, this would produce a focal length in excess of 4,000 ft., compared to the target board distance of 600 ft.

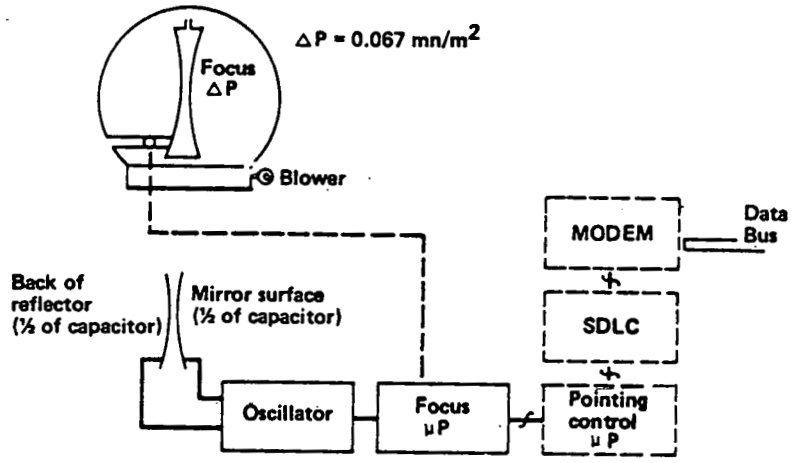

Figure 2.3.1.2-1. Focus Control

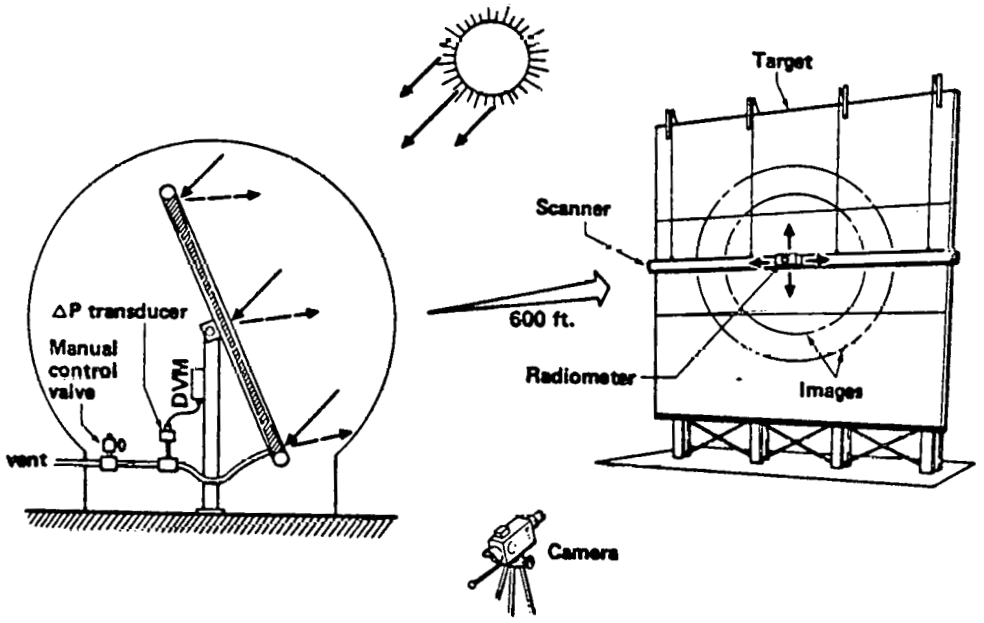

Figure 2.3.1.2-2 Vacuum Focusing Test Schematic

Figure 2.3.1.2-3. Focusing Test at Livermore

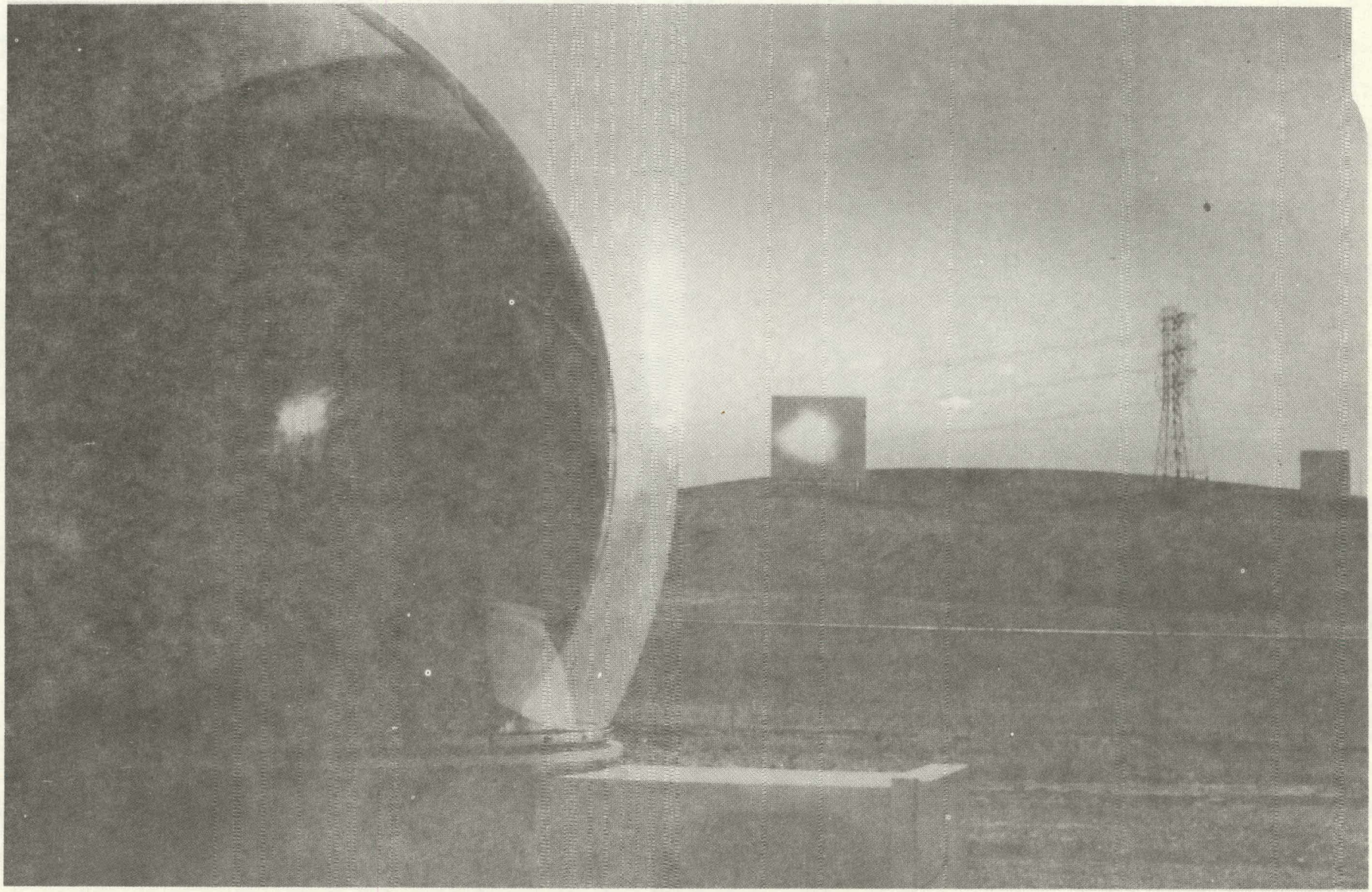

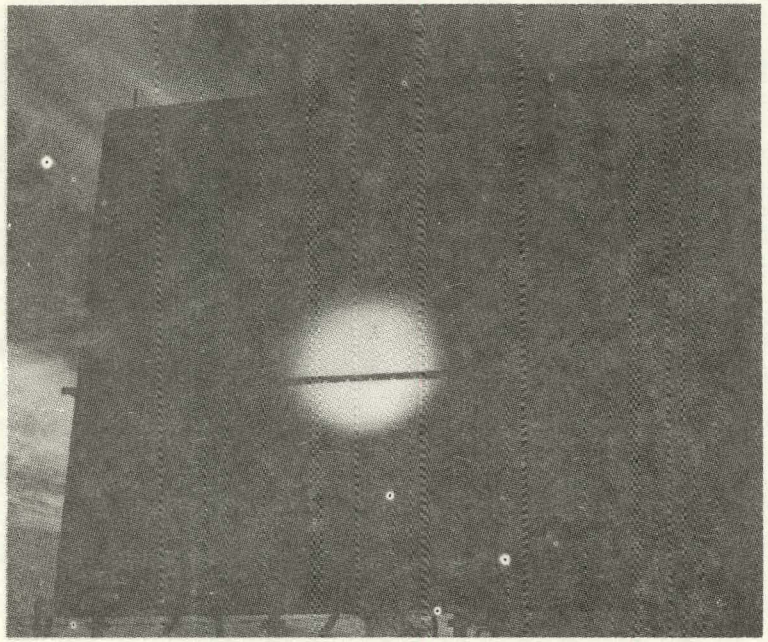

Vacuum Focusing

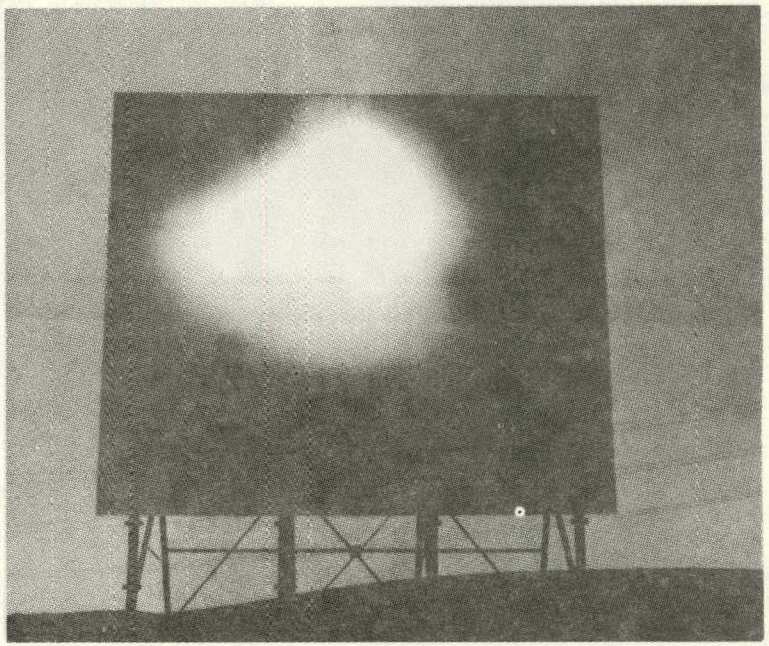

Partial Gravity Focusing

Figure 2.3.1.2-4. Visual Images at 600 ft Distance

concentration of energy due to vacuum focusing is illustrated in Figure 2.3.1.2-5. It should be noted that photographic film sensitivity does not provide an adequate measure of image size at the target. Mapping showed that the image intensity ratio of about 0.13 was the background level of diffuse light at the target. The visual image as shown by the photograph is somewhat smaller than the mapped image. The low intensity energy outside the visual image accounts for approximately 20 percent of the total energy.

Typical results of parametric analyses are shown in Figure 2.3.1.2-6. Energy delivered to the receiver is plotted for a far-field mirror (position A), utilizing a scattering error function of 0.12 (not final value). Data in the figure illustrates that beam pointing error is the most significant parameter in performance optimization. Total energy on target is essentially proportional to the reflector area; i.e., within the size range studied for the specified target, mirror size has a negligible affect on spillage.

Table 2.3.1.2-1 compares the percent of reflected energy delivered to receiver for gravity focused and vacuum-focused reflectors. Data shown in the table were calculated on the basis of a 9.15m diameter reflector, scattering error function of 0.12 degrees, and a 2mr (1σ) beam pointing accuracy. Results show that the difference in performance between gravity and vacuum focused reflectors is small. Considering the additional capital cost to provide vacuum focusing, gravity focusing was selected for the commercial plant heliostat design.

On the basis of data shown in Figure 2.3.1.2-6, and results of controls/gimbal preliminary design studies (Sections 2.3.5 and 2.3.6), a 2mr (1σ) beam pointing error was selected as a cost effective goal. Table 2.3.1.2-2 summarizes the beam pointing error budget established.

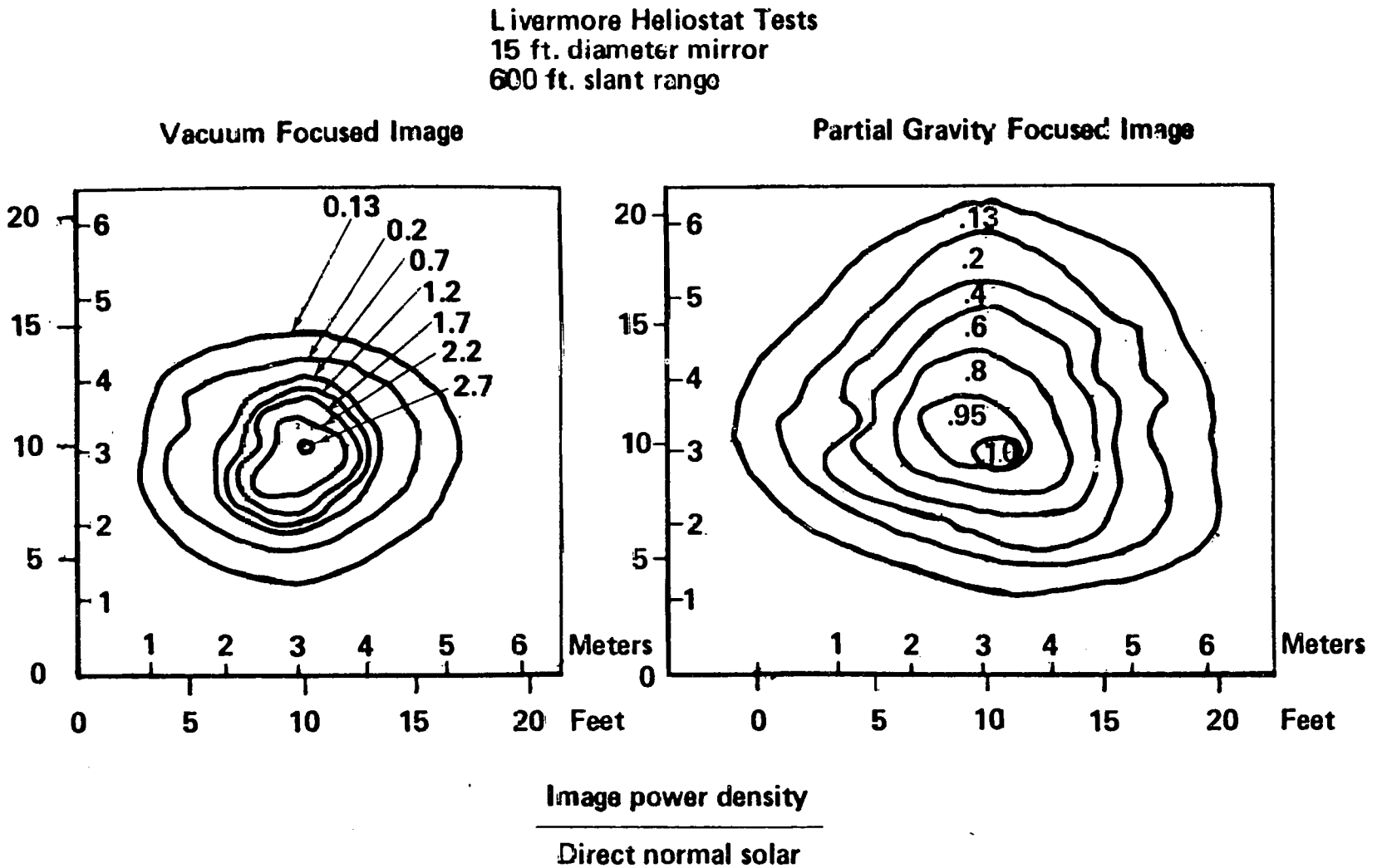

Figure 2.3.1.2-5 Image Power Density Distribution

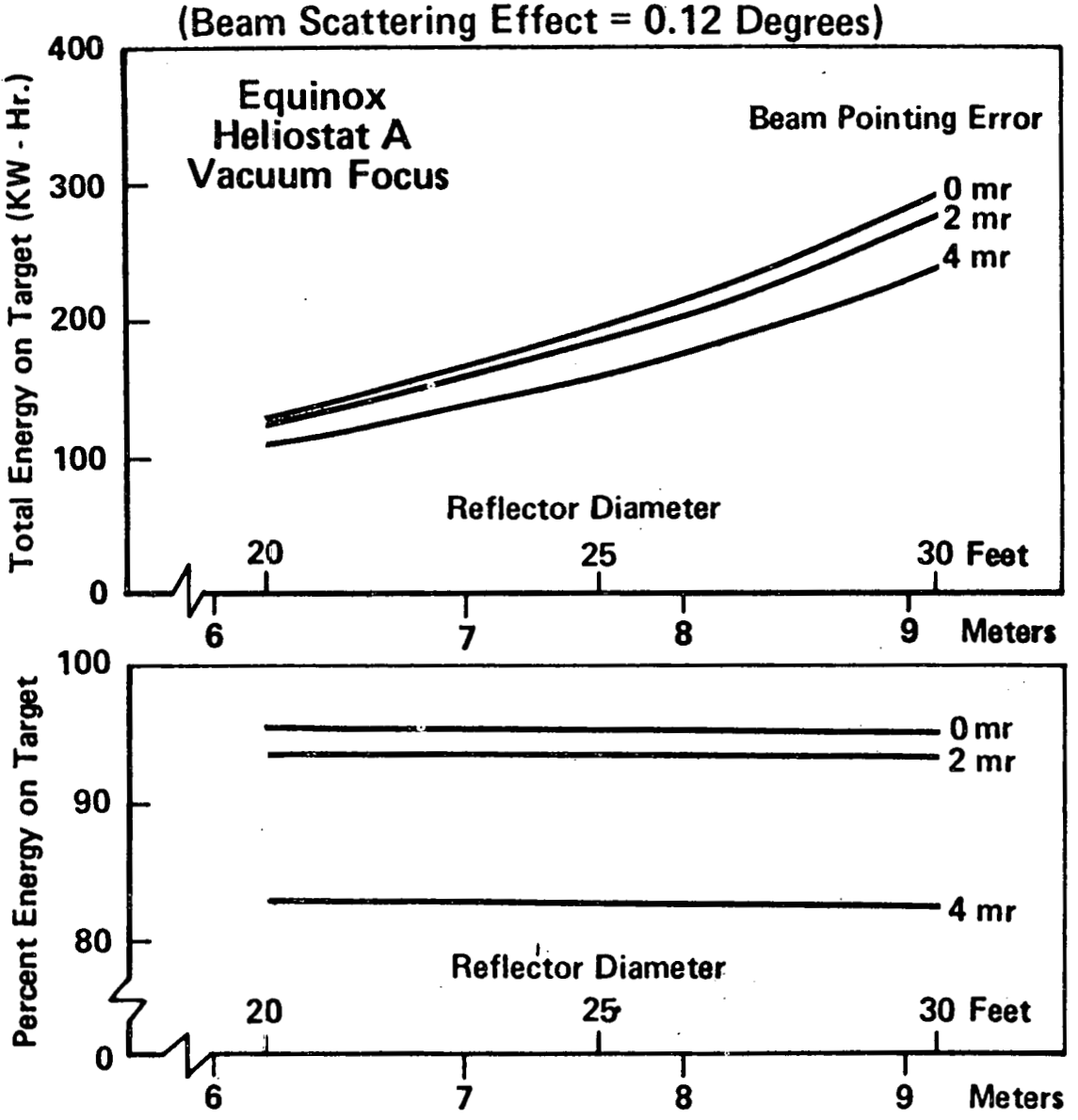

Figure 2.3.1.2-6. Significance of Beam Pointing Error and Mirror Size

TABLE 2.3.1.2-1 FOCUSING EVALUATION

BEAM POINTING ERROR = 2mr (1σ)

BEAM SCATTERING = 0.12^{o} (1σ)

	Focusing Method	Capture Efficiency Heliostat (vs Field Position)		
		A	B	C
Summer	Gravity	94.5	95.5	100.C
	Vacuum	94.5	95.7	100.0
Winter	Gravity	90.6	92.0	100.0
	Vacuum	90.8	92.6	100.0
Spring -Fall	Gravity	93.2	94.3	100.0
	Vacuum	93.2	94.6	100.0

NOTE: Efficiencies are averaged over;

Summer - 6:00 AM - 6:0C PM

Winter - 9:00 AM - 3:00 PM

Spring-Fall - 8:00 AM - 4:00 PM

Table 2.3.1.2-2

BEAM POINTING ACCURACY ERROR BUDGET

Source	Budget Allocation (1σ)	
Gimbal Actuator		
. Gimbal Actuator Error Cone	0.07	degrees
. Encoder Accuracy	0.03	
. Encoder Repeatability	0.03	
. Step resolution vs time (± 1/2 step)	0.008	
RSS	0.08	degrees
	(1.40 mr)	
Control System		
. Ephemeris Data	0.0060	degrees
. Angle Calculation	0.0036	
. Clock Resolution	0.0010	
. Alignment	0.0746	
RSS	0.075	degrees
	(1.31 mr)	
TOTAL STATIC	0.1	degrees
	(1.74 mr)	
Pedestal, Actuator, Mirror Dynamics	0.032	degrees
	(0.56 mr)	
Total Errors RSS	0.114	degrees
	(2.0 mr)	

Selection of heliostat size was based on optical performance data (Figure 2.3.1.2-6) and cost per unit reflector area. As discussed earlier, no significant reduction in performance occurred by increasing reflector size up to 10m diameter. Relative heliostat cost per unit reflector area, plotted in Figure 2.3.1.2-7, shows that cost does not significantly decrease at diameters greater than about 9 meters. On the basis of these data, a reflector size of 9.3 m diameter was selected as near optimum.

2.3.1.3 Results of Optical Performance Analysis

Finalized optical performance was calculated based on the following configuration:

1) Gravity focused reflector.
2) Effective reflector area of 65.7 sq. meters (9.3 m diameter)
3) Solar reflectance of 0.91.
4) Dome transmissivity of 0.88.
5) Heliostat scattering error factor of 0.05 degrees.
6) Beam pointing error of 2mr (1σ).

The parasitic power requirements for the controls and pressurization blower will be approximately 40 watts electrical during operation and 10 watts electrical during shutdown. These values, at 1 electrical equals 5 thermal, were subtracted from the incident energy on the receiver to establish net power performance as presented in Table 2.3.1.3-1. The percent of reflected energy intercepted by the cylindrical receiver is presented in Table 2.3.1.3-2.

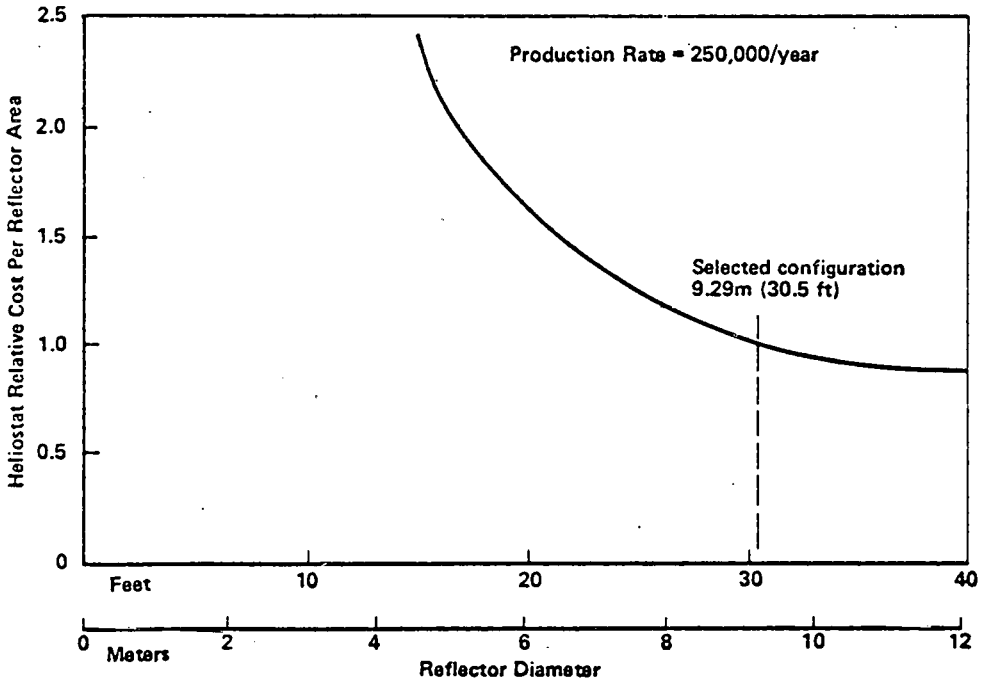

Figure 2.3.1.2-7 Heliostat Size/Cost Optimization

TABLE 2.3.1.3-1 NET DAILY INCIDENT ENERGY ON RECEIVER (KW-HR)

	HELIOSTAT		
PERIOD	A	B	C
Spring & Fall Equinox	285	277	231
Summer Solstice	363	362	393
Winter Solstice	230	220	146

TABLE 2.3.1.3-2 PERCENT REFLECTED ENERGY INCIDENT ON CYLINDRICAL RECEIVER

PERIOD	HELIOSTAT A	B	C
Spring & Fall Equinox	99.1	99.3	100.0
Summer Solstice	99.0	99.6	100.0
Winter Solstice	98.6	98.6	100.0

2.3.2 Protective Enclosure

2.3.2.1 Configuration

The protective enclosure (Figure 2.3.2.1-1) is a transparent weatherized polyester material thermoformed to a spherical shape. The spherical enclosure is truncated at a 45^{o} angle from the spherical center to interface with an attachment fitting at the base support ring.

The diameter of 9.69 m (31.8 ft.) provides a clearance of 19.8 cm (7.8 inches) from the reflector support ring. This clearance accommodates assembly and installation tolerances plus enclosure deflection due to the maximum design winds.

The enclosure is thermoformed from an 0.05cm (0.020 in.) thick weatherized polyester film. The thermoforming results in a finished dome with a minimum film thickness of 0.008cm (0.003 inches).

The enclosure interfaces with the base/foundation at a retention fitting which provides the tension load path and a positive air pressure seal. The design objectives for the retention fitting are:

1) Positive pressure seal
2) Adequate load path
3) Ease of assembly (minimum labor)
4) Ease of disassembly (minimum labor)
5) Minimum cost of materials
6) Long life

Several configurations of the retention device were evaluated. Seven of these are shown in Figures 2.3.2.1-2 and 2.3.2.1-3. The "Clip Wrapped Joint" which is discussed in the following paragraphs was chosen based on simulated testing, design analysis and cost data.

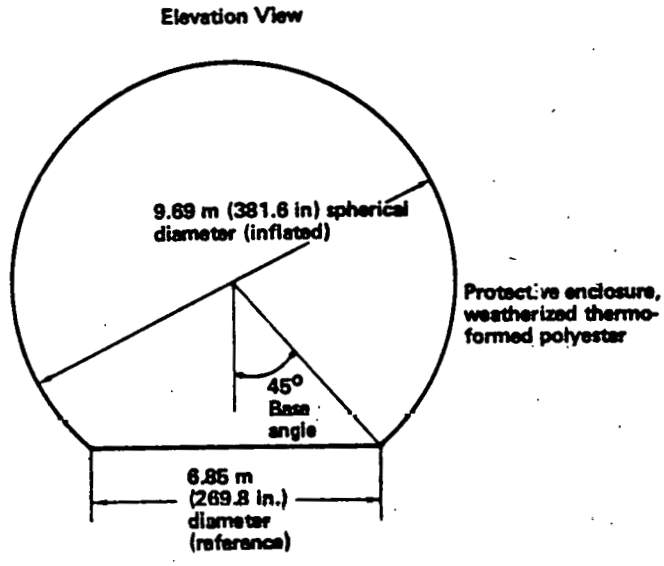

Figure 2.3.2.1-1. Protective Enclosure Envelope—Elevation View

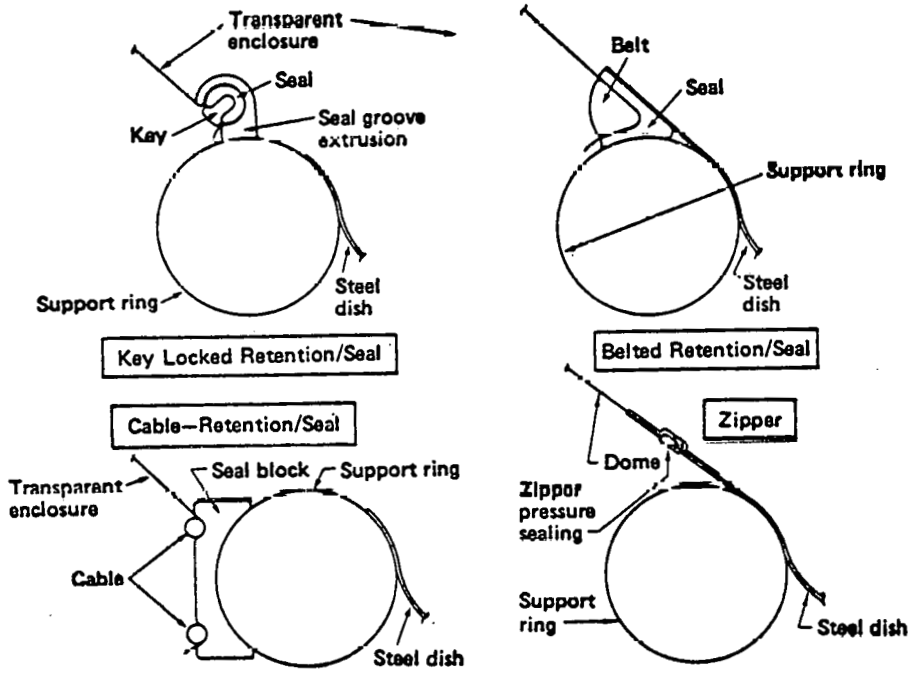

Figure 2.3.2.1-2. Interface Concepts (Non-energizing)

The clip wrapped joint uses an FEP Teflon "L" shaped extrusion sized such that it fits inside the rolled lip of the base dish. The dome material is wrapped around the extrusion causing a self energizing retention force as shown in Figure 2.3.2.1-4. The bottom edge of the dome is indexed during thermoforming to assure correct alignment. The "L" extrusion is in the form of a continuous cord, pre-coated with pressure-sensitive adhesive. The extrusion is cut to length on assembly. The adhesive strip is protected by a film which is peeled off during assembly.

The overall dome assembly procedure, using the "clip wrapped joint" attachment technique is as follows:

Step 1 - Place uninflated dome over reflector assembly.

Step 2 - Locate "L" extrusion on dome index line, using exposed adhesive to hold in place.

Step 3 - Locally wrap dome edge around extrusion and slide combination into rolled dish edge. (See Figure 2.3.2.1-4)

Step 4 - Inflate dome, after entire circumference has been installed per Step 3.

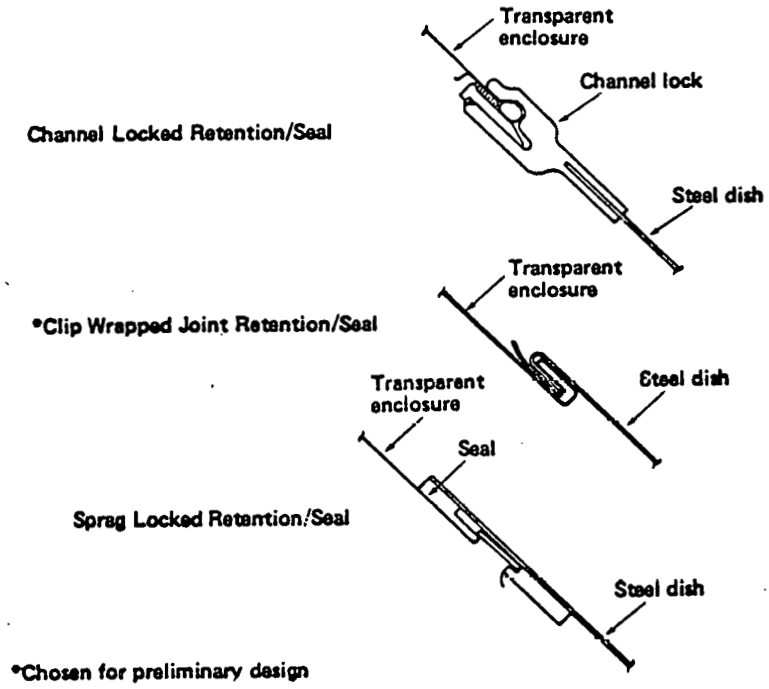

Figure 2.3.2.1-3. Interface Concepts (Self-energizing)

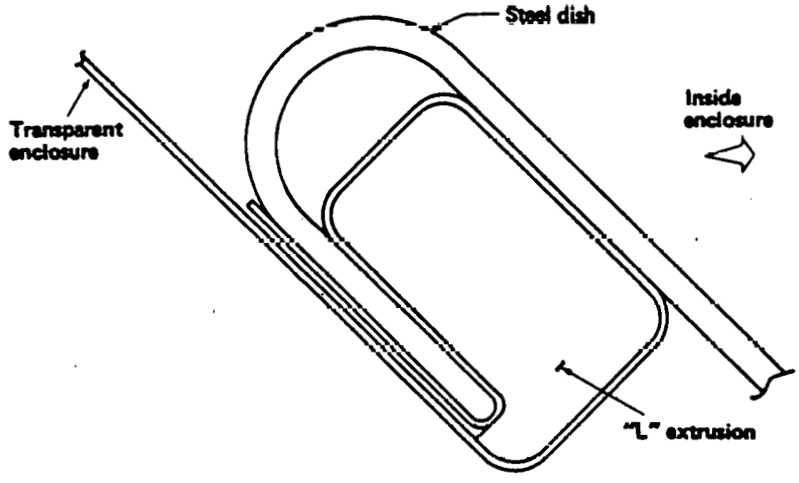

Figure 2.3.2.1-4. Clip Wrapped Joint

2.3.2.2 Protective Enclosure Materials Evaluation

Shortly after contract go-ahead a series of trips were taken to search the plastic film industry for candidate enclosure and reflector materials. A total of 14 companies were visited. In addition, many firms were contacted by telephone. Many were interested in participation in the development program. Some had a few candidates they could supply in the short term; however, the majority required additional time to make special process runs for this application. The result was a considerable delay in the start of materials screening tests and the realization that promising candidates would be supplied over a period of time rather than all at one time. Table 2.3.2.2-1 lists the suppliers that have participated to various extents, and the materials that they supplied.

One supplier contacted late in the program was ICI Ltd. - Welwyn Garden City, England. They have developed an improved technique for internal stabilization of polyesters. Initial tests at ICI show promising ultra-violet resistance and high transmittance. They will be providing specimens for enclosure and reflector material which can be evaluated in follow-on related contracts. Included will be stabilized oriented samples (reflector material) and stabilized unoriented (enclosure thermoforming material) samples.

The materials test plan prepared early in the program called for screening tests to be performed on all promising candidates. This consisted of measuring the mechanical (yield strength, ultimate strength, percent elongation, thickness uniformity) and optical (specular transmittance) properties prior to, during and following exposure to accelerated ultraviolet exposure testing. The most promising materials were then included in real-time and accelerated desert exposure testing. These tests are still underway at the Desert Sunshine Exposure test facility near Phoenix. The following paragraphs describe results of tests on enclosure materials completed in the contract.

TABLE 2.3.2.2-1

ENCLOSURE MATERIAL SUPPLIERS

SUPPLIER	MATERIAL	STATUS
ALLIED CHEMICAL	NON WEATHERABLE POLYESTER (PETRA)	- SCREEN TESTED - DESERT TEST UNDERWAY
MARTIN PROCESSING	WEATHERABLE POLYESTER (MELINEX "O")	- SCREEN TESTED - DESERT TEST UNDERWAY
NATIONAL METALIZING	WEATHERABLE POLYESTER	- SCREEN TESTED - DESERT TEST UNDERWAY
PENNWALT	FLUOROCARBON (KYNAR)	- SCREEN TESTED - DESERT TESTED
W.R. GRACE (CRYOVAC)	WEATHERABLE POLYCARBONATE	- SCREEN TESTED - DESERT TEST UNDERWAY
HERCULES	WEATHERABLE POLYPROPYLENE	- SCREEN TESTED
MORTON CHEMICAL	WEATHERABLE POLYESTER	- SCREEN TESTED
DUPONT	FLUOROCARBON (TEDLAR)	- SCREEN TESTED - DESERT TESTED
ICI AMERICAS	POLYESTER	- SCREEN TESTED
TEIJIN AMERICA	WEATHERABLE POLYESTER	- SCREEN TESTED

Mechanical Properties

Table 2.3.2.2-2 shows the initial mechanical property data for materials. All materials in the table exhibited adequate initial mechanical properties.

Joint samples were prepared using Kynar-C and Melinex "O" to demonstrate the fabrication process for enclosures in Phase II. Table 2.3.2.2-3 shows results of tensile tests on joint samples. Melinex "O" was joined with a thermosetting polyester adhesive; and Kynar-C by heat sealing with application of pressure and a hot wire (similar to Tedlar sealing) Ref. 2.3.2.2-1. The polyester joint was as strong as the parent material. Kynar failed adjacent to the joint, suggesting the material had thinned during the application of heat and pressure. Although adequate strength was demonstrated, it is believed that refinement of the technique would result in improvement in strength.

Extruded plastic materials may show considerable thickness non-uniformities in the machine and transverse roll directions. These variations must be considered in design. Table 2.3.2.2-4 provides thickness variation data for those materials that were supplied as roll stock. Most candidate materials were supplied as small hand prepared samples and would not provide representative machine produced thickness variations. The latter were not measured. A maximum variation of 30% from nominal was measured on one material while negligible variation was measured on others.

Specular Solar Transmittance

Many material samples had specular solar transmittances that were within the acceptable range ($\geq$ .86). Some were submitted for purposes of determining initial mechanical properties and weatherability, with plans (by supplier) to modify or improve the transmittance at a later time if the material looked promising. The last data column of Table 2.3.2.2-2 shows the transmittances for materials received.

TABLE 2.3.2.2-2

INITIAL MECHANICAL AND OPTICAL PROPERTIES FOR CANDIDATE ENCLOSURE MATERIALS

MATERIALS	Ultimate Stress MN/m^2 (PSI)	Yield Stress MN/m^2 (PSI)	Ultimate Elongation %	Specular Transmittance ▷
POLYESTERS				
PETRA A - Non-Weatherable; Allied Chemical	74.5 (10,800)	62.8 (9,100)	544	.89
MELINEX "O" - Weatherable; Martin Process	140 (20,300)	105 (15,200)	90	.84
MELINEX "C" - Weatherable; National Metalizing	185 (26,870)	132 (19,200)	132	.85
POLYESTER - Weatherable; Morton Chemical				.67
POLYESTER - Weatherable; Teijin America				.86
POLYCARBONATE				
POLYCARBONATE - Weatherable; W. R. Grace - 4 MIL	79.9 (11,590)	57.4 (8,320)	141	.88
W. R. Grace - 8 MIL	70.1 (10,170)	56.4 (8,180)	129	.85
POLYPROPYLENE				
POLYPROPYLENE - Non-Weatherable; Hercules	198 (28,740)	44.2 (6,410)	69	.80
Weatherable; Hercules	140 (20,270)	31.0 (4,490)	83	.76
FLUOROCARBONS				
KYNAR - Weatherable Polyvinylidine Fluoride; Pennwalt - KYNAR A	162 (23,520)		80	.89
KYNAR B	167 (24,170)		72	.88
KYNAR C	153 (22,160)		82	.89
TEDLAR - 7826B - Weatherable Polyvinylidine Fluoride; DuPont	78.2 (11,340)	34.5 (5,002)	180	.87

▷ 0.5 cone angle; normal incidence; AM 2 spectrum

TABLE 2.3.2.2-3

JOINT TENSILE DATA FOR ENCLOSURE MATERIALS

MATERIAL	FAILURE STRESS MN/m^2 (PSI)	FAILURE MODE/REMARKS
POLYESTER JOINT (MARTIN PROCESS MELINEX "O") THERMOSETTING POLYESTER ADHESIVE BOND	210 (30,520)	SEPARATION - NOT AT JOINT
FLUOROCARBON JOINT (PENNWALT-KYNAR-C), FIRST ATTEMPT HEAT SEAL	70.3 (10,200)	SEPARATION ADJACENT TO JOINT

TABLE 2.3.2.2-4

MATERIAL THICKNESS NON-UNIFORMITY

MATERIAL	NOMINAL THICKNESS (INCHES)	MAXIMUM DEVIATION FROM NOMINAL (INCHES)
WEATHERIZED POLYESTER (MELINEX O - MARTIN)	.002	.0000
POLYESTER (PETRA-ALLIED)-1	.004	.0010
-2	.004	.0012
POLYCARBONATE (CRYOVAC) -1	.010	.0026
-2	.004	.0008
TEIJEN	.007	.0000

NOTE: MICROMETER MEASUREMENTS TAKEN AT EDGE, CENTER, OPPOSITE EDGE AT 3 POSITIONS DOWN ROLLS PROVIDED BY EACH SUPPLIER (9 DATA POINTS EACH MATERIAL)

Accelerated Ultraviolet Tests

Figures 2.3.2.2-1 and 2.3.2.2-2 show the physical test setup, consisting of a solar simulator (Spectrolab X-200) and the target plane. Samples were held to a water-cooled panel and temperature controlled to approximately $80^{o}F$. The integrated acceleration rate for the region of 250-400 nanometers was 10 air mass 2 SUNS. Test results are shown in Appendix Figures F-1 through F-8.

KYNAR showed the least degradation, both in optical and mechanical properties. The material is known to be inherently resistant to UV. Degradation rates of polyesters were similar, making ranking difficult. Polypropylene embrittled to the point where it could not be handled after 360 hours.

Examination of the above data would lead to the following ranking:

1) Kynar
2) Polyesters
3) Polycarbonate
4) Polypropylene

Predictions of film life is being accomplished in actual desert exposure by simultaneously exposing samples in environments of one sun and multiple sun levels. Dome material coupons were transmitted to the Desert Sunshine Exposure Test Facility (DSET) in March where they are being exposed to one and eight sun environments. Comparisons of damage rate data will be made, and the acceleration factor estimated. The accelerated data curves can be adjusted by this factor and material property versus real time predictions made.

The only material for which applicable real time exposure data was found is an oriented polyester film which was UV stabilized by the Martin processing. This material was removed from a greenhouse in Illinois after a 15 year exposure (calculated to equal 10.5 years in Arizona).

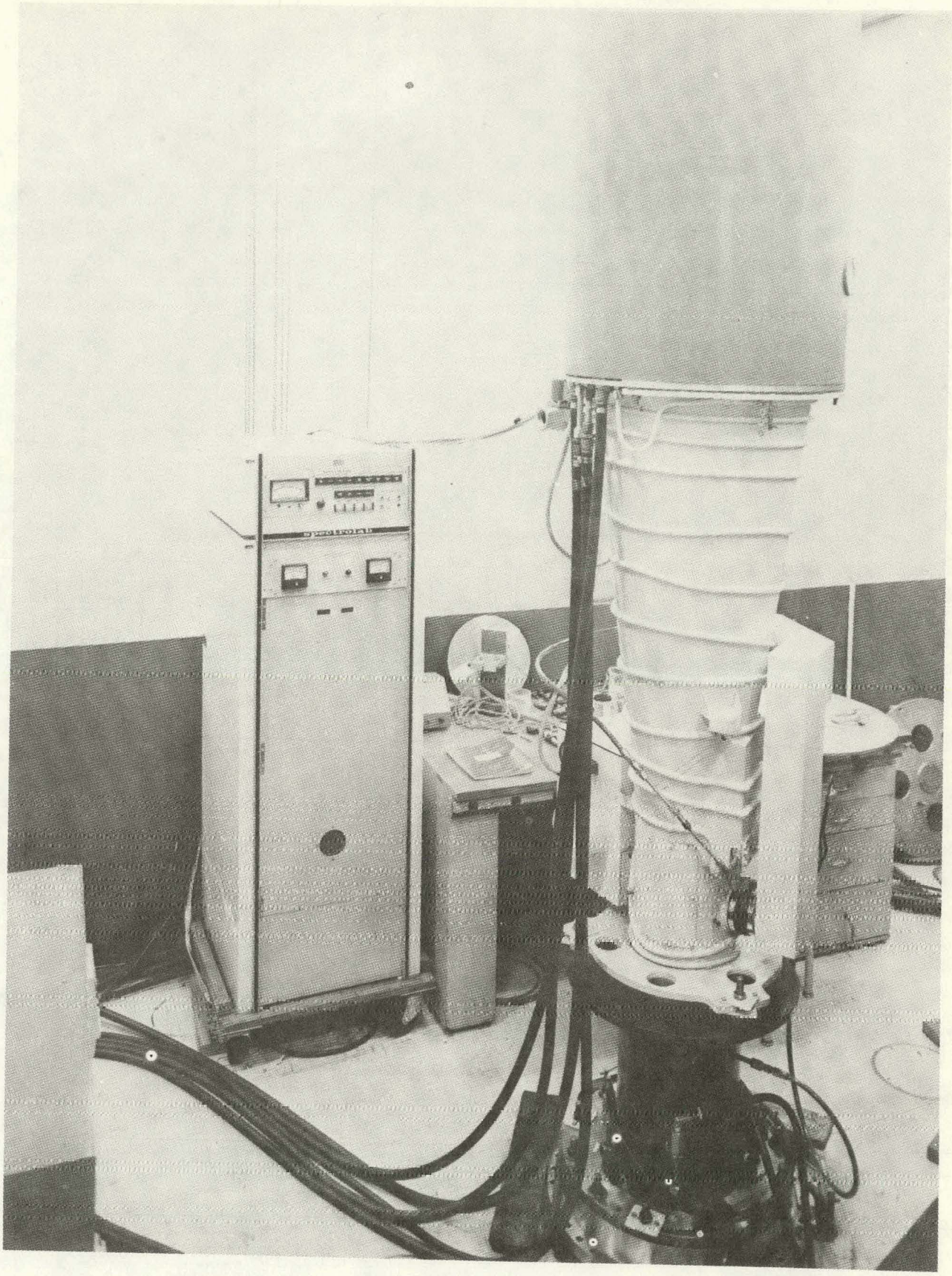

Figure 2.3.2.2-1 *Solar Simulator Lamp House & Power Supply*

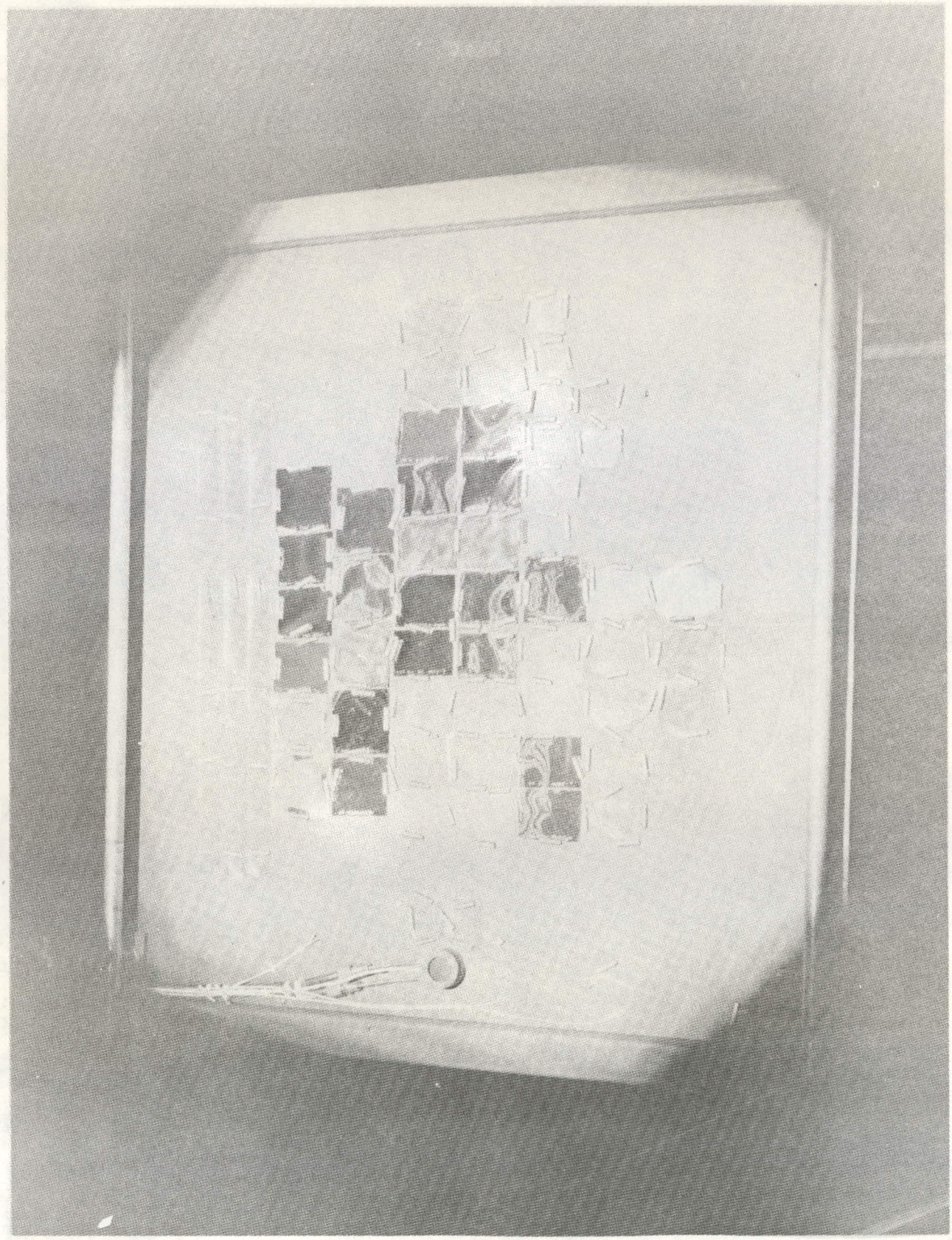

Figure 2.3.2.2-2 Target Plane with Material Coupons

The surface of the sample was scratched from tree branches and leaves, washing, and handling, precluding valid specular transmittance measurements. The ultimate strength and percent elongation of the 15 year old material were reduced only 35 percent and 12 percent respectively, which is safely within design allowables. The material obviously has not reached the end of its life in the mechanical sense.

Examination of the accelerated ultraviolet test data (Figures F-1 through F-8) revealed a much greater rate of mechanical property degradation for the polyester than observed on the Illinois greenhouse. Accordingly, the spectral content of the solar simulator and the spectral sensitivity of polyesters was evaluated in an attempt to explain the discrepancy in test results. Table 2.3.2.2-5 shows the most damaging wavelengths for several materials.

Table 2.3.2.2-5

SPECTRAL SENSITIVITIES OF SELECTED MATERIALS

POLYMER	WAVELENGTH OF GREATEST SENSITIVITY (Nanometers)
Polycarbonate	295
Polyethylene	300
Polypropylene	310
Polyvinyl Chloride	310
Thermoplastic polyester	290-320
Unsaturated polyester	325

Figure 2.3.2.2-3 compares the detailed spectral content of the solar simulator with that of the AM-2 sun in the ultraviolet wavelength region. While the simulator did provide an integrated 10 AM-2 UV sun level, it can be seen that at specific bands, higher or lower levels were present.

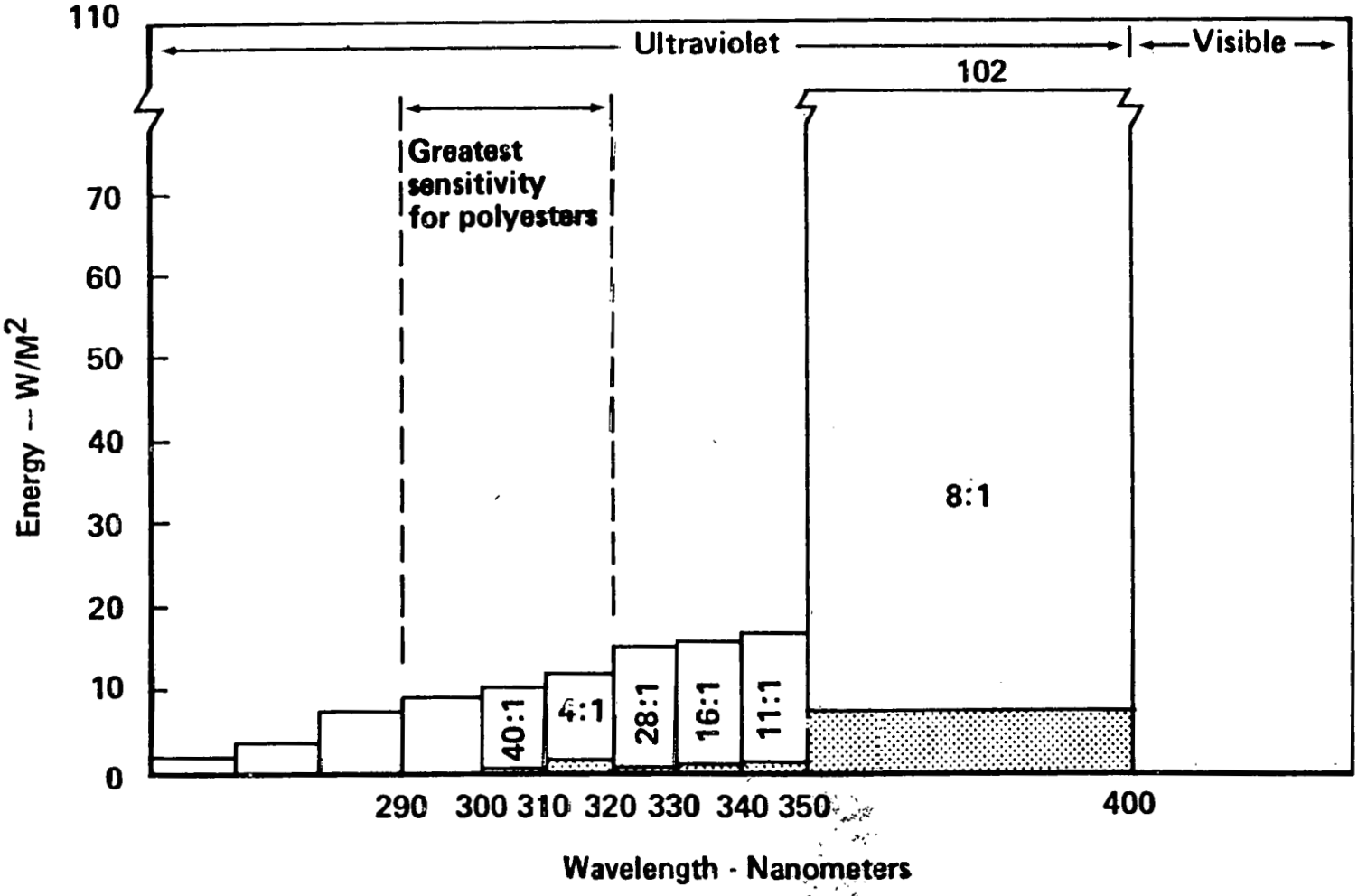

Figure 2.3.2-3. Solar Simulator/AM2 Energy Distribution (Solar Simulator at 10 UV Suns 250 to 400 nm)

With the exception of the 310-320 nm band, all wavelength UV below 350 nm were greater than 10 suns. In the 300-310 nm band, which includes the wavelengths of greatest sensitivity for polypropylene and thermoplastic polyesters, the level was 40 suns. Polycarbonate is most sensitive to 295 nm UV, which for practical purposes does not exist in the AM-2 solar spectrum, but was present to some extent in the test. The principle message from the above is that the acceleration rates will vary for different types of polymers. Furthermore, the acceleration rate for polyester was considerably higher than 10 suns.

Cost Analysis

Table 2.3.2.2-6 shows approximate projected costs for Tedlar, Kynar and polyesters, using preliminary cost per unit area data derived from discussion with suppliers. The last column gives cost per unit area per unit transmittance (squared).

Table 2.3.2.2-6

ENCLOSURE MATERIALS RELATIVE COSTS

MATERIAL	ANTICIPATED COST $/m^2	SPECULAR TRANSMITTANCE	COST $/m^2 τ^2
Tedlar (8 mil)	11.76	.875	15.46
Kynar (4 mil)	2.07	.905	2.52
Polyester (3 mil)	0.54	.875	0.703

In conclusion, both Kynar and weatherized polyesters exhibit the ability to function satisfactorily as enclosure material. Kynar was shown to be UV stable in the accelerated testing and is known to be inherently stable. The 15 year greenhouse experience verified the ability of film processors to long-term weatherize polyesters that would otherwise be subject to embrittlement. Since polyester films have the lowest cost and stabilization appears feasible, a weatherized polyester is recommended for commercial plant protective enclosures.

2.3.2.3 Structural Analysis

The enclosure consists of a transparent spherical dome segment attached to a steel support ring which is supported by three steel stanchions. As shown in Figure 2.3-1, the enclosure sphere is truncated at a 45^{o} angle. A steel dish, welded to the steel support ring, forms the lower segment of the pressurized sphere.

Details of the structural analysis which support the design are described in the following sub-sections.

Design Loads - The principle loads acting on the enclosure are those caused by the environment (wind, snow, ice, and earthquake), and the internal static air pressure used to support the membrane enclosure.

Wind Loads - Undisturbed wind above smooth terrain is known to assume logarithmic velocity profile, according to atmospheric boundary layer theory. Design wind profiles are commonly specified by power laws which give results similar to a logarithmic description. These take the form:

$$V_z = V_{REF}\left(\frac{z}{H_{REF}}\right)^{\alpha}$$

where V_z = Wind velocity at height z above ground.

V_{REF} = Wind velocity at reference height H_{REF}

α = Exponent affecting shape of profile.

Specification 001 requires that:

1) heliostats be designed for wind according to a power law with H_{REF} equal to ten meters, and α equal to 0.15, and
2) heliostats shall survive without damage a maximum wind velocity, including gusts, of 40 meters per second (90 mph) at ten meters above the ground.

Reference 2.3.2.3-1 gives the following equations for lift and drag respectively.

$$L = K_L \; q \; R^2$$

$$D = K_D \; q \; R^2$$

where K_L = Lift coefficient

K_D = Drag coefficient

q = Wind dynamic pressure

R = Dome radius

A wind tunnel test program (Reference 2.3.2.3-2) was carried out to determine the pressure distribution on enclosures and the affect on pressure distribution of "sheltering" due to the density of the array plus a peripheral fence. Testing was performed in the University of Washington Aeronautical Laboratory (UWAL) low-speed wind tunnel. Tests ranged from single units to 60 enclosure models in square and diagonal arrays, at varying spacing densities. Test runs were made with and without the peripheral fence and at different fence locations.

The aerodynamic lift and drag coefficients obtained from these tests are shown in Figures 2.3.2.3-1 and 2.3.2.3-2. These have been used to calculate lift and drag forces on the heliostat. Compared with the loads obtained from the previous equations, and used for earlier design, the

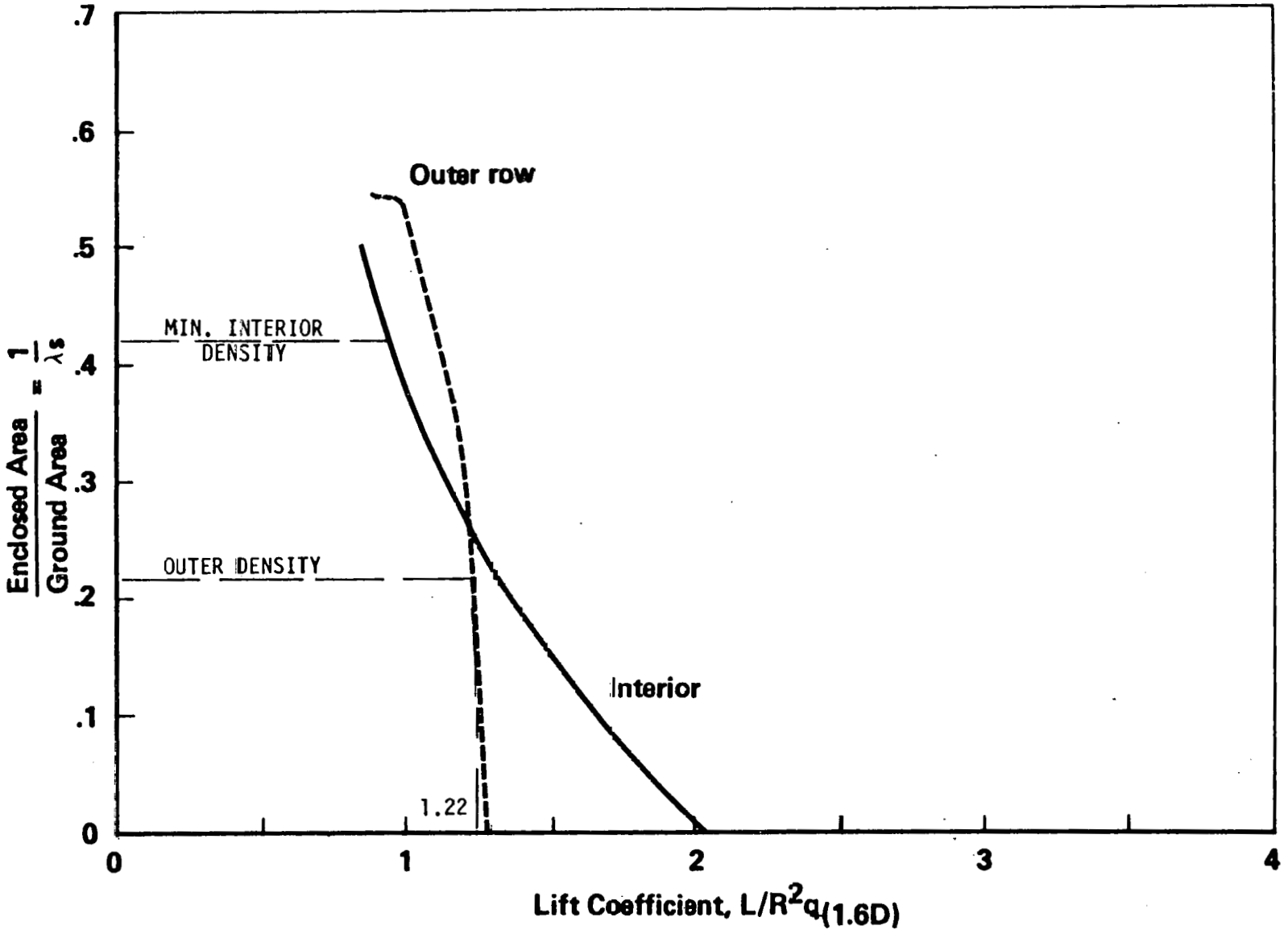

Figure 2.3.2.3-1. Wind Tunnel Test Data

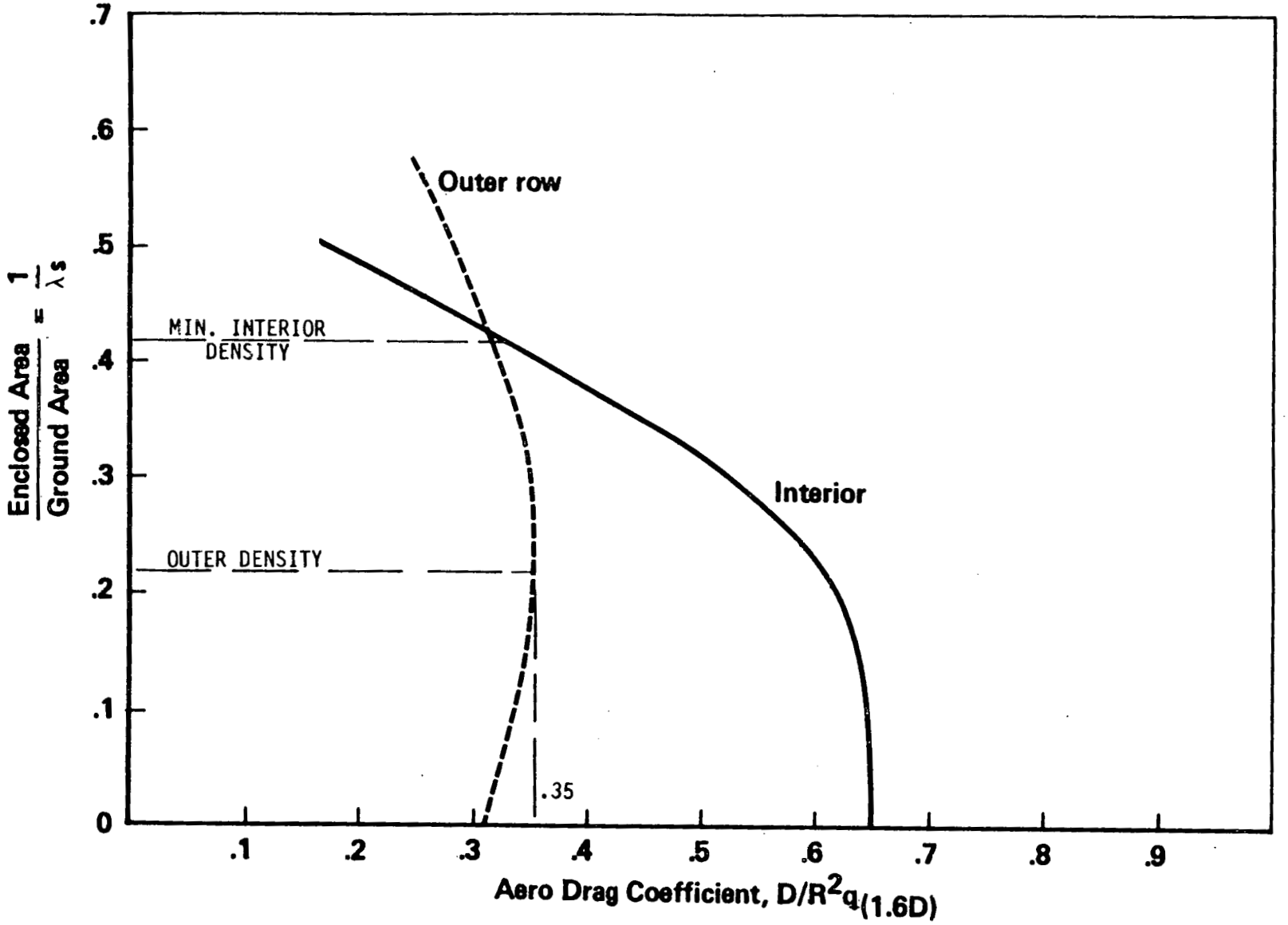

Figure 2.3.2.3-2. Wind Tunnel Test Data

loads obtained from wind tunnel test data show a reduction in drag force of 21 percent for a 9.69 m (31.8 ft.) diameter dome; but the lift force has not changed appreciably. Therefore, the loads obtained from wind tunnel test data have been used to determine the lowest cost design for the prototype heliostat. The lift and drag forces acting on the heliostat due to the peak survival wind of 40 meters per second (90 mph) are:

LIFT LOAD L = 32,399 Newtons (7,284 lb.)

DRAG LOAD D = 9,296 Newtons (2,090 lb.)

These maximum loads occur at the minimum array density of 0.22.

Enclosure Analysis

Transparent enclosure size is controlled by wind velocity and the allowable stress of the membrane material. The design nomograph obtained from the heliostat wind tunnel test program, (Figure 2.3.2.3-3), permits determination of the allowable enclosure size based on array density, enclosure configuration, and enclosure material allowable strength.

Mechanical properties for weatherized oriented polyester supplied by the manufacturer gives a typical average value yield strength of 100 MN/m^2 (14,500 psi) with a reduction to 75.8 MN/m^2 (11,000 psi) at maximum design temperature (132^oF). Limited room temperature testing at Boeing has verified this data. Figure 2.3.2.3-4 shows a typical stress strain curve comparing Boeing test data with the manufacturer's test data. From Figure 2.3.2.3-3, at an array density of 0.22 and with an allowable membrane stress of 75.8 MN/m^2 (11,000 psi), the 9.69 m (31.8 ft.) diameter enclosure requires a membrane thickness of 0.003 inches.

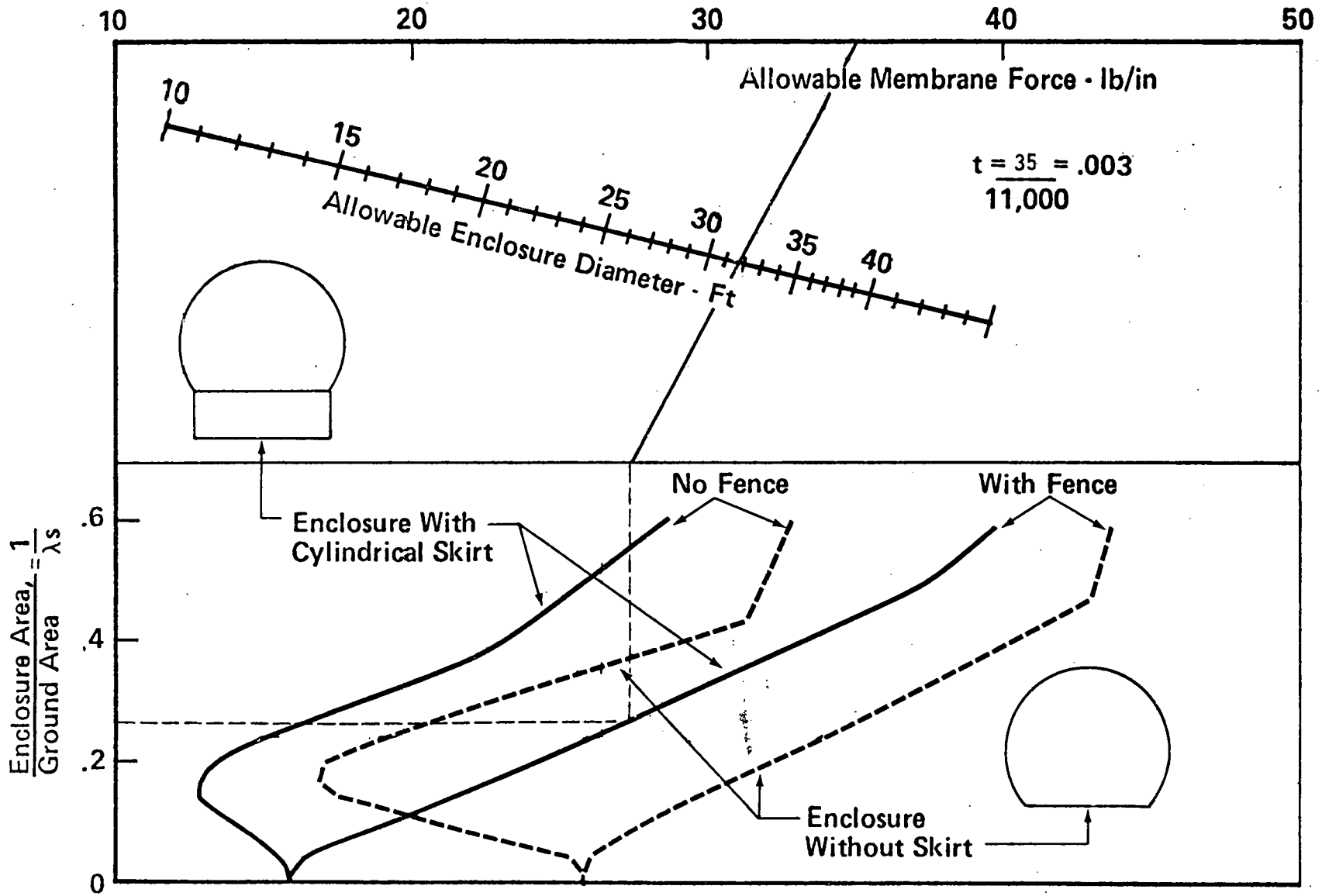

Figure 2.3.2.3-3. Allowable Enclosure Diameter from Wind Tunnel Test Results

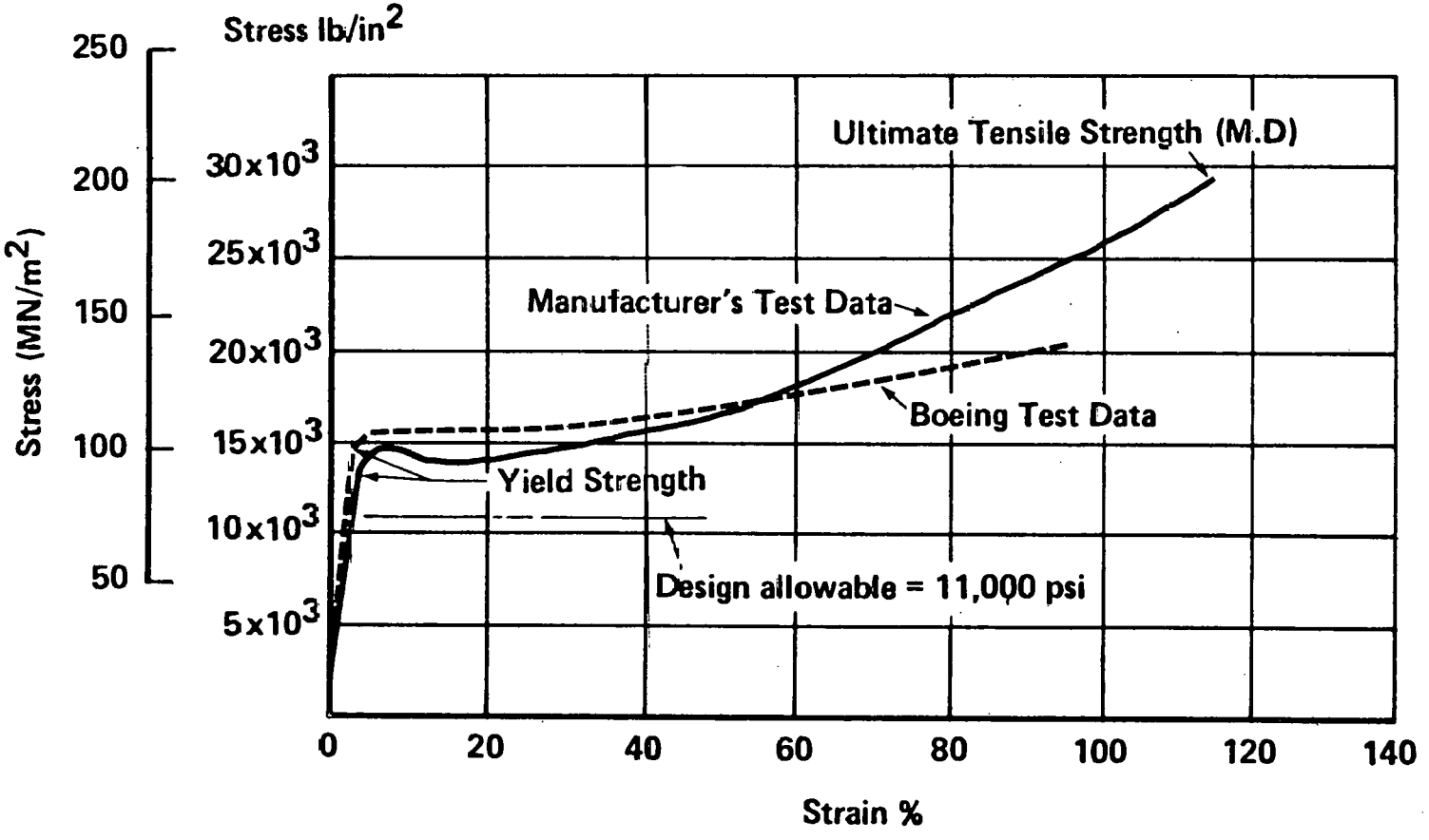

Figure 2.3.2.3-4. Stress-Strain Curves for Weatherized Oriented Polyester

Analysis of enclosure deflection was correlated to actual measured test deflection of the research heliostats at Boardman, Oregon. The data was then scaled linearly with dome diameter and as the square of the wind velocity. The analysis, as given by Reference 2.3.2.3-2, shows very little difference in deflected shape between truncated base angles of 50^{o} and 45^{o}. Accordingly, the base angle for the selected configuration has been reduced to 45^{o} which considerably reduces the size and cost of the base ring and dish structure. The deflected shape, with a maximum deflection of 5.31 cm (2.09 in.) is shown in Figure 2.3.2.3-5.

Internal Pressure Loads - The internal air pressure maintains the spherical integrity of the enclosure shape under maximum wind conditions. A pressure of 0.689 KN/m^2 (0.1 psi) exceeds the maximum 90 mph wind stagnation pressure.

Snow and Ice Loads - Specification 001 requires survival under a snow load of 250 Pascals (5 lb/sq ft.) and survival under a deposited ice layer 5.1 cm (2 in.) thick. It is assumed that snow and ice are deposited in a cosine distribution on the upper hemisphere. Pressure on the dome due to this coating of snow or ice is only 35 percent of the internal pressure.

Earthquake Loads - An earthquake analysis of the enclosure using the uniform building code approach (Reference 2.3.2.3-3) has been made. Using the most conservative values for all coefficients gives an equivalent lateral force of 0.53 g's for Zone 4 Earthquake Design. Applying this acceleration to the mass of the enclosure, plus the mass of the enclosed air, results in a lateral force of 309 Kg (682 lb.) and a radial deflection 32 percent of that caused by the peak survival wind. Film stresses, due to earthquake loading, will be considerably less than that for the design maximum wind condition because the larger non-uniform aerodynamic pressure distribution will not be present.

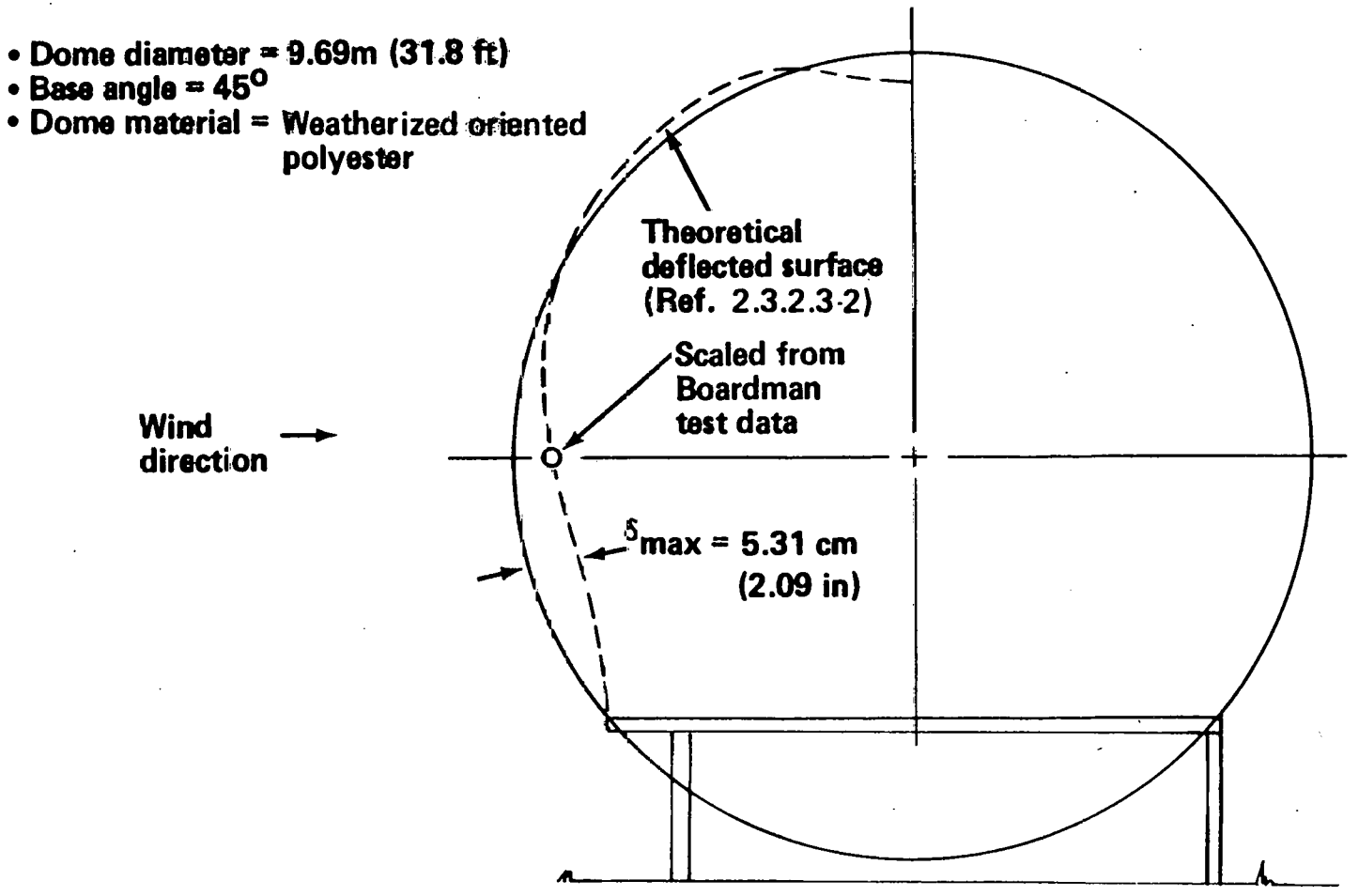

Figure 2.3.2.3-5. Dome Deflections at Peak Survival Wind Velocity

Hail Loading - Specification 001 requires survival without damage of 25 mm (1 in.) hailstones at a velocity of 23 m/s (75 fps). Reference 2.3.2.3-4 documents the Boeing hailstone test program. The test results are shown in Table 2.3.2.3-1. These results show no penetrations at specification conditions for any of the materials tested. The minimum velocity required to cause penetration was 140 percent of the terminal velocity (75 fps). The larger hailstones did cause small indentations in the enclosure materials. Analysis of the environment and the effect of indentation on Tedlar show (see Figure 2.3.2.3-6) an optical transmittance loss after 15 years of 0.1 percent to 1.6 percent for the average and maximum areal density of hailstorms, respectively. Similar effects are expected for other dome materials tested.

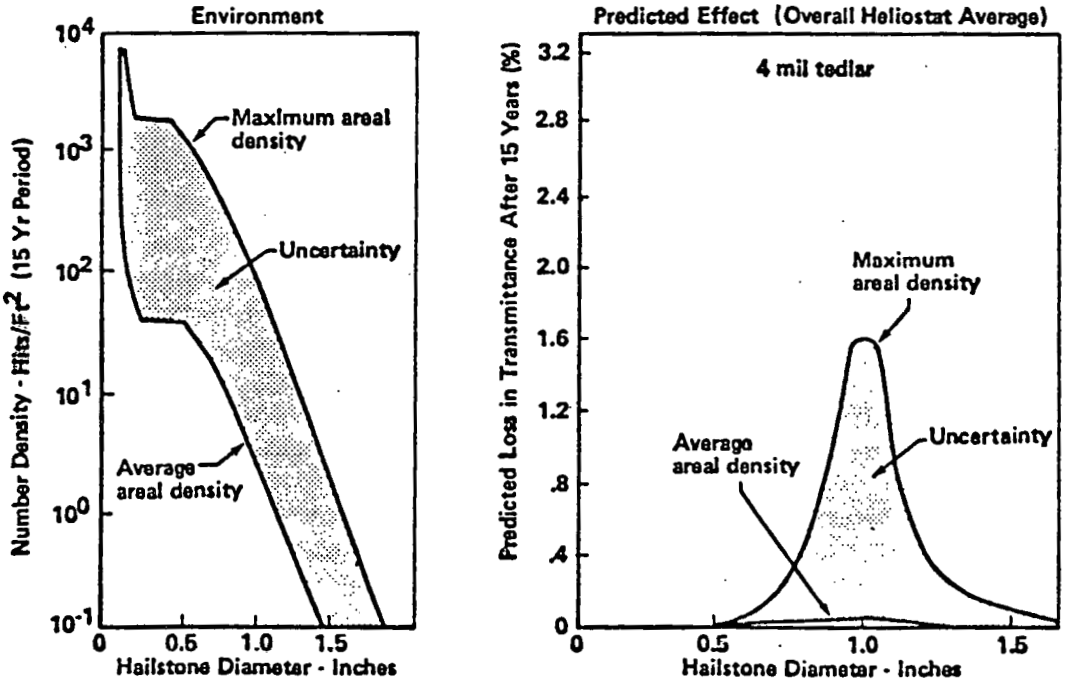

Figure 2.3.2.3-6. Effect of Hailstone Environment on Optical Performance

Table 2.3.2.3-1 Hailstone Test Results
(1 inch Diameter Hailstones)

MATERIAL	Film Thickness (Mils)	Hailstone Weight Avg. (Grams)	Angle From Normal Incidence	Velocity (FPS)	DAMAGE				
					Indentation Diam. (Inches)	Specular Transmittance (%)	Loss In Yield Strength (%)	Loss In Ultimate Strength (%)	Velocity at Failure (FPS)
TEDLAR (Polyvinyl Flouride)	4	7.9	0°	76.3	.40	56	0.7	0.9	122
• In Laboratory		8.8	45	74.8	[1]	--	---	---	---
		8.6	60	74.8	NONE	--	---	---	---
• On Heliostat In Field	4	8.0	0°	76.2	.39	--	---	---	106
		8.1	45	77.8	[1]	--	---	---	---
		7.9	60	77.8	NONE	--	---	---	---
MELINEX O (Polyester)	2	8.4	0°	74.8	.37	77	2.9	0	113
		7.3	45	74.8	NONE	--	---	---	---
		9.1	60	73.4	NONE	--	---	---	---
PETRA A (Polyester)	5	7.5	0°	74.8	.23	71	0	0	104
		9.0	45	74.8	NONE	--	---	---	---
		---	60	----	----	--	---	---	---
POLY CARBONATE	3.5	7.8	0°	73.4	.46	24	0	9.5	>117
		7.0	45	73.4	NONE	--	---	---	---
		---	60	----	----	--	---	---	---

[1] Fine Scratch Lines, ½ inch long

2.3.3 Base/Foundation

2.3.3.1 Configuration

The base/foundation (Figure 2.3.3.1-1) consists of the above and below ground structure required to support and environmentally protect the reflector, reflector drive system and the transparent protective enclosure. The air supply system is considered part of the base/foundation. The above ground structure consists of a steel hemispherical dish segment welded to a circular steel pipe support ring. Loads are transferred from the transparent protective enclosure across the steel dish and into the support ring. Three steel pipe stanchions provide a load path from the support ring to the subground structure. A steel pipe forms the pedestal mount for the reflector and gimbal. A diaphram seal provides air tight penetration of the pedestal through the bottom of the steel dish. The subground structure used to support the stanchions and pedestal consists of four auger-cast concrete piles.

The base/foundation design selected provides simplicity, minimum use of materials, and factory assembly of the entire heliostat adjacent to plant sites. The latter results in minimum use of field labor to install heliostats; thus minimizing overall costs. Approximately 900 Kg (3,000 lbs.) of steel and 0.84 m^3 (1.1 $yds.^3$) of concrete are used in the fabrication of the base/foundation. Details of the base/foundation are given in the following paragraphs.

Pile Design and Installation

All four concrete piles (Figure 2.3.3.1-2) have a 35.6 cm (14.0 in.) diameter. The three stanchion piles are embedded 2.4 m (8.0 ft.) below ground level. The monument (reflector support) pile is embedded to a depth of 1.8 m (6.0 ft.). The above dimensions assure that

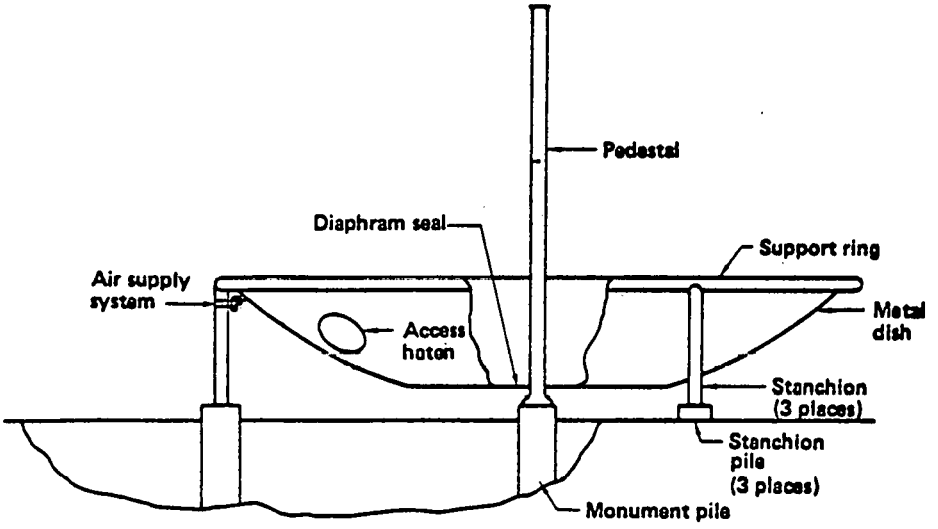

Figure 2.3.3.1-1. Base Foundation

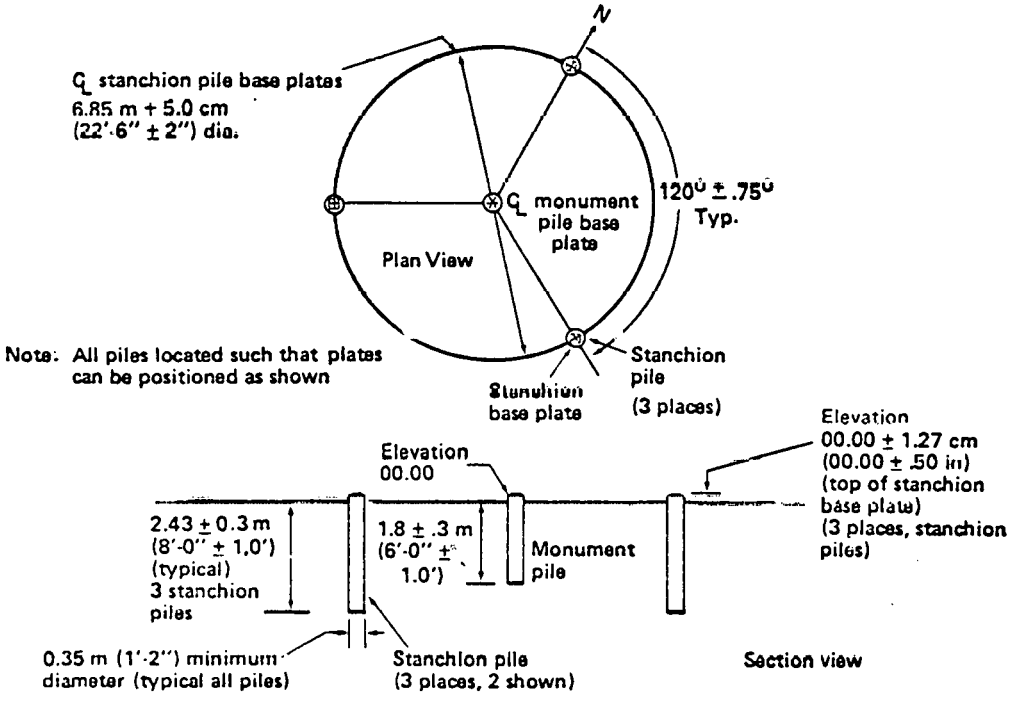

Figure 2.3.3.1-2. Pile Plot Plan

adequate soil adhesion is developed to resist the forces generated at the pile surfaces by the gravity forces and maximum wind loads. Each pile is capped with a steel plate, which provides the welding surface for the stanchion tie down. Loads are carried into the piling by four concrete anchors which are stud welded to the caps prior to placement. The concrete anchors overlap a single rebar located in the concrete pile. This approach minimizes fabrication costs and provides adequate strength. The same arrangement is also employed on the monument pile.

A conceptual design of automated equipment capable of installing 40 heliostat foundations/per day/per machine is described in Section 3.0. This equipment will maintain placement tolerances depicted in Figure 2.3.3.1-2, and does not require extensive site preparation.

Support Ring and Stanchions

The support ring and stanchions transmit enclosure loads to the stanchion piles (see Figure 2.3.3.1-3). The choice of pipe material and size was determined by a stress/deflection analysis versus cost. This optimization resulted in a standard 10.16 cm (4.0 in.) pipe for both the ring and stanchions.

Preformed Metal Dish

To capitalize on the inherent advantages of factory assembly-line rates and low costs, the dish is designed for press forming. Using present metal technology, it is estimated that a dish can be formed with a resultant average thickness of 0.066 cm (0.026 in.). This results in a dish weight of 226.5 Kg (500 lb.).

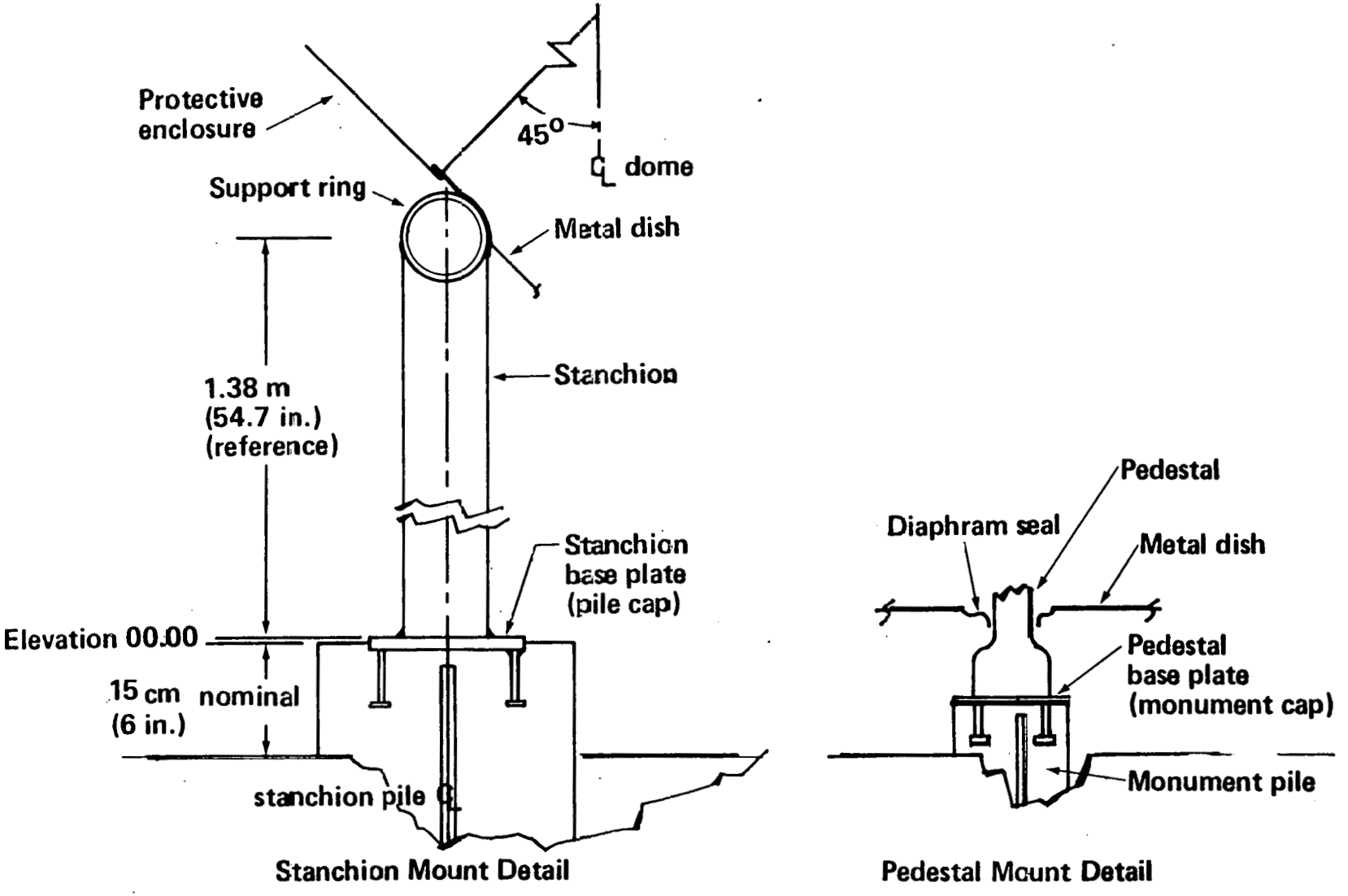

Figure 2.3.3.1-3. Base/Foundation Details

The access hatch located on the dish is elliptical in shape. This has the dual advantage of an inside pressure augmented sealing force, yet allows complete removal of the hatch by rotating and tipping. This removal aspect provides rapid maintenance of the electronics package which is mounted on the inside surface of the hatch.

Pedestal

The pipe pedestal provides a positive reference point for the gimbal drive assembly. Structural analysis (described in Section 2.3.4.3) resulted in selection of a 14.12 cm (5.56 in.) outside diameter of the steel pedestal which allows only a 0.048 cm (0.019 in.) deflection during maximum dynamic loading conditions.

Air Supply System

To limit deflection of the protective enclosure the air supply system maintains an enclosure pressure equal to or greater than the wind impact pressure generated by a 40 m/s (90 MPH) wind. The air used by the system is filtered to the extent necessary to assure 15 years of continuous duty without cleaning the reflector. The simplicity of the system results in a high reliability over its 30 year life. The individual components and their placement in the system package facilitate the 15 year scheduled maintenance period, which consists of changing the primary filter and replacement of the compressor vanes. A diagram and system layout of the air supply assembly are shown in Figures 2.3.3.2-4 and -5. Four components make up the system; a prefilter, a rotary vane compressor, a primary filter and a pressure relief valve. These components are located external to the heliostat in a sheet metal cannister. The maximum power consumption of the air supply system is 10 watts.

A positive internal pressure 6.9 KN/m^2 (0.1 psig) above external ambient pressure is required to maintain clearance between the inflated enclosure and the reflector structure during specified 40 m/s (90 MPH) wind velocity. This differential pressure was calculated by integrating the wind impact pressure distribution over the frontal area of the protective enclosure.

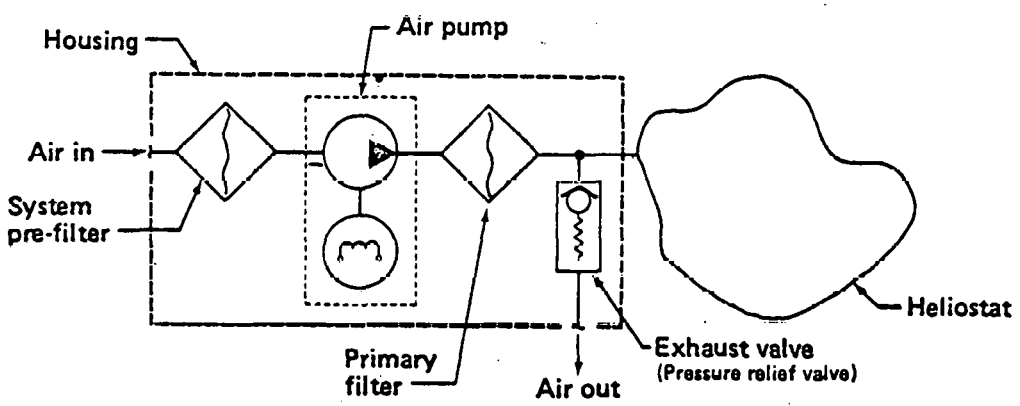

Figure 2.3.3.2-4. Air Supply System Layout

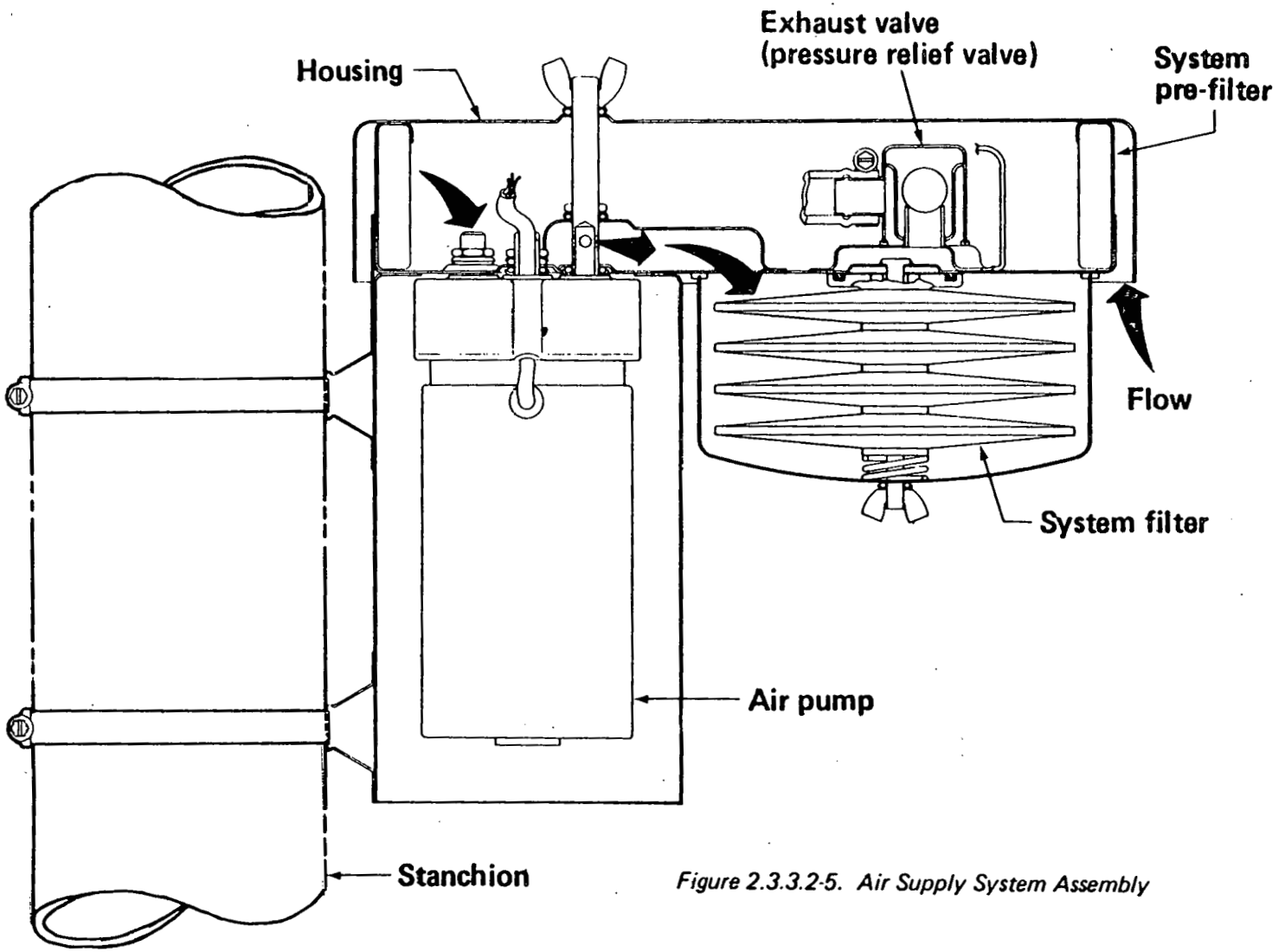

Figure 2.3.3.2-5. Air Supply System Assembly

Ambient temperature and pressure variations result in the requirement for variable air flow into and out of the enclosure. This variable flow rate plus steady state leakage are additive. The air supply system must be sized for the maximum demand, coinciding with the worst-case climatic conditions, to compensate for this flow rate variation. Analysis of climatic data for New Mexico indicates that to maintain constant pressure, flow rate will vary between +0.04 m^3/min (+1.48 cfm) to -0.05 m^3/min (- 1.73 cfm), the minus sign indicating flow out of the enclosure.

Enclosure leak rate is considered a negative flow and is determined by summing the individual points of leakage. As shown in Table 2.3.3.1-1 a total leak rate of 0.006 m^3/min (0.2 cfm) has been estimated for the commercial plant design.

TABLE 2.3.3.1-1 ENCLOSURE LEAK RATE BUDGET

POTENTIAL LEAKAGE SOURCE	DESIGN LEAKAGE LIMIT m^3/min @ 6.9 KN/m^2
Interface Seal	0.004
Pedestal/Dish Seal	0.0006
Access Hatch Seal	0.0012
Other Penetrations	0.0
DESIGN TOTAL	(-0.006m^3/min @ 6.9KN/m^2) (-0.20 cfm @ 0.10 psig)

Combining the above rates indicates that the air pump must supply a peak air flow of 0.05 m^3/min (1.68 cfm) at 6.9 KN/m^2 (0.1 psig) and that the enclosure must vent a total of 0.043 (1.53 cfm) at 6.9 KN/m^2 (0.1 psig). To provide this peak air flow, a rotary-vane constant displacement pump was selected. This configuration was chosen because of its nearly

constant output flow versus increasing impedance from the filters (see Figure 2.3.3.2-4) it is designed to run at approximately 800 RPM and is sized to supply 0.06 m^3/min (2.0 cfm) at 14 KN/m^2 (2.0 psig). To meet the 30 year life criteria the .03 hp, 120 volt ac pump motor uses a permanently lubricated and sealed porous bronze bearing sized to provide 30 years of lubricant. This motor arrangement is similar to motors presently used in commercial appliances. The compressor consists of a ported dye cast aluminum housing with a hard anodized bore. Four spring-loaded fiber reinforced teflon vanes, a rotor shaft and a teflon coated bushing make up the rotating unit.

In operation ambient air is drawn through the system prefilter, compressed, forced through a primary filter, and expelled through into the enclosure. As shown in Figures 2.3.3.2-4 and -5, a pressure relief valve has been incorporated in the manifold to vent excess compressor air and air from the enclosure which occasionally must be released due to ambient temperature or pressure changes. The pressure relief valve incorporates a sharp-edged seat and ball poppet. Relief pressure is determined by the weight of the ball versus the net unseating force generated by the internal heliostat pressure. This scheme eliminates springs which are difficult to tune and prone to failure. To prevent compressor-generated contaminates from entering the enclosure, the primary filter is located between the compressor and enclosure. This imposes a constant-flow variable-pressure requirement on the compressor caused by long-term filter loading. The pressure drop across the primary filter is not expected to exceed 14 KN/m^2 (2.0 psig) during the fifteen year filter life. The pre-filter is placed on the suction side of the air pump. This arrangement protects the pump from potential wear problems associated with ingestion of airborne particulates. The primary filter consists of four separate filter disks which provide parallel air flow. Each filter disk has 294 cm^2 (47 $in.^2$) of filter area, for a total of 1175 cm^2 (188 $in.^2$) of filter area. Each filter disk uses an injection molded plastic perforated disk to support a layered filter cover. Incoming air first passes through a Gelman

Type-E glass-fiber depth-filter, then through a Gelman Acropor membrane filter with a pore size of 0.45 um. A layer of glass scrim separates the two filter medias. The first filter layer will entrain 99.7% of the total mass of airborne particulate. 99.99% of the remaining mass will be filtered out by the membrane layer.

A porous polyurethane foam provides the filter media for the pre-filter. The filter is constructed from 1.3 cm (0.5 in.) thick foam which is held rigid by the housing. The total frontal area of the filter is 94 cm^2 (47 $in.^2$). The holding capacity of the filter is equivalent to 5 or more years of service in the southwestern United States.

Selection of filters was based on a design goal to eliminate the need for reflector cleaning over a 15 year period. For design purposes, it was assumed that the degradation in specular reflectance due to dust accumulation must be less than 5 percent in 15 years. Both air flow rate and cleanliness are involved in selection of filters. These factors where taken into account by the light scattering versus dust accumulation model described in the Appendix C. This model used airborne particulate data for both the Grand Canyon area and Phoenix Arizona. The results of the model indicated that a two-stage filtration system, passing 0.014 m^3/min (0.5 cfm) of air, would provide 15 years of operation with a total decrease in reflector efficiency of less than 5%. A coarse pre-filter was selected to trap larger particles, and a depth-type glass fiber filter backed with a membrane filter traps residual fine particles. Since the predicted average air flow rate into the enclosure is approximately half the value used in the foregoing contaminant analysis model (Appendix C), a 2 to 3 percent loss in reflectance (vs 5 percent) is expected over a 15 year life.

The various components of the air-supply package are mounted external to the heliostat in a formed sheet metal cannister. The cannister is designed to prevent water from entering the system. Pressurized air is

transferred from the cannister to the heliostat through a 1.3 cm (0.5 in.) diameter air hose which connects the cannister supply port to a penetration fitting on the base shell. Air flow within the cannister is directed by integral sheet metal manifolding. The bonnet of the cannister is retained by a single wing nut. When the bonnet is removed the electrical plug between the compressor motor and electrical supply is exposed, along with the pressure relief valve and pre-filter. The cannister body is mounted to the North foundation stanchion by a metal bracket and two straps.

The air supply and its components are designed for thirty years of continuous duty with the exceptions of a 5-year cleaning or replacement cycle for the pre-filter, and a 15-year replacement of the compressor vanes and primary filter. To facilitate this scheduled maintenance the components are mounted individually in the housing cannister. Removal of the compressor involves taking off the bonnet, unplugging the electrical supply, and removing 3 nuts. With the bonnet off, the pre-filter can be lifted out and replaced without shutting down the system. The primary filter is changed by removing a wing nut and dropping the primary filter can down.

Protective Enclosure Retention

The interface between the protective enclosure and the base/foundation is discussed in Section 2.3.2 "Protective Enclosure."

Finishes

The above ground base structure will be primed and painted with synthetic white enamel. This includes the interior of the dish. Painted components will be baked to prevent long-term contamination of the reflector surface by outgassing.

Installation Welds

Anchoring of the heliostat assembly is accomplished by field welding the three stanchions and pedestal to pile caps. The welding procedure and welder qualification will conform with those established by the "American Welding Society" for structural welds.

2.3.3.2 Structural Analysis

The lift and drag forces on the dome due to the maximum survival wind conditions are reacted at ground level by horizontal and vertical loads plus an over-turning moment as shown in Figure 2.3.3.2-1. The overturning moment results in an up load on the windward side of the dome and a down load on the opposite side. These loads are reacted with adequate margin of safety by three concrete piles 35.56 cm diameter (14 in.) which are buried 2.44 meters (8 ft.) in the ground. The loads are transferred from the pile by side friction between pile and soil and by bearing pressure at ground level. Soil bearing pressure due to foundation weight is only 21.5 KN/m^2 (450 psi) and no soil stabilization is required.

The lift and drag forces on the dome are transferred to ground level by a circular support ring mounted on three vertical stanchions. The support ring is made from steel pipe and is designed by limiting bending between vertical supports. Figure 2.3.3.2-2 shows the stress levels and deflections for pipe sections between 8.89 cm O.D. (3.5 in.) and 13.97 cm O.D. (5.5 in.) due to 90 mph wind loads. Support ring deflection was limited to 13.2 cm (5.2 in.) in order to ensure adequate clearance between the dome and the reflector, with the reflector in the most adverse position. Four inch A.P.I. 5LX x 52 steel pipe (4.5 in. O.D.) was selected for the support ring material, to limit the ring deflection under load and also to achieve the lowest cost design for the heliostat support structure. Figure 2.3.3.2-2 shows that with this pipe section, the stress levels are below the yield stress of the material and that adequate clearance is ensured at maximum survival wind condition.

The support ring is welded to the top of the stanchions which are also made from the same 4" diameter pipe material. The bottom of each stanchion is welded to a 1.27 cm (1/2" thick) A.537 steel base plate mounted on top of the concrete pile (see Figure 2.3.3.2-1). The base plate is welded to four 1.59 cm diameter (5/8 in.) A615 steel rebars embedded in the concrete pile.

The stanchions transfer horizontal shear, and vertical loads, from the support ring to ground level. The loads cause bending, direct tension, and shear stresses in the stanchion. Stress level in the 4 in. pipe section is 91.63 MN/m^2 (13,290 psi), well below the 358.5 MN/m^2 (52,000 psi) yield strength of the material.

The stress level at the weld between stanchion and base plate is 154.4 MN/m^2 (22,391 psi) due to the maximum survival wind condition. This is safely within the allowable value of 165.5 MN/m^2 (24,000 psi) for fillet welds proposed in Table 1.5.3 of the Manual of Steel Construction.

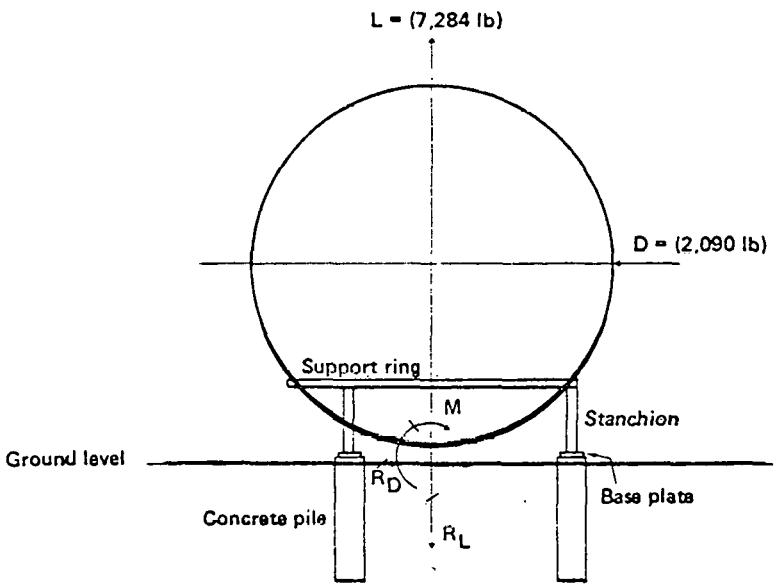

Figure 2.3.3.2-1. Heliostat Base Support Loads

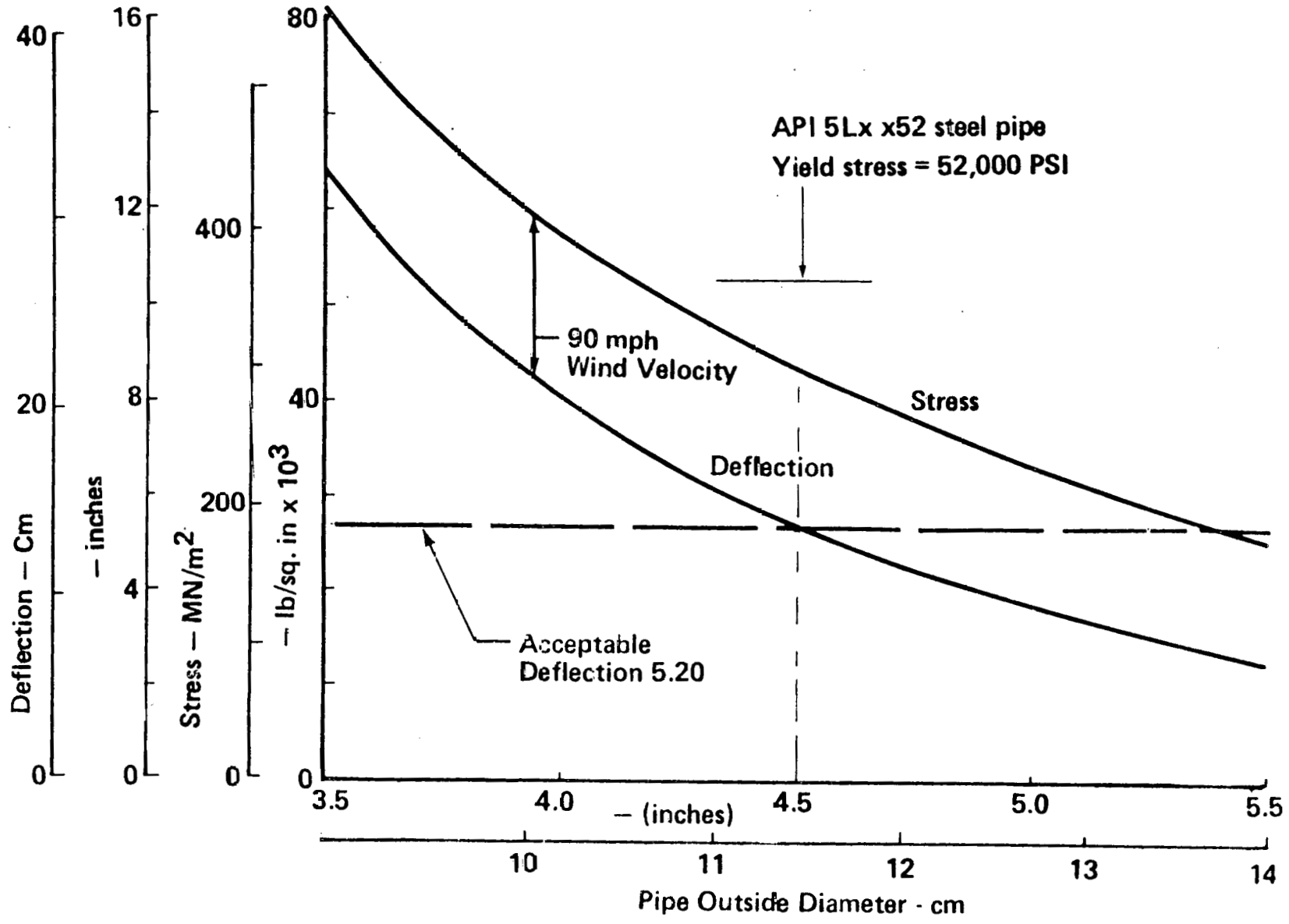

Figure 2.3.3.2-2. Stress and Deflection for Heliostat Support Ring Mounted on 3 Piles

2.3.4 Reflector Assembly

2.3.4.1 Configuration

The reflector assembly consists of a bi-axially stretched reflective aluminized polyester membrane bonded to a light-weight circular aluminum frame (Figure 2.3.4.1-1). The overall diameter of the reflector assembly is 9.3 m (30.5 ft.). This size was selected on the basis of the cost/performance optimization as discussed in Section 2.3.1.3. The reflector is gravity focused by pre-tensioning the reflective membrane during assembly. This procedure results in a controlled sag due to gravity. The controlled sag produces a parabolic reflector with a predictable focal length. A 8.0 MN/m^2 (1,150 psi) pre-tension stress level was selected to produce a correct focal length for far field heliostat A. This focal length (pre-tension) provides best field performance when used for all heliostats in the array.

Reflector Frame

The reflector frame consists of three circular rim segments, three T-fittings, three spokes, and a center hub. The circular rim segments are produced by ram forming thin-walled, 12.7 cm (5.0 in.) diameter aluminum-alloy tubing. The spokes also use the same type of tubing. The T-fittings and center hub are aluminum alloy castings. The T-fittings couple the rim segments to the spokes. Spokes are located below the rim to provide reflector membrane clearance. The center hub is designed to attach to the spokes and also accommodate the gimbal such that the elevation axis closely coincides with the reflector frame center-of-gravity; thereby, eliminating a counter-weight. Joints in the reflector frame are made by electromagnetic swaging. This method of joining has been utilized in a previous reflector assembly and represents a substantial savings in cost versus welded or conventional mechanical type joints.

Reflective Membrane

The reflective membrane is made by thermo/adhesive joining wide panels of 0.005 cm (0.002 in.) thick aluminized polyester film. Laboratory measurements have established a solar specular reflectance value of R = 0.91 and a joint ultimate stress of 105 MN/m^2 (15,190 psi).

Dispersion Errors

The frame is designed for stiffness to minimize overall dispersion characteristics of the reflector surface. Analysis of the design indicates that the maximum dispersion angle is 0.0006 radians due to out of plane static sag of the frame. Maximum frame sag occurs when the reflector is in the horizontal position. The sag diminishes as the reflector is rotated out of the horizontal plane, thereby reducing the dispersion angle.

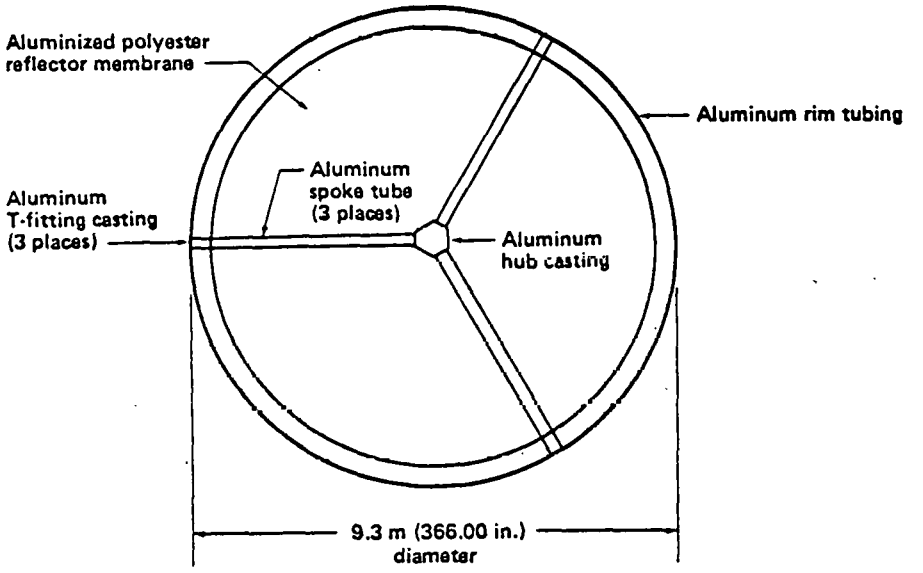

Figure 2.3.4.1-1. Reflector Assembly

2.3.4.2 Reflector Material Selection

A weatherized polyester substrate (weatherized Mylar D or Melinex "O") with an unprotected aluminum coating has been specified for the commercial plant reflector design. A weatherized substrate is specified because it is expected that some UV will pass through the enclosure material. Unprotected aluminum was specified based on earlier studies which showed that unprotected aluminized films do not degrade optically over long term (9 years) in a protected laboratory environment. Development of a protective coating for aluminum was, however, initiated in this effort to assure availability if required.

Screening testing was performed on various types of metalized polyester films with and without protective coatings and weatherized substrates. Candidate films prepared cooperatively by industry suppliers were first screened for specular reflectivity and, if promising, were exposed to accelerated simulated sunlight testing. Those candidates showing most promise were then tested for mechanical properties and submitted to Desert Sunshine Exposure Test Facilities for real-time and accelerated outdoor desert exposure testing. As discussed in Section 2.3.2.2, the start of reflector material screening testing was delayed due to late delivery of candidate materials.

Table 2.3.4.2-1 lists the materials and respective suppliers for candidates received for test. To the right, in the appropriate columns, are shown the specular reflectances taken on the Boeing bi-directional reflectometer at 0.15^{0} cone angle with a 633 nanometer wavelength source. As can be seen, a variety of film processors are represented. The reflectance is, of course, generally higher as the cone angle is increased from 0.15^{0} upward. (Figures F-9 through F-12 in Appendix F are plots of specular reflectance as a function of cone angle for the various candidates.)

The protective coated material supplied by National Metalizing was improved in two iterations from a reflectivity of .71 to .89 (at 633 nm wavelength). This compares with reflectivity of .91 for an unprotected aluminized surface at the same wavelength.

TABLE 2.3.4.2-1

SPECULAR REFLECTANCE FOR VARIOUS SUBSTRATE/COATING COMBINATIONS

	SPECULAR REFLECTANCE @ .15° Cone Angle	
	No Overcoat	Overcoated
MYLAR (Unknown Designation) - ALUMINIZED (National Metalizing)		.89
MYLAR D - ALUMINIZED (National Metalizing)	.91	
MYLAR D - ALUMINIZED (Dunmore)	.89	
MELINEX 442 - ALUMINIZED (Dunmore)	.86	.79
MELINEX "O" - (UV Stabilized) - ALUMINIZED (Martin Processing)	.81	
MELINEX "O" - ALUMINIZED (Morton Chemical)	.88	.69
POLYESTER (Unknown; U/V Stabilized) - METALIZED (OCLI)		
SILVERIZED	.91	.90
ALUMINIZED		.68

NOTE: All data shown are single wave length data (633 NM) that have been corrected upward 3% for integrated air mass 2 reflectance.

Dunmore provided Mylar D in earlier research and it was seen to have a 633 nm reflectance of 0.89 for the present effort, they provided candidates of overcoated and uncoated aluminized Melinex 442. As seen in the table, the reduction in specular reflectance due to the overcoating was 0.07, an unacceptable loss. Melinex "O" provided by Martin Processing exhibited a large amount of scattering at small cone angles (see Figure F-11). This is possible due to the stabilization process and its effect on the surface quality of the substrate. Late in the program, Morton Chemical provided aluminized polyester with and without overcoating for evaluation. Test results were a 633 nm reflectance of 0.88 without overcoating, and 0.69 with overcoating. Further iterations may improve the low value obtained for overcoated material. Aluminized polyester with overcoating, and silvered polyester with and without overcoatings were provided by Optical Coating Laboratory. The overcoated aluminized material had low reflectivity at all cone angles and was not a viable candidate as received. The overcoated silvered material had comparable reflectance to the best aluminized specimens evaluated thus far.

As noted at the bottom of Table 2.3.4.2-1, values in the table have been upward adjusted by about 3 percent to convert to integrated solar specular reflectance (AM-2).

Accelerated simulated sunlight exposure tests were performed on selected specimens. The purpose of this testing was to evaluate resistance of protective coatings to UV. As discussed in Section 2.3.2.2, the testing was quite severe because of the spectral mismatch between the simulator and real sunlight in wavelengths of high sensitivity for polyesters. No attempt was made to relate exposure time under the simulator with equivalent real time under sunlight. The samples submitted for test did not generally have acceptable reflectivities, but were exposed primarily to evaluate the coatings.

Mechanical and optical property versus time plots for the materials provided early enough in the program to be exposure tested under the solar simulator are shown in Appendix Figures F-13 through F-19. Generally, the reflectances remained constant, while the mechanical properties dropped with exposure. The tests revealed no optical degradation of the metalized surface, but did substantiate the need for substrate protection from the ultraviolet.

Based upon the initial and accelerated U/V data, samples of National Metalizing and OCLI overcoated materials were selected for real time and accelerated exposure testing in the desert. Although the Dunmore material reflectivity was lower than desired, its survival to the accelerated U/V test exposure was good. All samples have been enclosed in weatherable polyester "bags" to simulate the protection they would receive in a heliostat protective enclosure. The bag material used was Martin Processing weatherable polyester (Melinex "O").

2.3.4.3 Reflector Structural Analysis

The reflector support structure consists of a circular ring 9.29 m (30.5 ft.) in diameter, and three radial support arms all made from aluminum tube 12.7 cm (5.0 in.) diameter with 0.198 cm (.078 in.) wall thickness. The radial arms are joined together at a central hub casting which is attached to the gimbal mounted on the vertical reflector pedestal. The hub casting accommodates the gimbal drive motors such as to eliminate the reflector imbalance about the gimbal elevation axis.

2.3.4.3.1 Design Loads

The reflector assembly is protected from the severe elements of the environment (wind, snow and ice) by the protective enclosure. Design loads are due to membrane tension, gravity, temperature, reflector motion, and earthquake. These loading conditions are discussed below.

Membrane Tension

The reflective membrane is tensioned by pre-stretching to a uniform biaxial tension of 8.0 MN/m^2 (1,150 psi) and bonding to the circular support ring. Polyester material of 0.05 mm (.002 in.) thickness is used for the reflective membrane. Prestress in the membrane is low compared to the material yield stress of 100 MN/m^2 (14,500 psi). Therefore, long term creep effects will not cause significant loss of membrane tension.

Variations in temperature and humidity will cause changes in membrane stress. Differential expansion of the polyester and aluminum support structure over an extreme temperature range of 60°C (140°F) to -30°C (-20°F) will result in a change of plus or minus 30 percent from the nominal membrane stress of 8.0 MN/m^2 (1,150 psi). The effect of humidity on membrane stress is less pronounced than that of temperature. It tends to reduce the effect of temperature because relative humidity generally decreases as temperature increases.

Gravity Loadings

A convenient way of expressing reflector membrane deflection in relation to performance is given by the reflector focal length corresponding to the parabolic deflection mode that the membrane assumes. Figure 2.3.4.3-1 shows focal lengths for a uniformly stretched circular membrane as a function of membrane stress and angle of tilt of the reflector plane from vertical. Focal length is independent of membrane thickness and diameter. Focal lengths as indicated in the figure were included in performance optimization studies which resulted in selection of the 8.0 MN/m^2(1,150 psi) membrane prestress. The axis of the deflected parabolic surface remains essentially normal to the plane of the reflector support ring, regardless of the angle of tilt. Therefore, gravity deflections will not significantly affect beam pointing accuracy.

The reflector structure was analysed using a Nastran Computer Program for loads due to gravity, temperature, and membrane tension. Figure 2.3.4.3-2 shows the "Math Model" for this analysis. Stress levels were found to be very low, thus the structure is designed by stiffness. With the reflector horizontal, the maximum out-of-plane deflection of the circular ring between support arms, due to the combined loading condition, is 0.14 cm (0.057 in.)(see Figure 2.3.4.3-3). This is the displacement of grid point 101 relative to grid point 105. This deflection causes a maximum angular deviation of a small portion of the reflector surface from the normal reflector plane of less than 0.012°, which will have negligible effect on performance. The vertical deflection at the ends of the support arms causes a rigid body downward translation of the ring of 3.4 cm (1.34 in.). Adequate clearance (0.85 cm) between the reflector plane and the central mounting hub is provided to accommodate, without interference, the vertical deflection of the ring plus sag of the membrane.

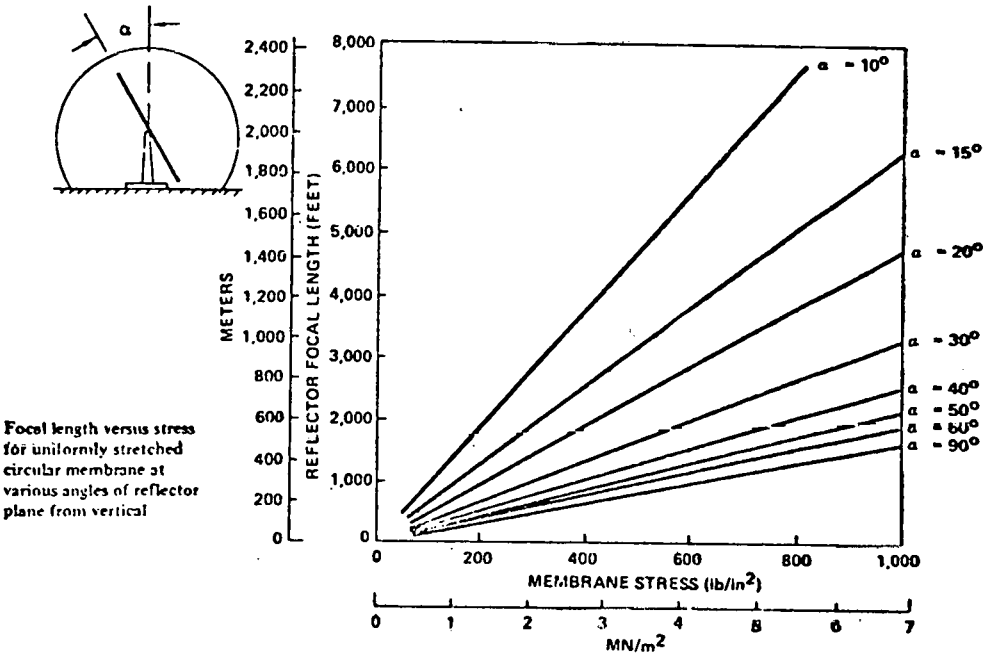

Figure 2.3.4.3-1. Reflector Focal Length

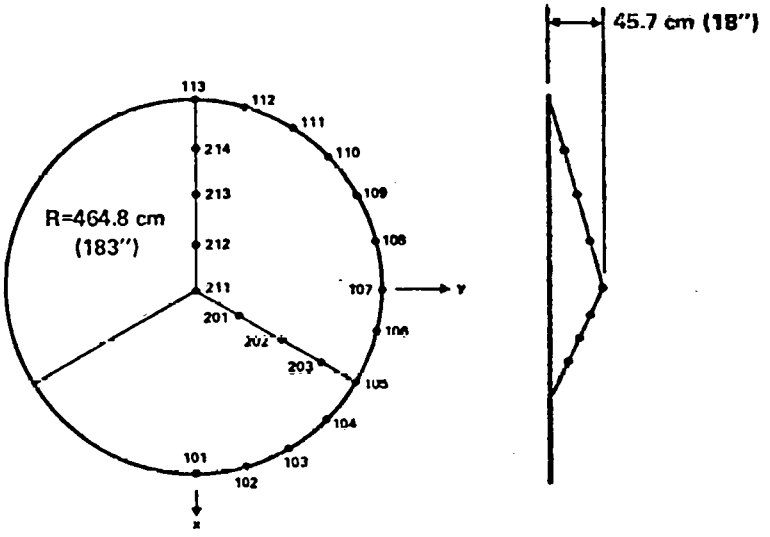

Ring radius = 464.8 cm (183")
Ring section = 12.7 cm (5 in.) O/diameter x 0.198 cm (.078 in.) wall thickness
Support arm section = 12.7 cm (5 in.) O/diameter x 0.198 cm (.078 in) wall thickness

Figure 2.3.4.3-2. Reflector Structure Math Model

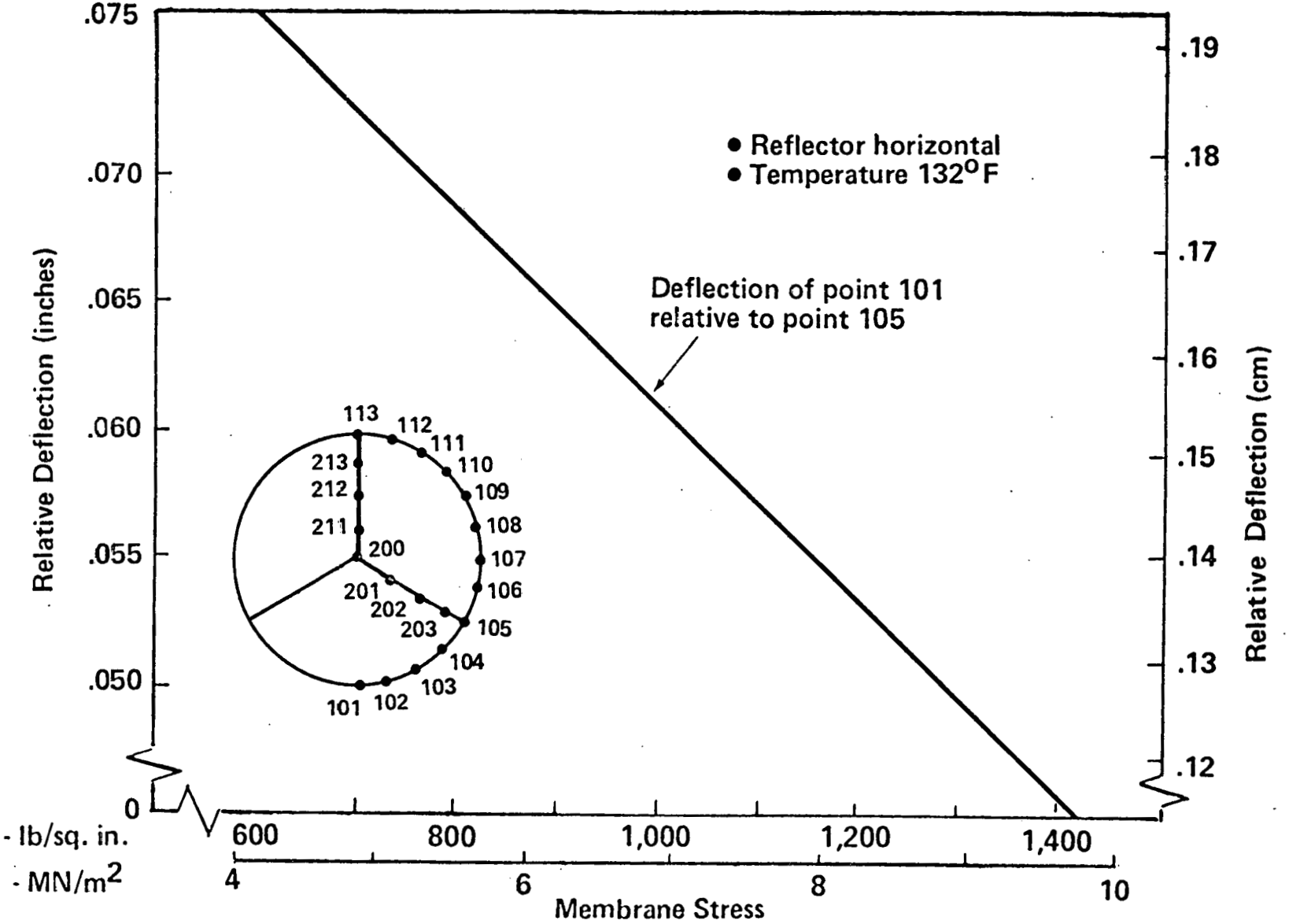

Figure 2.3.4.3-3. Reflector Structural Deflection Related to Membrane Stress

Stress levels in the central mounting hub are also low, but in order to limit the reflector ring deflection, the minimum bending section through the hub is designed to maintain the stiffness of the basic support arm.

The reflector pedestal is made from a 12.7 cm (5 in.) diameter A.P.I. 5LX x 52 steel pipe. The base of the pedestal is bell shaped to a 21.9 cm (8.63 in.) diameter. This is welded on installation to a base plate on the pedestal foundation pile. The 1.8 m (6 ft.) augured pedestal foundation pile is embedded with four 1.59 cm (5/8 in.) diameter A.615 steel rebar welded to the 1.27 cm (1/2 in.) thick steel base plate. The pedestal carries gravity loads plus torque loads due to the motor driven reflector as shown in Figure 2.3.4.3-4. The pedestal has been analyzed as a beam column. The stress levels are minimal and the deflection at the top of the pedestal is only about 0.01 degrees.

Earthquake Analysis

A seismic analysis of the reflector assembly has been conducted using the design earthquake response spectra shown in Figure 2.3.4.3-5, as taken from Reference 2.3.4.3-1. A peak ground acceleration of 0.35g's was assumed equal to that measured in the 1940 El Centro Earthquake, as reported in Reference 2.3.4.3-2. This approach meets the requirements of Seismic Zone 3 (Uniform Building Code) which is the design requirement defined in Specification 001. The fundamental frequency of the reflector assembly supported by a 12.7 cm (5 in.) diameter steel pipe was calculated to be 2.094 Hz. The peak response of this dynamic system to the above seismic environment, assuming 2 percent of critical damping, is then 7.44 cm (2.93 in.) and 1.31g's. Adding this displacement to the maximum seismic deflection of the enclosure (0.68 inches) gives a total deflection of 9.17 cm (3.61 in.). The design provides a clearance of 19.8 cm (7.8 in.) between the reflector and the dome. Peak bending stress in the reflector pedestal support due to earthquake loading is 54 MN/m^2 (7,836 psi) which is well below the design allowable.

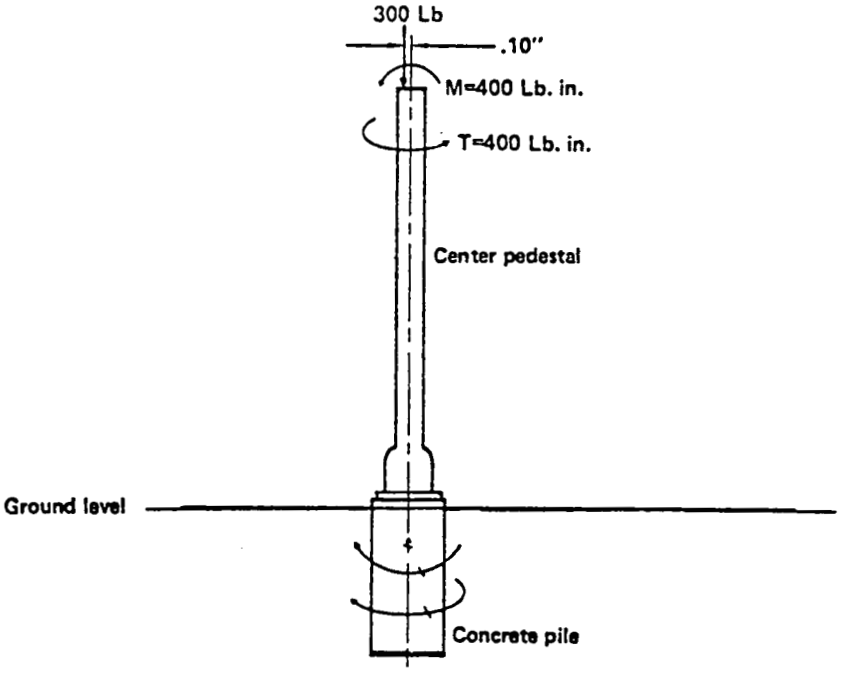

Figure 2.3.4.3-4. Pedestal Loads

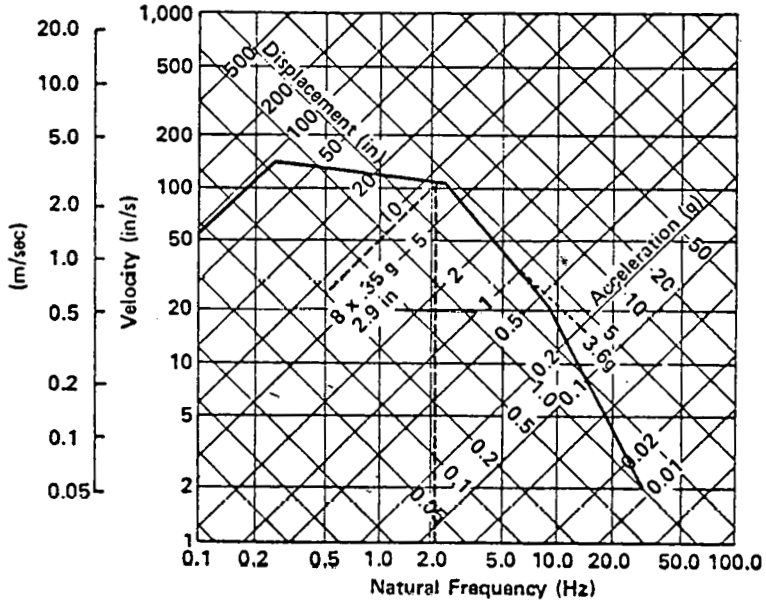

Figure 2.3.4.3-5. Horizontal Design Response Spectrum for 2% Critical Damping – Scaled to 1g Horizontal Ground Acceleration

2.3.5 Gimbal Actuator Assembly

Early in the program, a decision was made to go to industry for a cost effective gimbal actuator design. The intent was to obtain an integrated assembly from a single source. Toward that end, a new specification control drawing (SCD) was prepared to delineate gimbal/actuator requirements. The SCD was written to permit as much design flexibility as possible, and the prospective subcontractors were encouraged to innovate. Only certain parameters were tightly controlled; i.e., those which affect total system performance such as pointing accuracy. Clifton Precision Inc., Clifton Heights, N.J., and Berger Lahr Corp., Jaffrey, N.H., were modestly funded to prepare preliminary designs and cost estimates for various production quantities up to 1,000,000 units/yr. Although not funded, others were sufficiently interested in the program to prepare conceptual designs and cost estimates. As a result of design and cost comparisons, the Clifton Precision assembly was chosen for the commercial plant preliminary design. Details of this design are discussed in the following section. Discussion of other gimbal/actuator designs considered is given in Appendix A.

2.3.5.1 Gimbal/Actuator Design Description

The gimbal/actuator assembly shown in Figure 2.3.5.1-1 is designed to meet the Boeing specified requirements for a low cost electromechanical azimuth elevation heliostat drive system. The design includes an elevation actuator and an azimuth actuator which, when coupled together, act as an integral gimbal/actuator assembly. The method of coupling provides adjustment for perpendicularity of the azimuth axis relative to the elevation axis. The assembly is capable of rotating the reflector $\pm$ 180^{o} in the azimuth axis, and a total of 178^{o} in the elevation axis.

The internal design of the individual actuators is identical, i.e., a stepper motor is coupled through a spur gear train to the rotary output shaft. A multipole synchro transducer is directly coupled to the output shaft. This arrangement provides reflector position feedback information without introducing gear train errors. To achieve long life, a brushless design is used for both the stepper motor and synchro transducer. The only design difference between the azimuth and elevation axis is their cast metal housings.

Electrical excitation and feedback signals are conducted through a separate cable assembly for each actuator. The cable assemblies terminate at the control electronics package located on the heliostat access hatch.

The synchro transducer feedback signals are converted to a binary output equivalent to those produced by an encoder. The conversion will take place in the electronics package using a microprocessor-based synchro-to-digital converter. The encoded positon of the mirror will be compared to the stored position sent to the heliostat, and the resulting error will be used to drive the stepper motor to correct the position. The system identified is closed loop, thereby correcting for gear and backlash errors. The position accuracy of the "encoded" synchro is expected to be about 15 bits.

The Clifton Precision approach utilizing a multipole synchro transducer optimizes design performance versus maintenance by eliminating the inherently short life light source incorporated in photoelectric encoders. The synchro transducer approach also allows placement of reflector-positon signal-conditioning electronics on the heliostat access hatch. This facilitates maintenance of failed electronic components. To further minimize maintenance, the actuators utilize life-sealed bearings and dry film lubricated gears which eliminates the need for oil. These features allow for scheduled maintenance of the pedestal mounted gimbal/actuator components to coincide with the protective enclosure change.

In summary, the Clifton Precision concept was chosen primarily for its low cost and ease of maintenance of electronics associated with the syncro position sensor.

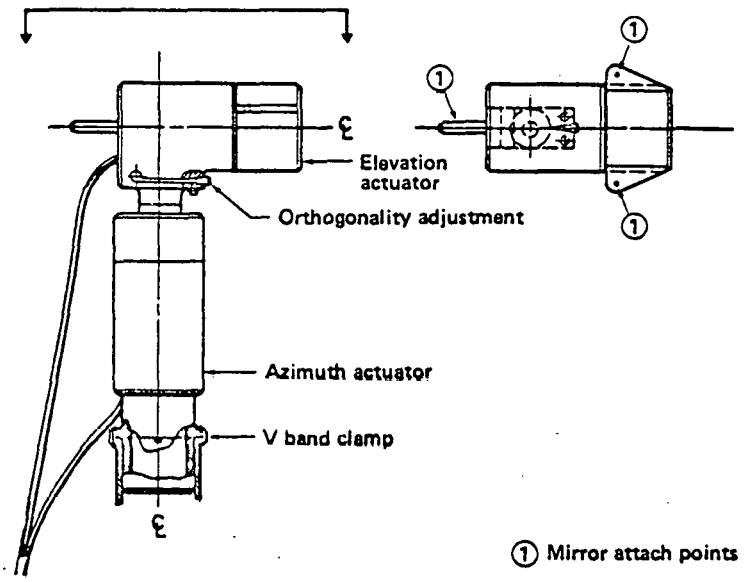

Figure 2.3.5.1-1. Heliostat Gimbal/Actuator

2.3.6 Controls

2.3.6.1 Heliostat Controller Design

The design of the heliostat controller has been refined and simplified to enhance high volume, low cost production. The block diagram in Figure 2.3.6.1-1 shows the current configuration which uses state of the art large scale integrated (LSI) devices, some of which were not available one year ago. A detailed system description can be found in Reference 2.3.6-1, Paragraph 3.3.4, page 72. Functionally, there has been no change.

The refined design, shown in Figure 2.3.6.1-2, incorporates improvements which eliminate all hand soldering and most hand assembly, reduces parts count by combining parts with a common function, and improves reliability by reducing parts count. A single power transformer with three secondaries has replaced the three transformers previously used in the three "off the shelf" power supplies. Rectifiers, filters and regulators were added to the single PC board. Push-on terminals are used for the power cable with a push-in strain relief. A card edge connector has been incorporated into the transformer for connecting transformer secondaries to the circuit board. Unregulated unfiltered DC is used for the stepper motors, filtered DC is used for the modem transmitter, and regulated filtered power is used for the remainder of the electronics including the micro-processors.

The printed circuit board provides for an edge connection to the transformer secondaries. All other electronic components are located on the board. Parts were selected to permit 100 percent automatic insertion and flow soldering. No hand wiring is required on the PC board.

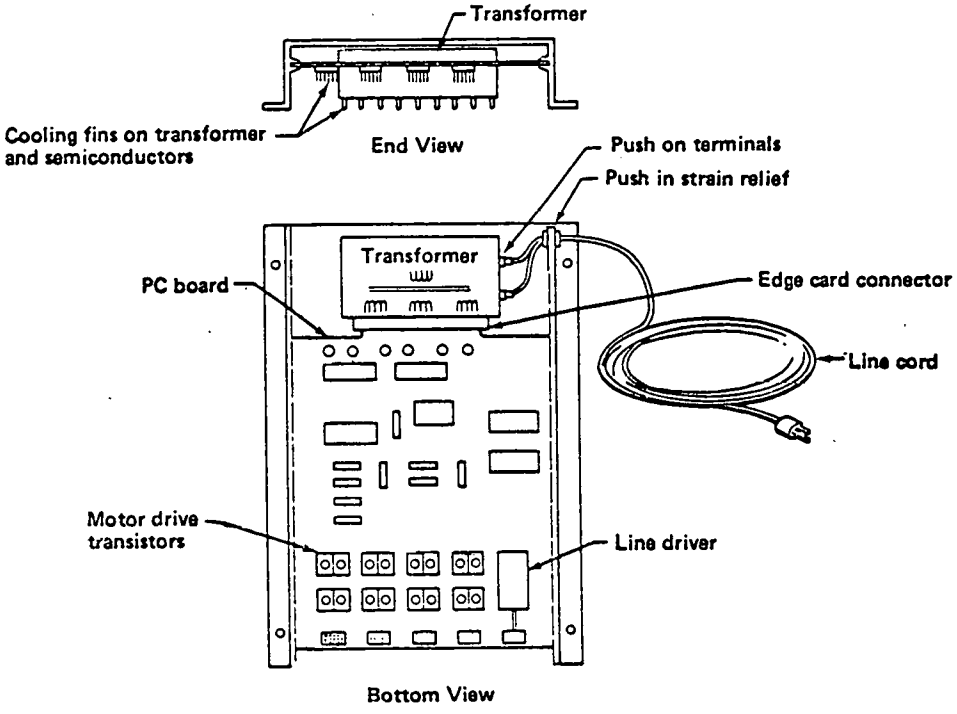

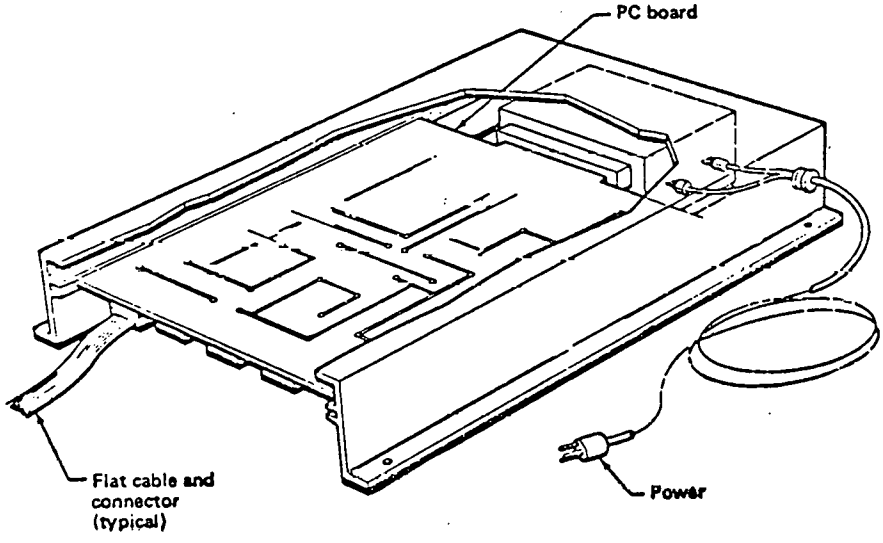

Figure 2.3.6.1-2. Heliostat Controller

To support a maintenance trade study, high reliability parts were substituted into the heliostat controller design for commercial parts which were significantly lower in hardware reliability. Heliostat controller failure rate was improved from 31.854 failures per million operating hours (MOH) to 5.79 failures per MOH. Unit cost increase to achieve this improvement is approximately 22% in quantities of 25,000. See Section 4.5 for a detailed explanation of trade study results.

The data bus coupling transformer has been redesigned to provide simplified field installation of the data bus cable (see Figure 2.3.6.1-3). The data bus "J" box with terminal strips is no longer required (see Figure 2.3.6.1-4). Installation time and hardware costs have been greatly reduced.

All inputs and outputs to and from the PC board are made via low-cost, machine installed connectors so that replacement of any part of the control electronics is quick and easy. This is especially important for field maintenance.

As a result of design improvements, a cost reduction of approximately 40% was realized for a unit fabricated with commercial parts, and a 30% reduction for a unit fabricated with high reliability parts, in quantities of 2500. Cost reduction is greater for larger quantities.

2.3.6.2 Alignment

The alignment approach selected for the commercial plant preliminary design allows non-precise installation of the reflector pedestal, and completely eliminates the requirement for future adjustment. The approach uses a circular sensor array installed on the tower below the receiver as shown in Figure 2.3.6.2-1. Hardware required is shown in the block diagram Figure 2.3.6.2-2, including the sensors and a sensor data acquisition system. Required sensor spacing is to be determined. Laser/geodolite survey equipment determines heliostat location in the field for alignment software. No other hardware is required for initial alignment or subsequent realignment.

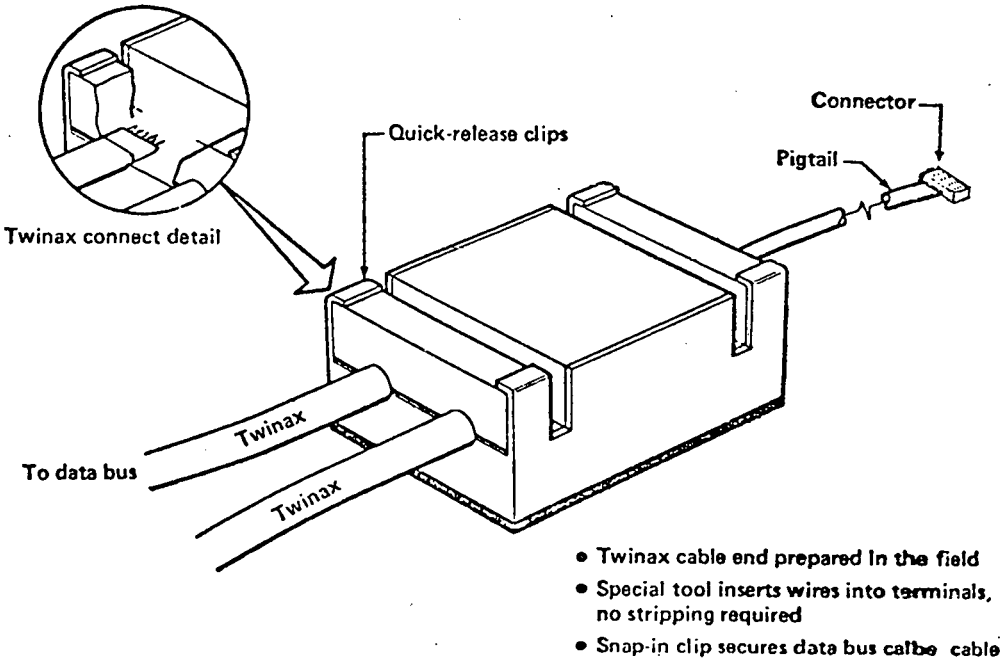

Figure 2.3.6.1-3. Data Bus Transformer

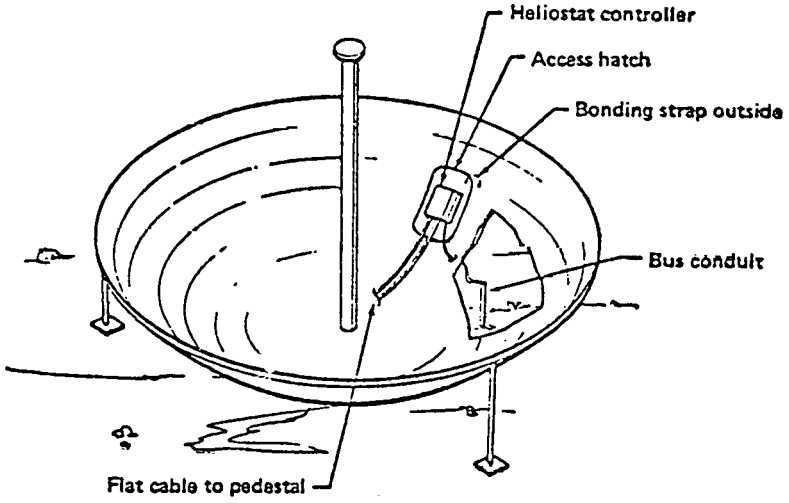

Figure 2.3.6.1-4. Heliostat Controller Installation

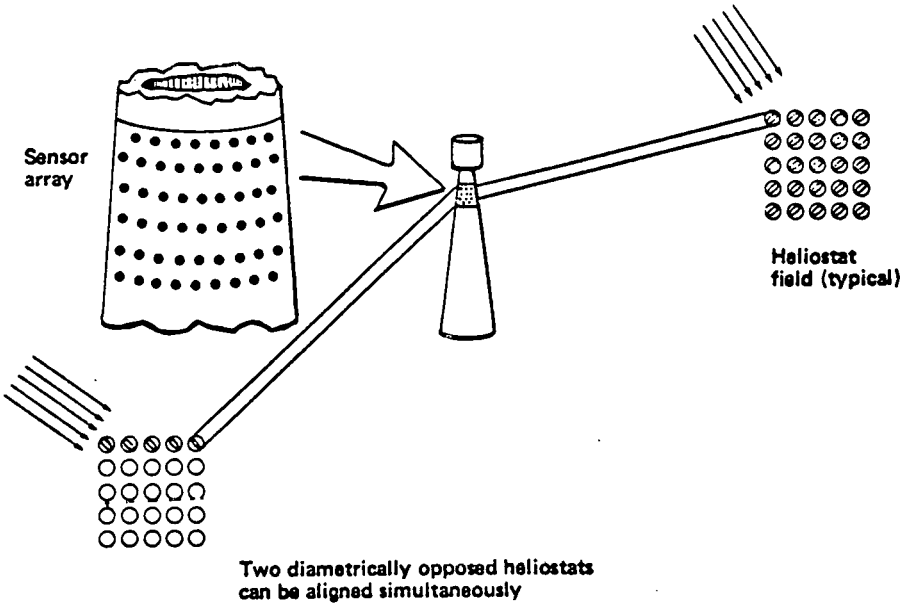

Figure 2.3.6.2-1. Alignment Schematic

Alignment Scenario

Heliostat foundations are installed on locations determined by conventional surveying. As each heliostat is installed, its position is determined using a laser/geodolite in the ranging and angle mode. Surveyed bench marks are used for directional reference. Receiver position is determined in a like manner.

Using a manual heliostat controller connected to a data bus, each mirror is manually positioned so that the reflected sun image falls within the boundaries of the alignment array. (The control system must be operational.) Upon command, the computer reads data from the sensor array and calculates the energy centroid. The following data are now available.

1) Absolute position of the center of the mirror,
2) Absolute position of the target.
3) Angular position of the sun, based on ephemeris data and time of day.
4) Energy centroid of the reflected image.
5) Angular position of mirror gimbal, azimuth and elevation with regard to a gimbal reference.

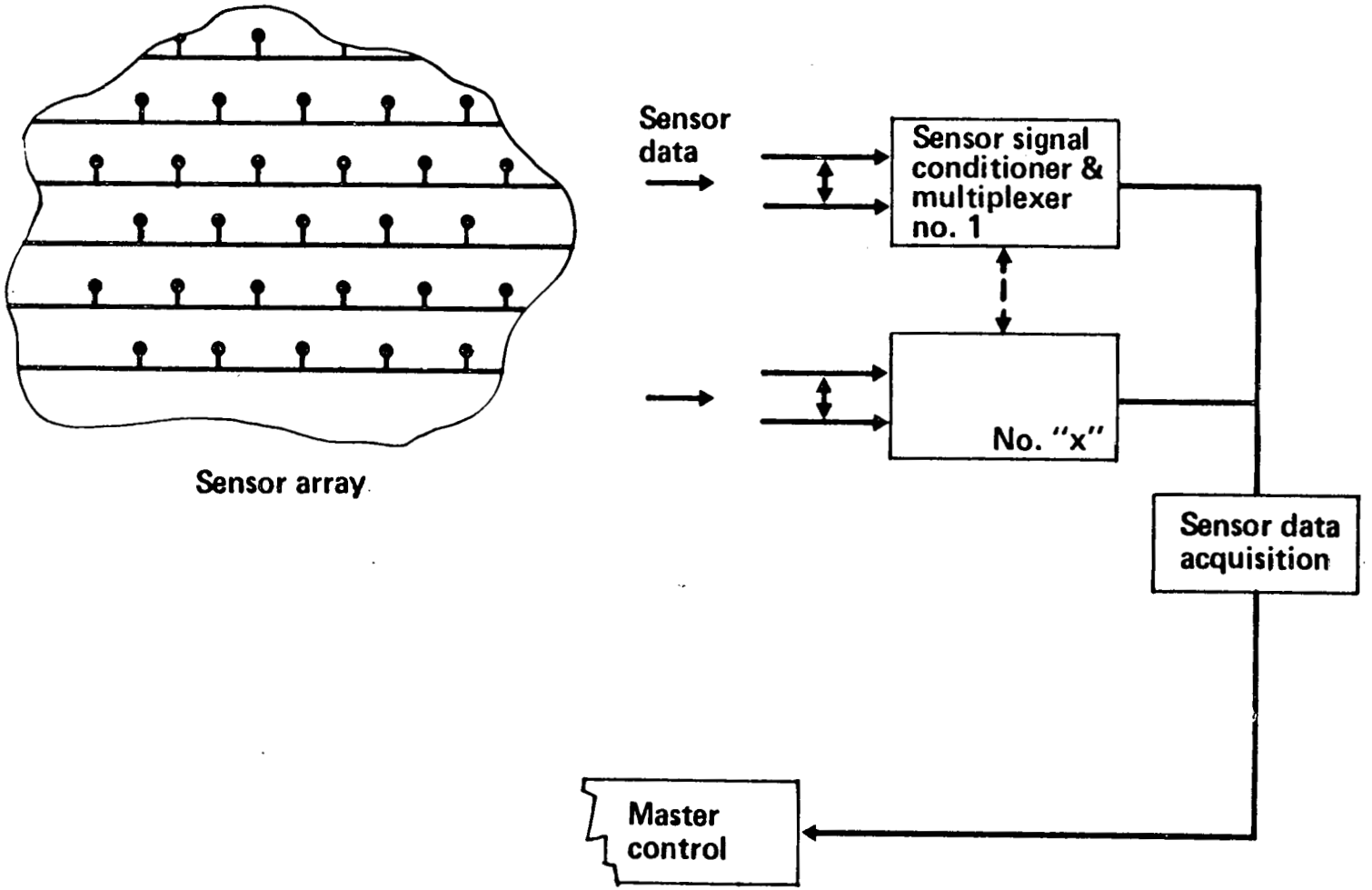

Figure 2.3.6.2-2. Block Diagram of Heliostat Alignment Electronics

Using this information the gimbal angles required to position the reflected image onto the target can be calculated. However, since the reflector pedestal was installed with loose tolerances, at a different time of day the image may not hit the target where programmed. This installation approach was selected to reduce installation costs. The amount of level offset must be known so that a gimbal azimuth and elevation angle transposition can be calculated to insure correct pointing throughout the solar day, and from day to day. Rather than make a direct measurement of this parameter, the alignment procedure is repeated one or more times at a different time of day. Each time, the gimbal correction required to align the image on the array is noted and a calculation made to determine gimbal offsets from level.

The alignment concept lends itself to automatic alignment checks after initial alignment is complete. At any time during the day the computer commands a heliostat first to a standby position, then to the align position (image on the alignment array). The energy centroid is calculated from the sensor data and the gimbal is automatically reoriented if required so that a line between the energy centroid and the center of the mirror is normal to the centerline of the tower. The required gimbal azimuth and elevation transposition angles are updated accordingly. Alignment checks can be made continuously if dictated by experience. Two diametrically opposed heliostats can be checked simultaneously. The sequence should allow up to four heliostats per minute to be aligned with no manpower, unless the sequence for an individual heliostat cannot be successfully completed. When this occurs, the problem heliostat is automatically taken out of service, the operator alerted, and maintenance personnel are dispatched.

2.3.7 Heliostat Thermal Analysis

A heat balance and thermal design verification is presented for the prototype heliostat. Design requirements are established based on the Barstow thermal environment. The heliostat system is required to operate with ambient air temperatures which range from -30 to 50^{o}C while being exposed to wind, sunlight, and other environmental conditions typical of the Southwest United States. Individual components such as reflector, enclosure, gimbal drive systems, and electronics each have their own operating temperature requirements which are established based on the commonly accepted limits for candidate prototype heliostat materials and components.

Prototype heliostat temperatures are described for "worst case" environmental conditions. These predictions show that the prototype heliostat design is thermally acceptable for the pilot plant environment.

This discussion covers three major topics. Heliostat thermal design requirements are described in 2.3.7.1. The analysis model developed for these studies is described in 2.3.7.2. Results and conclusions of the heliostat thermal analysis are described in 2.3.7.3.

2.3.7.1 Thermal Design Requirements

Two design days are utilized to define the range of environmental conditions which are expected for the Prototype heliostat. They characterize the Barstow site, or others having similar climatic conditions and latitude. Worst summer hot and winter cold days define the extreme conditions for which only occasional events can be expected but satisfactory short term performance is required. Table 2.3.7-1 describes the environmental conditions assumed for these days.

Table 2.3.7-1. Thermal Design Conditions Summary

		Design day	
		Hot Summer	Cold Winter
Daily temperature range $^{o}C(^{o}F)$	Max	50 (122)	-15 (+5)
	Min	34 (93)	-30 (-23)
Sky temperature ^{o}C		Ambient minus 6	Ambient minus 20
Average wind m/sec (mi/hr)		2.0 (4.5)	6.0 (13.4)
Direct total insolation at noon W/m^2		1,005	1,040

Figure 2.3.7-1 describes ambient air temperatures assumed for the design days. Nominal ambient temperature data are 30 day averages of hourly temperatures taken from the "Aerospace Data Tapes" for Inyokern, California, 1962 and 1963. The summer data is collected for 15 days, each side of August 7, and winter for 15 days each side of December 21. The hot summer day temperature profile results by equally increasing the nominal summer day profile so that it reaches a daily maximum of $50^{o}C$ ($122^{o}F$). The cold winter day, generated similarly from nominal winter data, reaches a daily minimum of $-30^{o}C$ ($-22^{o}F$).

Figure 2.3.7-2 describes "Direct Total Insolation" as affected by solar elevation angle and time of year. Here, rather than utilizing only direct insolation, total solar flux is used. The "Direct Total Insolation" includes all solar radiation which reaches the ground and assumes it to be direct and circumsolar flux. The data are best suited for thermal analysis on clear days, a typical condition for both the hottest summer and coldest winter days.

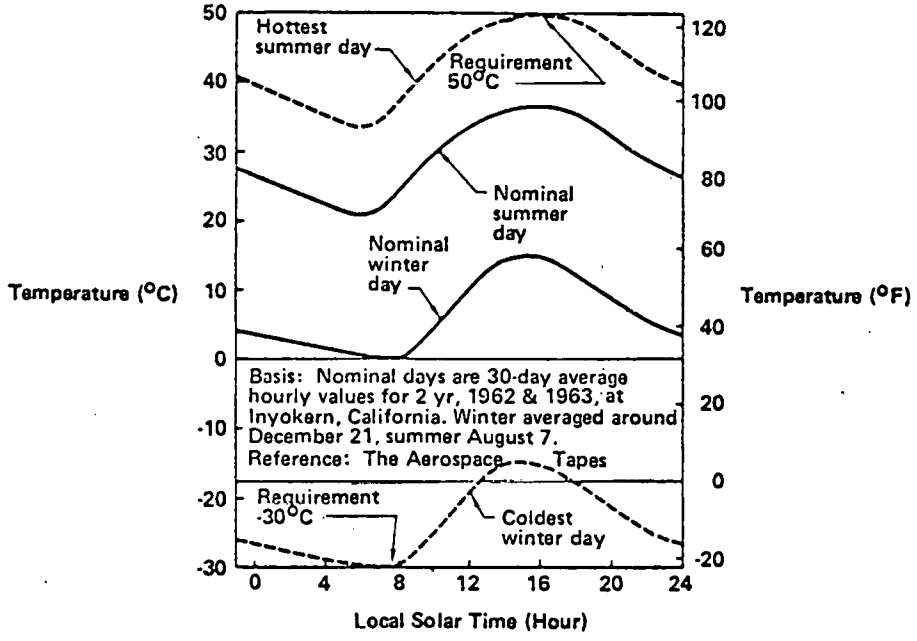

Figure 2.3.7-1. Ambient Temperatures for Design of PD Heliostat

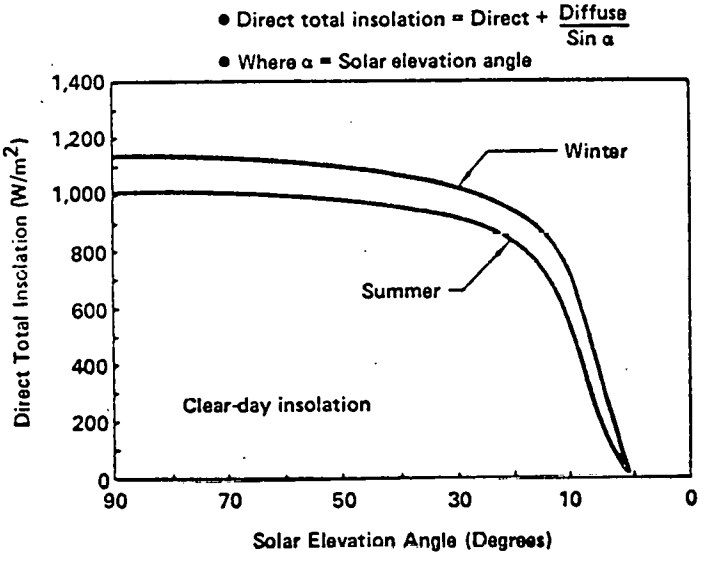

Figure 2.3.7-2. Design Insolation Values — Barstow, California

The wind speed assumed for the thermal analyses were determined from the speed frequency distribution included in the specifications. For the cold winter case a 6 m/s value was assumed. This represents a maximum for approximately 70% of the time. This should maximize the convective loss from the dome, thereby producing coldest temperatures. Similarly, 2 m/s was chosen for the hot summer day.

Temperature critical components of the prototype heliostat are listed in Table 2.3.7-2, along with their operating and non-operating temperature limits. These temperatures are obtained from a variety of sources. Consultation with vendors and cognizant subsystem engineers provides initial operating temperature goals. These are the limits which result in negligible impact of operating temperatures on cost, performance, and reliability. The design is initially evaluated with respect to accomplishment of these temperature goals. The enclosure, reflector, gimbal drive motors, synchros and gear drive units did not require temperature range increases over their initial goals. The heliostat electronics temperature limits had to be increased from initial values to those shown in Table 2.3.7-2 by utilizing some mil-spec type components. Also the power supplies contained within this unit are designed with high conversion efficiency. Even so, the power supplies dissipate half of the approximately 50 watt electrical input to the operating heliostat.

TABLE 2.3.7-2 TEMPERATURE LIMITS

System environment and temperatures:
30^{o} to $+60^{o}$C nonoperating
-20^{o} to $+50^{o}$C operating
Humidity and insolation in southwest U.S.

Components	Temperatures (^{o}C)	
	Nonoperating	Operating
Enclosure	-35 to 55	
Reflector	-35 to 65	
Gimbal drive motor	-30 to 125	-20 to 100
Gear drive	-30 to 93	-20 to 93
Snychro	-65 to 95	-20 to 75
Heliostat electronics	-60 to 125	-60 to 100

2.3.7.2 Analysis Model

The Boeing Thermal Analyzer Computer Code has been utilized for these studies. It is a lumped parameter forward difference analyzer capable of steady state and transient simulations. The problem has been formulated by defining collector thermal interfaces throughout a 24-hr. day of interest. Initial temperatures are assumed and temperatures determined as functions of time for several consecutive identical days. When temperatures begin to repeat on a 24-hour cycle, the process is complete and final day temperatures are reported.

The thermal analysis model includes a single heliostat with thermal boundary conditions which include: air, sky and surrounding ground level temperatures and solar heating of components. A comprehensive listing of heliostat heat transfer mechanisms used in this analysis and their independent variables is shown on Table 2.3.7-3.

Table 2.3.7-3 Heat transfer Mechanisms - Prototype Heliostats

External mechanisms	Independent variables
Direct solar heating	Solar elevation, azimuth, intensity at ground
Radiation to sky surroundings	Temperatures of sky and surroundings
Forced convection	Air temperatures, wind velocity, heliostat geometry
Solar heating via reflection	Collector field layout, orientation of adjacent reflectors, solar elevation, azimuth, intensity solar reflectance of ground
Internal mechanisms	
Solar absorption reflection and shadowing	Heliostat thermal coatings, reflector orientation, solar azimuth and elevation
Free convection	Air and component temperatures, geometry
Radiant exchange	Heliostat thermal coatings, reflector orientation
Thermal capacity	Component mass and materials

The thermal analysis has assumed the heliostat was located 1200 meters north and 430 meters east of the tower. Solar incidence and reflector normal directions were calculated at hourly intervals for the winter and summer solstices. Solar input to each component was calculated for each incidence and normal direction combination. Thermal radiative interchange was calculated assuming the reflector was oriented at an "average" 45^{o} orientation to the horizontal.

2.3.7.3 Heliostat Thermal Performance Results

The Heliostat Thermal Model has been exercised for two operating conditions - cold winter and hot summer. The heliostat temperature variations are presented in Figures 2.3.7-3 and 2.3.7-4. Each of these cases actually represents a number of sequential identical days. In the thermal model the diurnal conditions are repeated until equal temperatures occur on successive days. This process generally requires 2 to 4 "days" operation.

In both the cold winter and hot summer cases, Figures 2.3.7-3 and 2.3.7-4 show the large-scale prototype heliostat component temperatures following closely the ambient air temperature. All the component temperatures remain within $10^{o}C$ of the ambient. Local temperature differences may be larger than this in the area of heat dissipative components, e.g. heliostat electronics and gimbal motors. The range of temperatures expected by these components will be discussed later.

Cold winter temperatures for the enclosure, reflector and inside air are, in general, lower than the ambient by about $2\text{-}3^{o}C$, whereas for the hot summer the difference is $1\text{-}2^{o}C$. This is caused by the radiation losses to the colder winter sky temperature over the warmer summer sky temperatures. The relatively larger heat capacitance of the dish is seen to produce a "lagging" effect in the dish temperature profile.

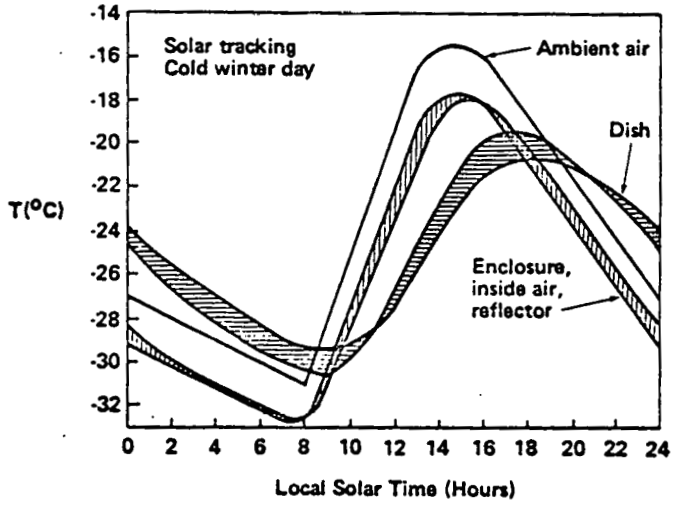

Figure 2.3.7-3. Prototype Heliostat Thermal Analysis

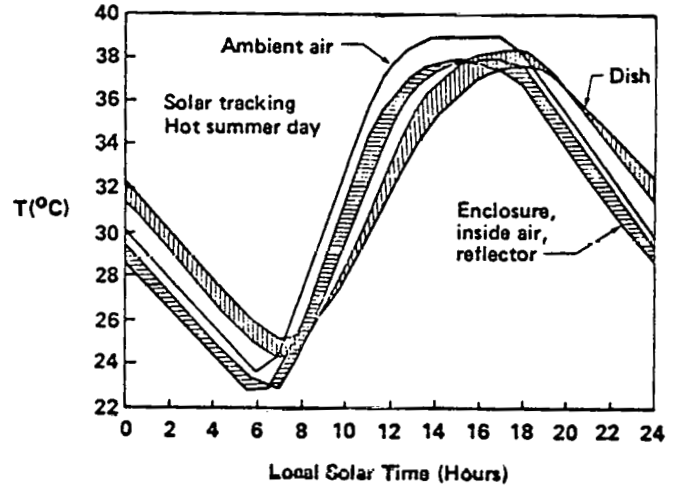

Figure 2.3.7-4. Prototype Heliostat Thermal Analysis

In order to estimate the effect of the above temperature data on the heliostat electronics and gimbal motor temperatures, a separate energy balance was performed on each of these components. The estimated dissipated power for the components was 29 watts for the heliostat electronics when operating, and 7 watts when in standby status; and 10.5 watts for the gimbal motors. These energy sources are negligible in comparison to the solar sources so they would not affect the large-scale component temperatures. However, the local temperatures of the heliostat electronics and gimbal motors would be affected by this heat dissipation. The temperature to which each component would rise to dissipate the appropriate power by natural convection to the heliostat inside air temperature was calculated at the maximum and minimum inside air temperature points. Table 2.3.7-4 presents the resulting prototype heliostat service temperatures. These data indicate only the gimbal motor in a nonoperating state on the cold winter day, would be outside the desired temperature limits. This condition could be averted by operating the gimbal motor when ambient temperatures drop below -20^{o}C.

Table 2.3.7-4 Prototype Heliostat Service Temperatures

	Max/Min Temperatures (^{o}C)		
	Temperature Limits	Hot Summer Day	Cold Winter Day
Ambient Air		49/33	-15/-31
Inside Air		48/33	-18/-33
Enclosure	55/-35	48/33	-17/-33
Dish - South Section		48/34	-19/-31
Dish - North Section		48/35	-21/-30
Reflector	65/-35	49/33	-18/-33
Heliostat Electronics			
Operating	100/-60	97/82	31/16
Standby		63/48	-3/-18
Gimbal Motor			
Operating	100/-20	70/55	4/-11
Non Operating		49/33	-18/-33*

*Temperature outside desired limits, system turned on early with ambient temperature below -20^{o}C.

3.0 MANUFACTURING/INSTALLATION CONCEPTUAL DESIGN

The conceptual design of manufacturing/installation processes has three major objectives:

1) To influence heliostat component design trade-offs to:
   - be compatible with maximum utilization of automated tooling
   - simplify design to minimize manufacturing/assembly functions
   - minimize the logistics of handling and transportation from raw materials to the completed heliostat on site
   - simplify the site preparation and installation procedures.

   All of these functions contribute to cost optimization.

2) To develop the fabrication/assembly/installation plans which:
   - can accommodate the specified production rates
   - provide conceptual designs of the automated tooling
   - evaluate production rates of the tooling to define total tooling required
   - define the total facility for manufacture, assembly and installation.

3) To develop manhours and manpower requirements for functions in the manufacturing/installation process, including the logistics of transporting heliostat assemblies from the manufacturing facility to each heliostat site.

The first objective above supported the optimization of cost whereas, the second and third objectives provided a firm basis for cost definition of the capital investment in facilities plus the manufacturing/installation labor cost.

To accomplish the above objectives, it was necessary to establish a scenario of plant sizes and plant locations to provide a basis for the manufacturing and installation planning which subsequently is used to define costs. The following defines the scenario (ground rules) for each of the three specified production rates:

1) A solar central receiver power plant has 25,000 heliostats.

2) Relatively small land areas will be dedicated to high density installation of solar power "parks." A solar power "park" is some multiple of individual solar plants, as defined in Item 6.

3) Solar parks are located in the reasonable vicinity of population centers to assure local availability of manufacturing, assembly and site installation labor. The number of solar power "parks" is a function of the specified production rates as defined in Item 6.

4) For the purpose of costing the delivery of materials, assume Phoenix, Arizona as an average location for sites.

5) Transport over dedicated roads will be utilized within the boundaries of the solar park. Solar parks are widely separated in the eight southwestern states, precluding dedicated roads between solar parks.

6) A separate scenario is assumed for each of the three specified production rates as discussed in the following and summarized in Table 3.0-1.

25,000 Heliostats Per Year

A solar park will contain 30 power plants (750,000 heliostats). The park will be completed in thirty years. Each plant within the park will be installed sequentially such that one plant installation is complete each year.

250,000 Heliostats Per Year

A solar park will contain 30 power plants (750,000 heliostats). Each power park is completed in thirty years at a rate of one plant per year. Ten parks are in simultaneous construction.

TABLE 3.0-1

SOLAR PLANT INSTALLATION ASSUMPTIONS

	Annual Production Rate		
	25,000	250,000	1,000,000
Heliostats Per Plant	25,000	25,000	25,000
Total Plants in 30 Years	30	300	1,200
Number of Solar Parks	1	10	20
Plants Per Park	30	30	60
Years to Complete a Park	30	30	30
Plants Complete Per Year Per Park	1	1	2
Number of Parks in Simultaneous Construction	1	10	20
Plants Complete Per Year	1	10	40

1,000,000 Heliostats Per Year

A solar park will contain 60 power plants (1,500,000 heliostats). Each power park will be completed in thirty years at a rate of two plants per year. Twenty parks are in simultaneous construction.

In utilizing the above scenario, the manufacturing/installation plan was further developed using the ground rules established in Table 3.0-2.

As seen in Table 3.0-2, the manufacturing plan provides for an on-site assembly facility at each solar park location. This facility completes all the fabrication and installation of heliostats for the 30 year construction period of the solar park. The following describes one such facility and the manufacturing concept which will achieve the high installation rates.

TABLE 3.0-2

MANUFACTURING/INSTALLATION GROUNDRULES

	ANNUAL PRODUCTION RATE		
	25,000	250,000	1,000,000
Heliostats per year per Facility (park)	25,000	25,000	50,000
Working days per year	250	250	250
Heliostat production per day per park	100	100	200
Number of shifts per day	2	2	2
Effective hours per day	16	16	16
Heliostats production per hour	6.25	6.25	12.5
Dimensions of Plant (miles on a side)	1.5	1.5	1.5
Dimensions of Park (miles on a side)	8.5	8.5	12.0
Average distance from Mfg. Fac. to site (miles)	4.0	4.0	6.5

3.1 HELIOSTAT MANUFACTURING CONCEPT

The smaller components and detail parts which are readily shipped by truck or rail will be procured from off-site sources. The large components such as the base dish and the enclosure will be manufactured on-site. Table 3.1-1 is a Make/Buy list for heliostat components. Figures 3.1-1 through Figure 3.1-9 illustrate the approach to the manufacturing plan. The incoming procured components and the raw material stock for the "make" components flow through receiving/inspection stores adjacent to the production assembly lines. The parts handling equipment and the manufacturing assembly tooling will be highly automated to achieve the production rates. Three basic branches of the assembly line are:

1) Support structure,
2) Reflector assembly, and
3) Enclosure fabrication.

These three basic lines feed to the final assembly area. The final assembly position installs and pressurizes the enclosure. The completed heliostat is then attached to the heliostat transporter and delivered to the heliostat site. The heliostat assembly fixture is the transportation fixture which is designed to also facilitate the installation at the site. The conceptual designs of the manufacturing processes and automated tooling are described in the following paragraphs.

On Site Fabrication and Assembly Facility

The on site assembly and checkout facility is contained in a single story building designed for a 30 year minimum life. The building will be provided with the normal utilities, conveniences and fire protection to conform to local building codes. See Figure 3.1.0.

Table - 3.1-1 MAKE/BUY PLAN

ITEM	Make (M) Buy (B)	Drawing Number
Support ring - segments	B	277-10048-41
Stanchions	B	277-10048-5
Pedestal	B	277-10048-6
Enclosure attach ring	B	277-10048-X
Reflector ring comps & spokes	B B B	277-10051-7 Tube ring 277-10051-8 Tube Supt 277-10051-9 Tube Supt
Hatch assy	B	277-10048-10
Flanges - hatch	B	277-10048-13 & -14
Gimbal assy	B	
Air Supply assy	B	277-10052-1
Relief Valve assy	B	277-10052-2
Electronics equipt. & Harness wire	B	
Piling installation	B	277-10050-1
Hub	B	277-10054-1
Tee's	B	277-10053-1, -2
Base dish	M	277-10048-3
Enclosure	M	277-10049-1
Heliostat Assy & instl	M	277-10048-1
Reflector assy	M	277-10051-1 & -2

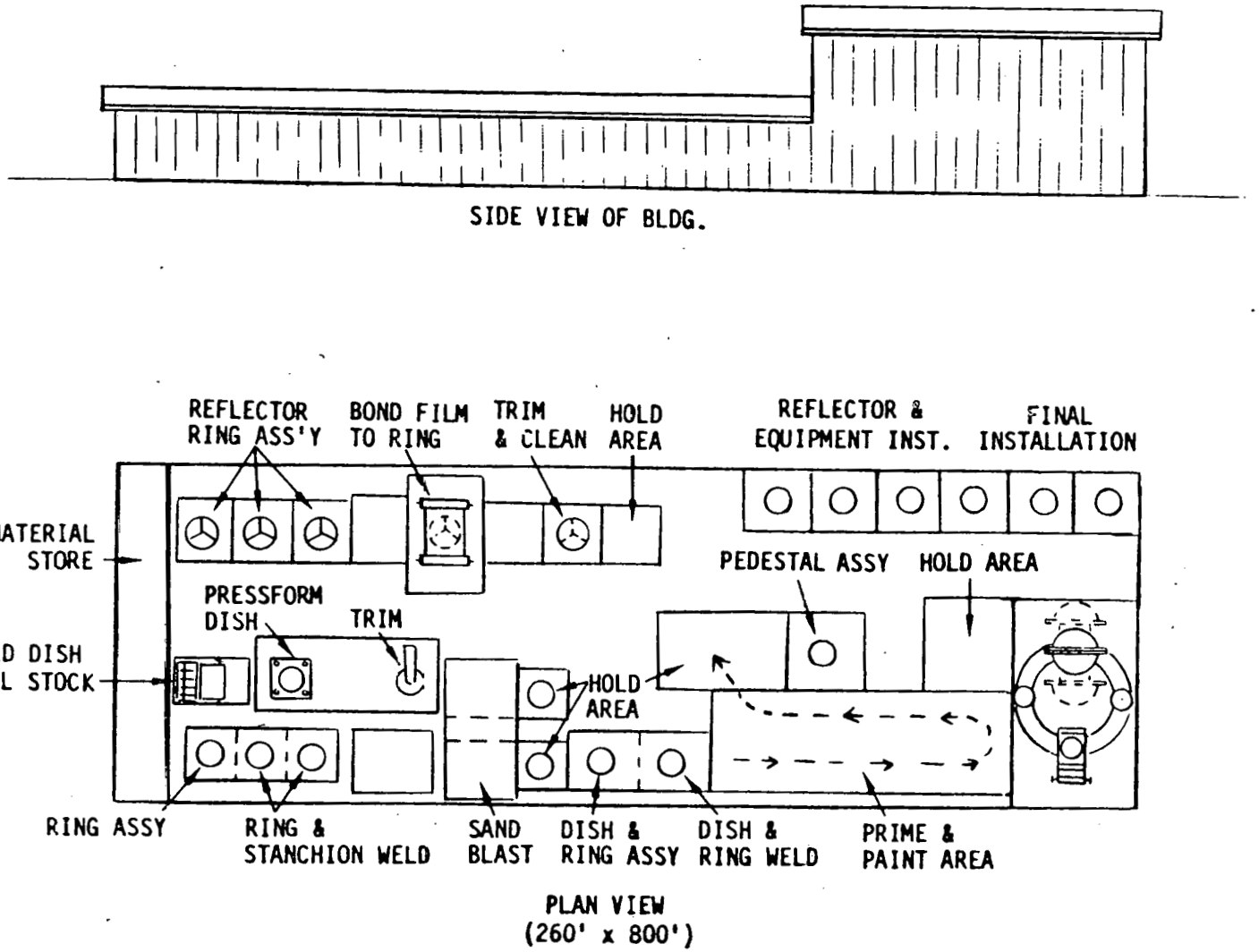

Figure 3.1. Onsite Assembly Facility

A high bay area of 35,000-45,000 sq. ft. is provided for the enclosure thermoforming area and the enclosure installation area to provide the necessary overhead hoist clearances. Exit doors to allow the heliostat to leave the final assembly area for the field will be 40' x 40'. All additional facilities such as specialized air conditioning, unique electrical power requirements and high volume air sources for the grit blast, vapor blast, painting facility and enclosure thermoforming area, are included in the cost of individual equipment.

Base Assembly

The support ring is fabricated from six component parts, three ring segments, and three stanchions. These are loaded into the assembly jig and welded as shown in Figure 3.1-1.

Ths dish is fabricated from five steel sheets (roll stock), butt welded together to form a single roll. This roll is passed through the forming press to shape the dish and then through the circle shear, where the dish is trimmed to net size. The sequence of operations is shown in Figure 3.1-2. The dish is now routed to the sub-assembly area where the prefabricated hatch and enclosure attachment ring are installed.

The support ring assembly is routed thru the grit blast area to remove scale and weld slag, the dish is routed to the adjacent vapor blast area to remove oil and other contaminates detrimental to painting. The ring assy. and dish are now routed to the weld area to be joined before routing to the painting facility where a primer coat will be applied and quick dried thru an infra red cure cycle. (See Figure 3.1-3). The finish coat will be applied in a similar manner. The support ring/dish assembly and the prefabricated reflector pedestal are then loaded into the base assembly fixture (see Figure 3.1-4) which will precisely locate the pedestal with respect to the base assembly. The fixture

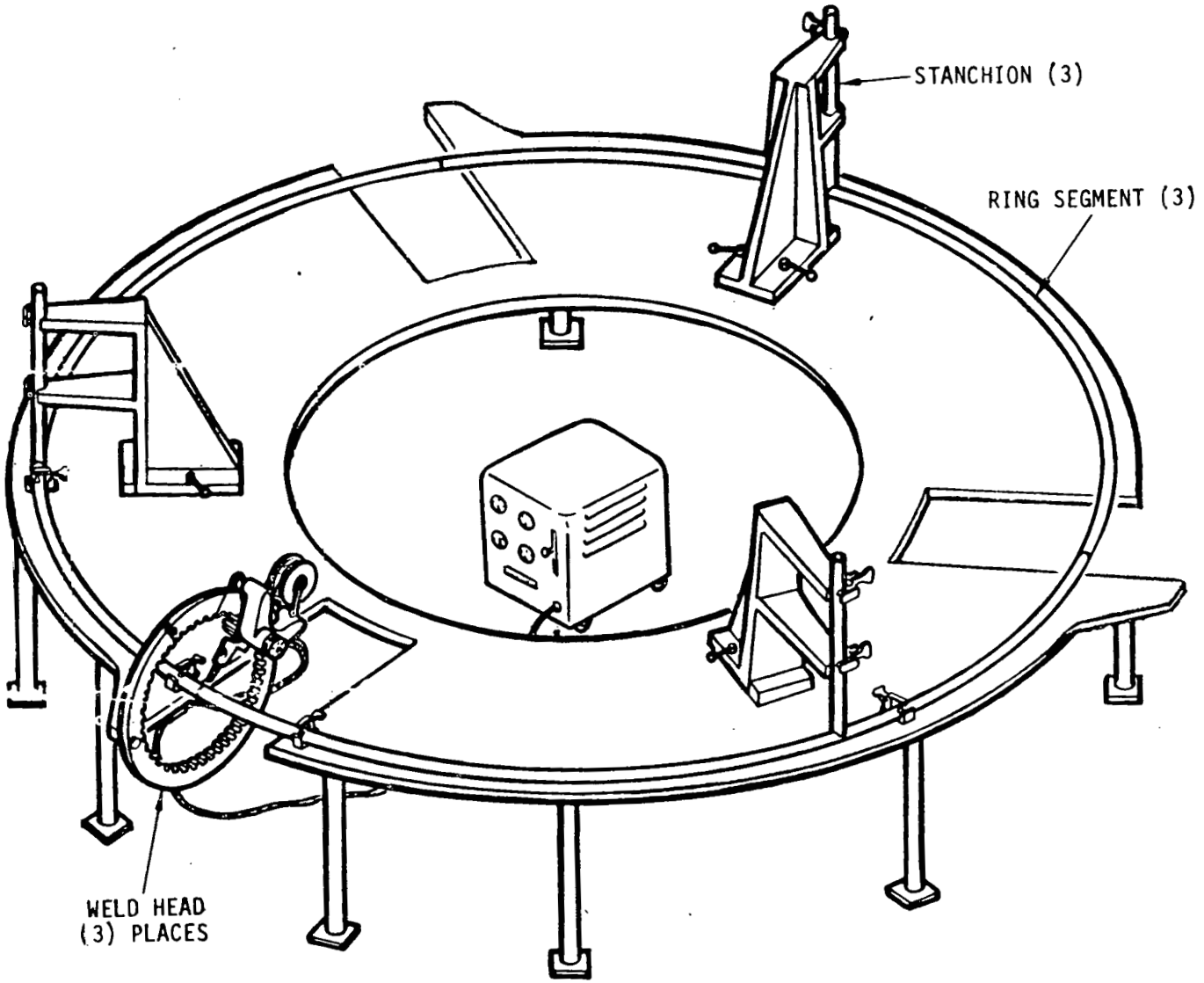

Figure 3.1-1 Support Ring Welding Fixture

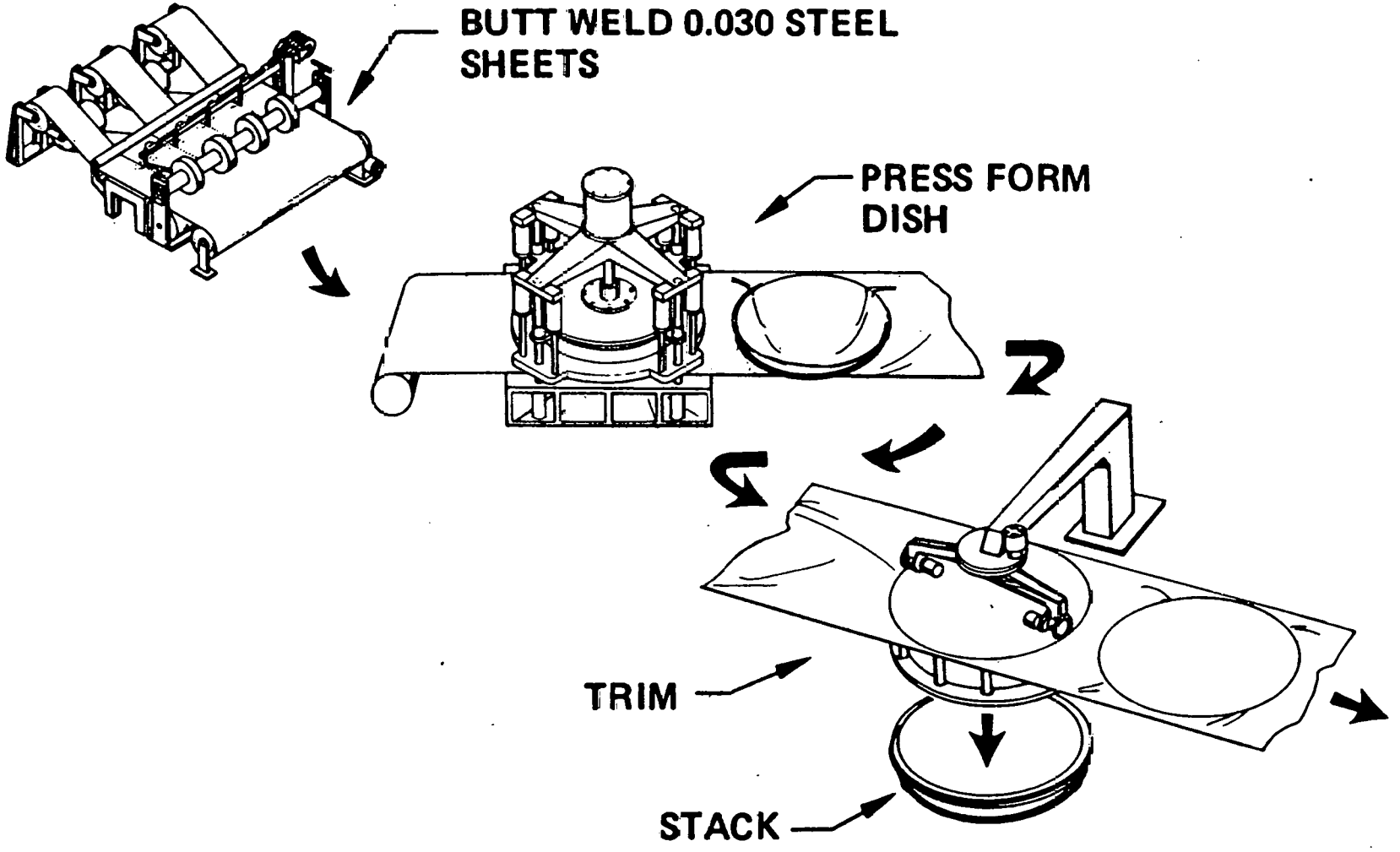

Figure 3.1-2. Dish Fabrication

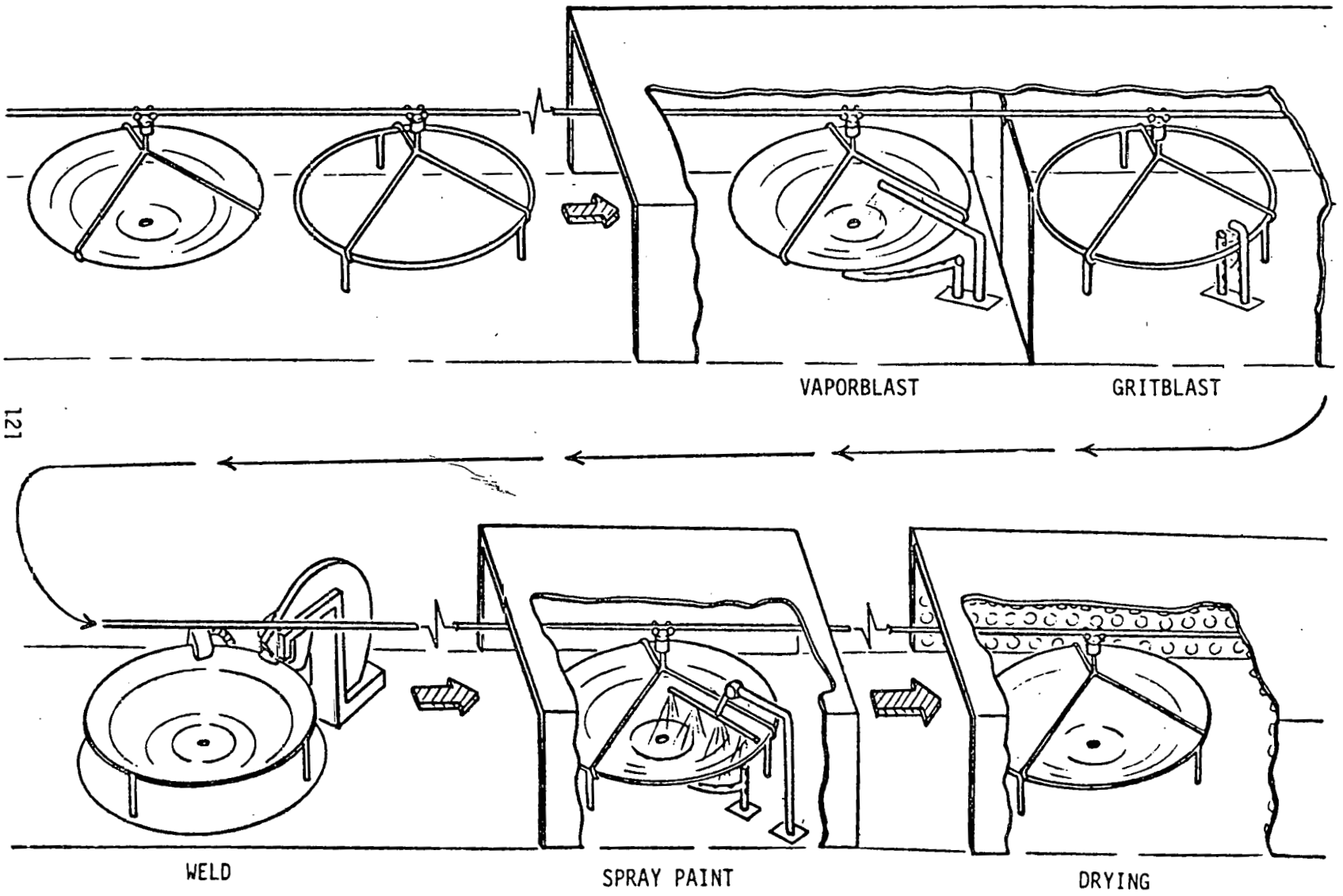

Figure 3.1-3. Clean, Paint and Weld Station

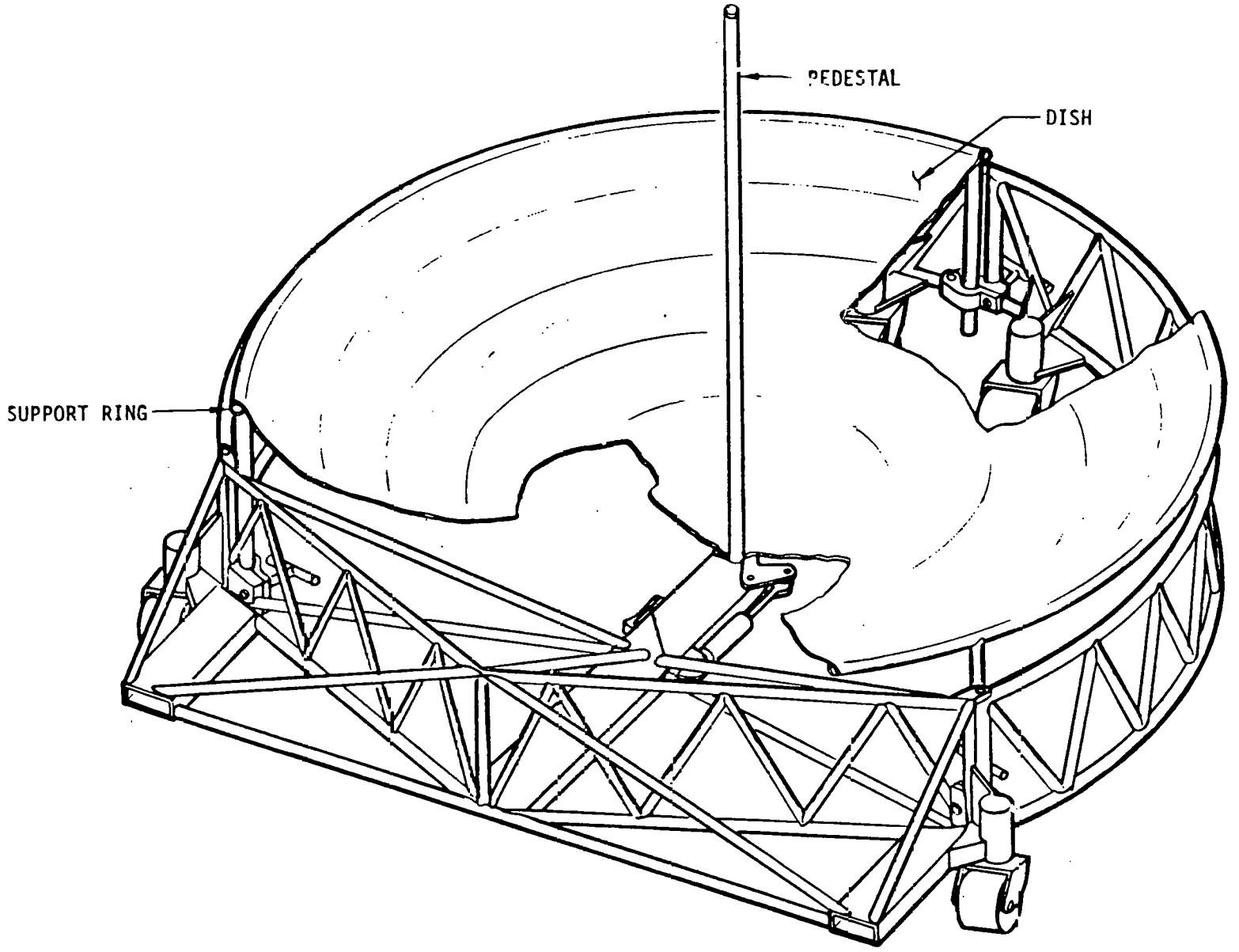

Figure 3.1-4 Base Assembly and Transportation Fixture

THE BOEING COMPANY
SEATTLE, WASHINGTON

provides a rigid structure to support the heliostat through assembly and will remain with the heliostat until installation in the field. This fixture and its interfaces with the transporter and the foundation at the site, will be further described in the installation conceptual design, Section 3.2.

Reflector Assembly

The three ram-formed reflector ring components, three spokes, attachment tees and the cast center hub fitting are purchased components. These items flow from reflector assembly stores to the fixture as shown by Figure 3.1-5 where the components are properly positioned and held to a planar surface during the electromagnetic swaging of each joint. The finished ring structure assembly is then moved to the final reflector assembly jig.

The aluminized polyester reflector membrane will be procured in the maximum practical width rolls. Each reflector membrane may require seven widths of the film. The strips will be bonded together on a continuous flow tool designed to handle, support and protect the delicate film. The bonded seams (six) will utilize a sandwich type lap joint with a solid form polyester thermosetting adhesive. The adhesive will be activated and cured in place by an electrical impulse heater.

The reflector ring is prepared for the membrane bonding operation by cleaning the bond surface of the ring with solvent. Heat activated adhesive tape is then positioned on the ring and heat-tacked at ten inch intervals. The polyester used as the reflective surface is handled on two rolls in a scroll arrangement as illustrated in Figure 3.1-6. A length of the film is rolled off the dispenser-roll across the area where the bonding is done. The scrap film is rolled up on a take-up roll. The reflector ring is then positioned under the length of film.

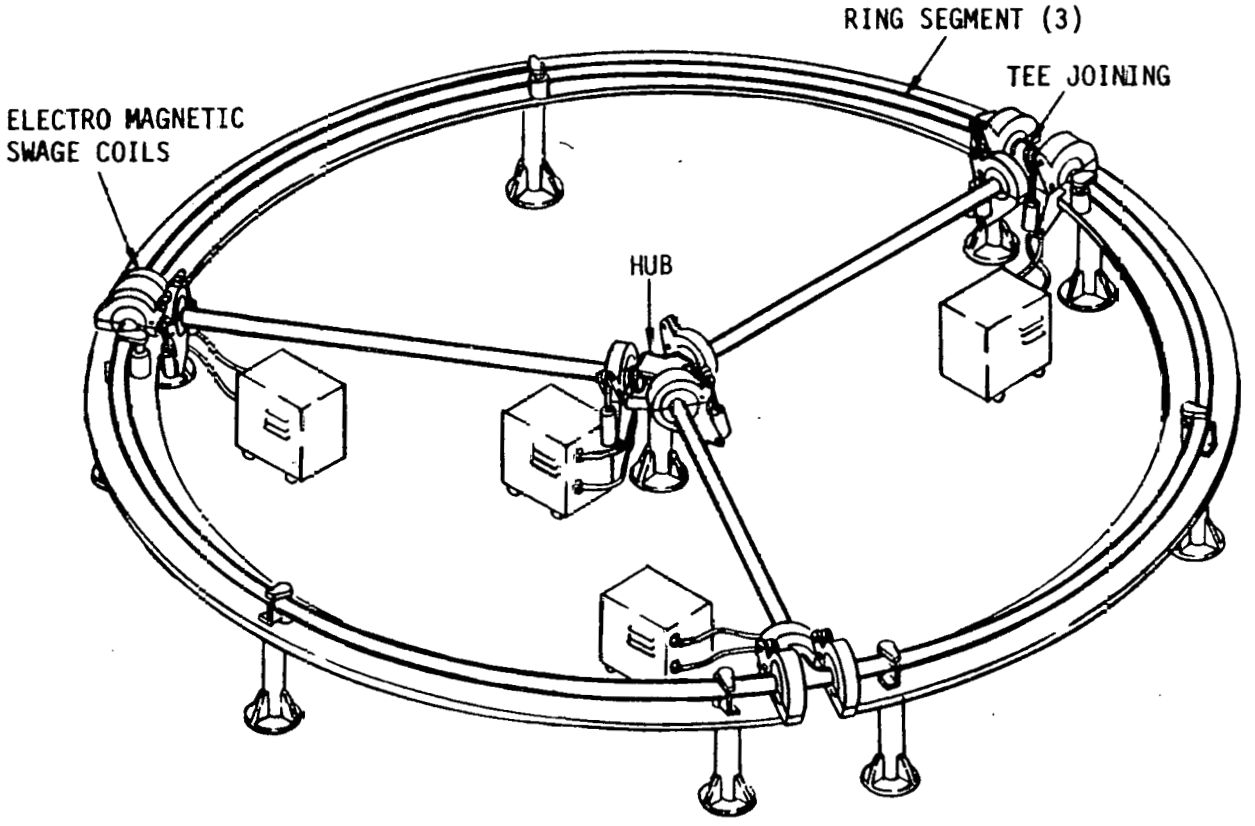

Figure 3.1-5. Reflector Ring Assembly Fixture

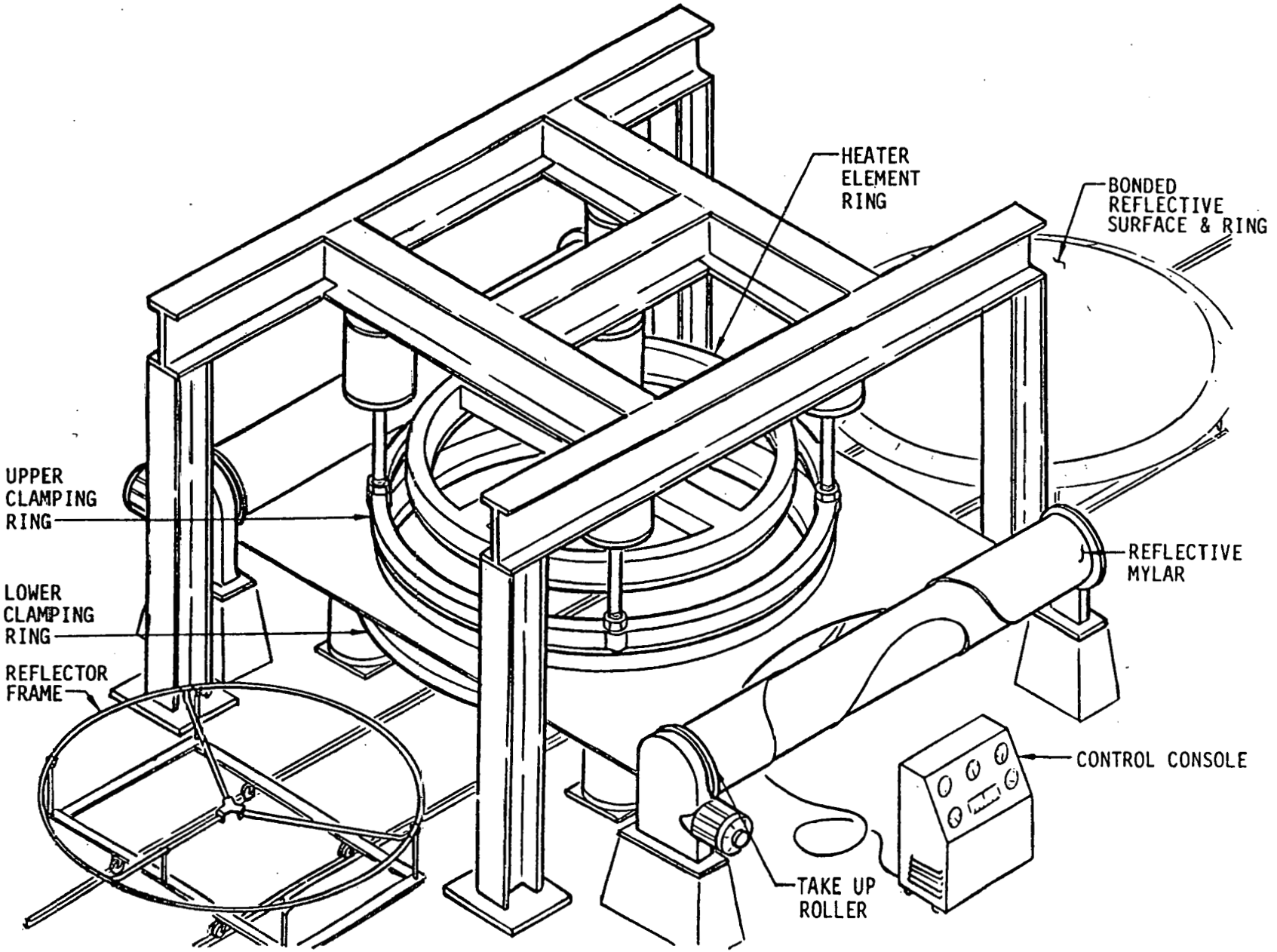

Figure 3.1-6. Bonding Reflective Surface to Ring Assembly

Clamp rings from above and below the film sheet, clamp the film and stretch it over the reflector ring. Simultaneously, a cutter on the upper ring shears off the circular section of film held by the clamps. Next, a heater ring drops down on the assembly to bond the reflective film to the reflector ring. After bonding, the clamp rings are released and the reflector moves on to have the film trimmed to the outside edge of the bond line. The completed reflector is then moved to position for assembly to gimbal mounting plate.

Enclosure

The enclosure is thermoformed from a weatherized polyester flat sheet blank. This thermoforming technique has been demonstrated by small models but requires further development for forming of full scale enclosures. The development work to date has been with unoriented polyester film. Radiant heat lamps have been used as the heat source in the facility diagrammed in Figure 3.1-7. A picture of a dome being formed is shown in Figure 3.1-8. Developmental tests have varied the heat rate and domes have been blown to various expansion ratios. The maximum expansion ratio achieved to date was approximately 30. This expansion ratio was limited by the heating capacity of the facility. Every increase in heat input to the film, during both heat-up and blowing has resulted in increased expansion ratios. A 9.7m (31.8 ft.) diameter enclosure will require expansion ratios of 40 and 110, if blown from blanks of 3.28m (10 ft.) and 1.85m (6 ft.), respectively.

The higher expansion ratios are expected to be feasible. However, since the available width of the polyester blanks may be limited, experimental domes have been successfully blown from blanks that have been joined. Hot-bar sealed joints and fused laminates have been blown to expansion ratios of six. If a seamed blank of width equal to the base diameter (6.86m) were used, the required expansion ratio would be approximately 6.8.

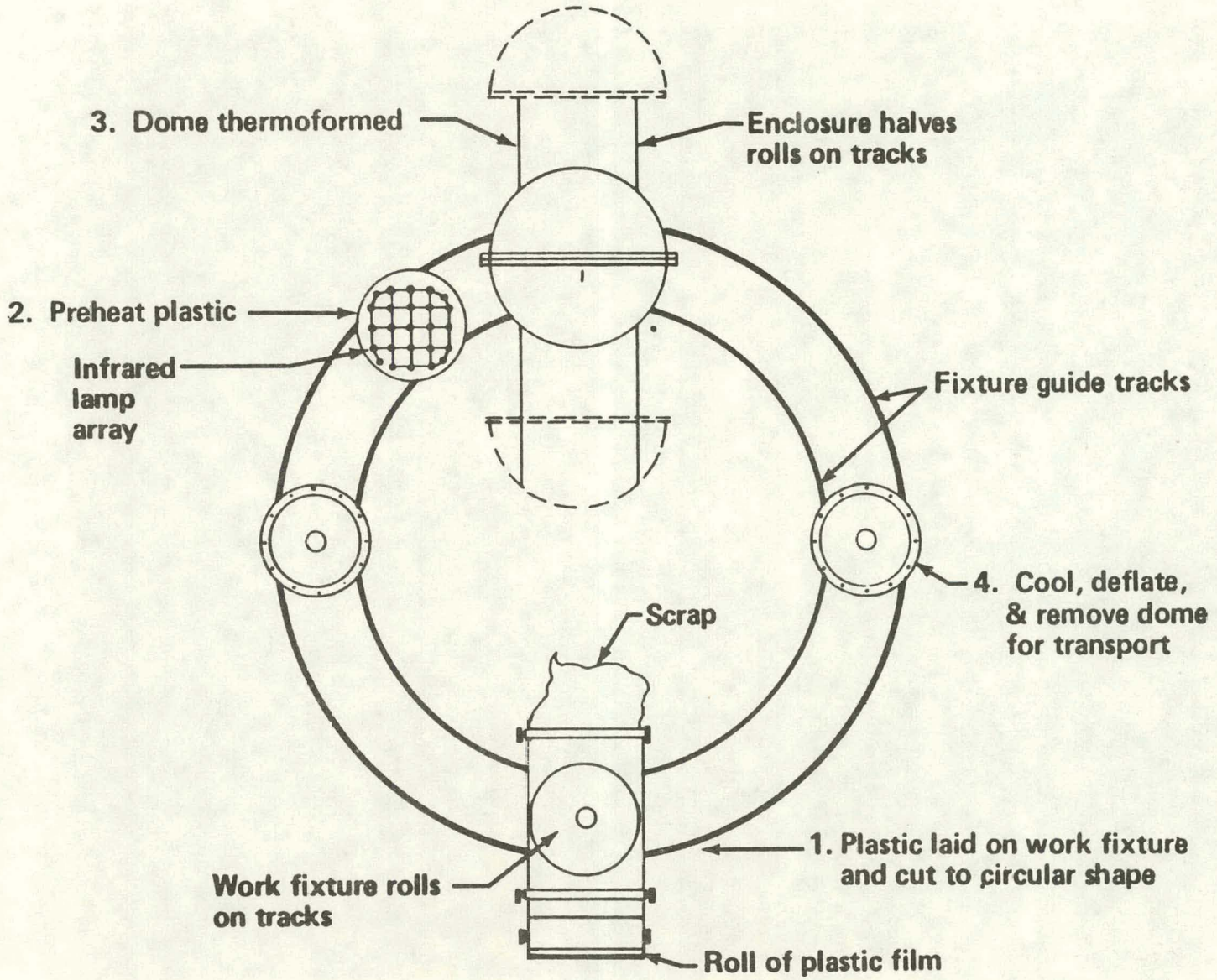

Figure 3.1-7. Enclosure Thermoforming Facility

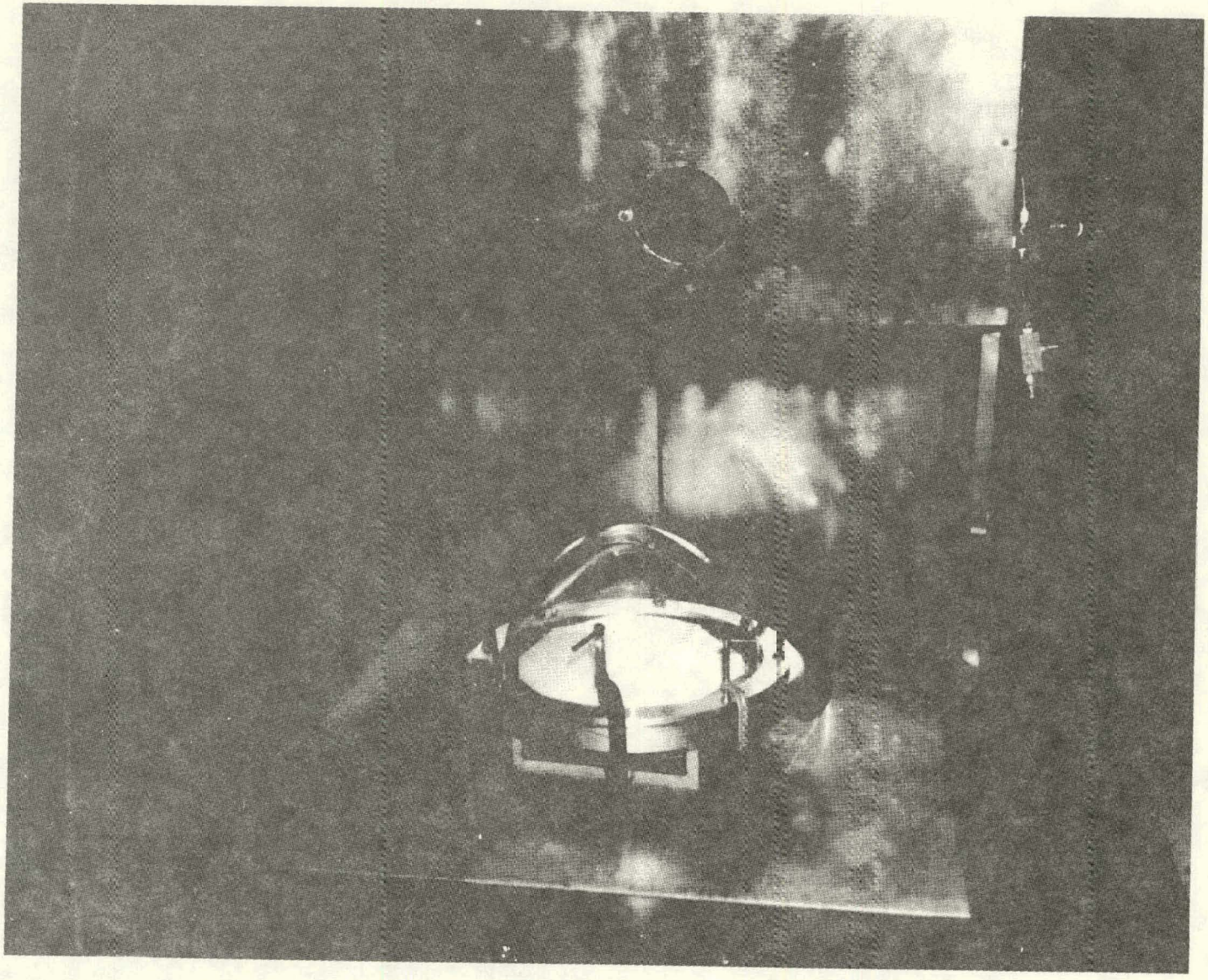

Figure 3.1-8. Experimental Enclosure Forming

Both the optical properties and the strength properties of the thermoformed enclosure material can be expected to be as good as or better than the initial properties of the film.

A conceptual design of the thermoforming facility is shown in Figure 3.1-9. This equipment will be located in a high bay, semi-clean room area of the manufacturing assembly facility. The blown enclosure is removed from the heat facility and moves directly to the final assembly area.

Final Assembly

The heliostat final assembly area will be a high-bay completely enclosed area in which a semi-clean room environment can be maintained. Before entering this area the painted base assembly will be vacuum cleaned to remove dust and other contaiminants accumulated in the welding and paint shops. The base assembly is now moved into the final assembly area to the first of two positions. Position 1 will install the heliostat controller, power and signal wire hardware, gimbal assembly, blower unit and reflector. Interconnecting wire harnesses will be hooked up and a functional test run to assure proper electrical operation (see Figure 3.1-10). Position 2 will install the enclosure using an overhead hoist and tag lines. During this operation the reflector will be rotated to a 60^{o} angle to facilitate enclosure installation. The enclosure is secured to the base, sealed and inflated see Figure 3.1-11.

The completed heliostat with its transportation fixture is then attached to the transportation tractor and leaves for the heliostat installation site.

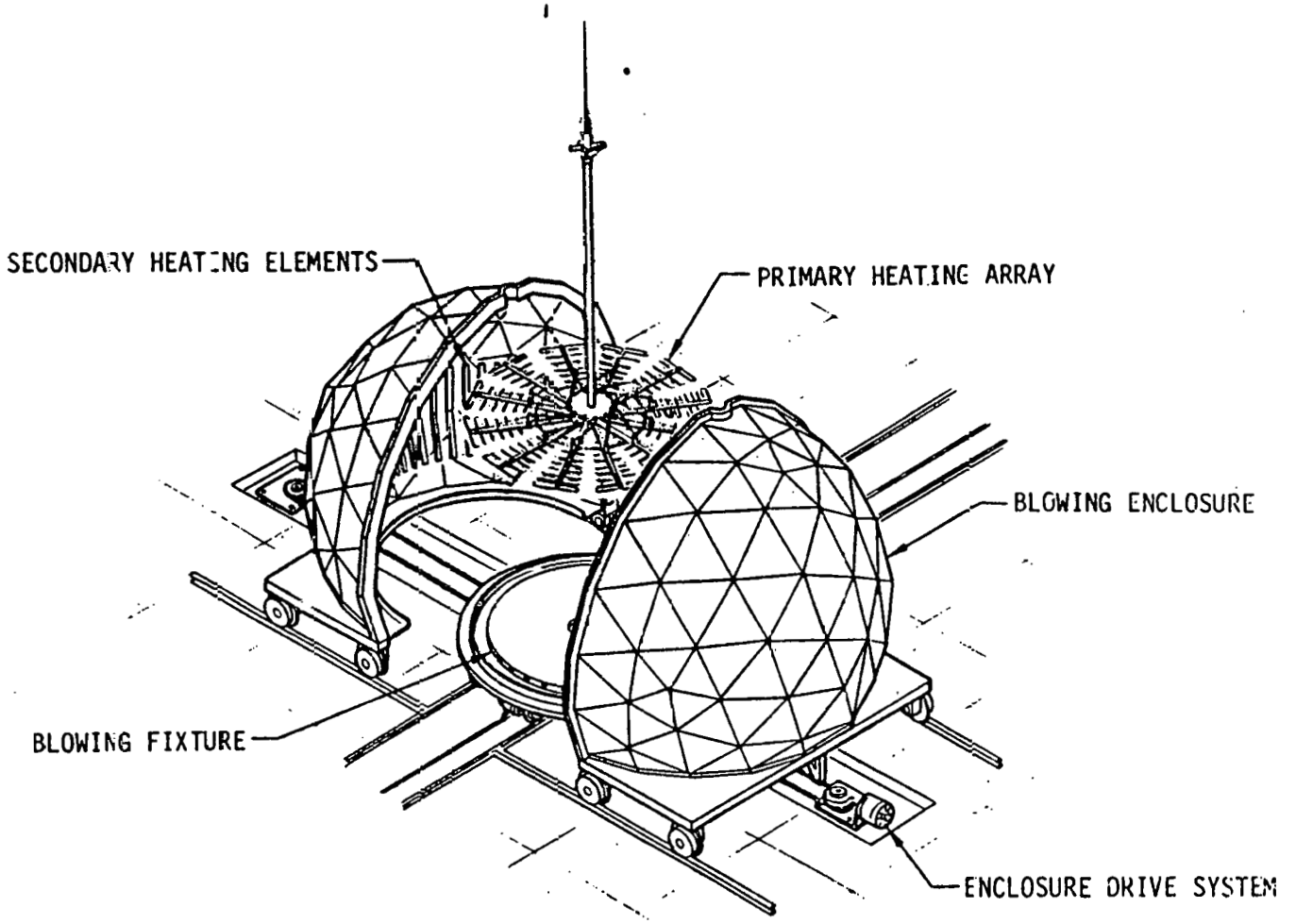

Figure 3.1-9. Thermoforming Facility

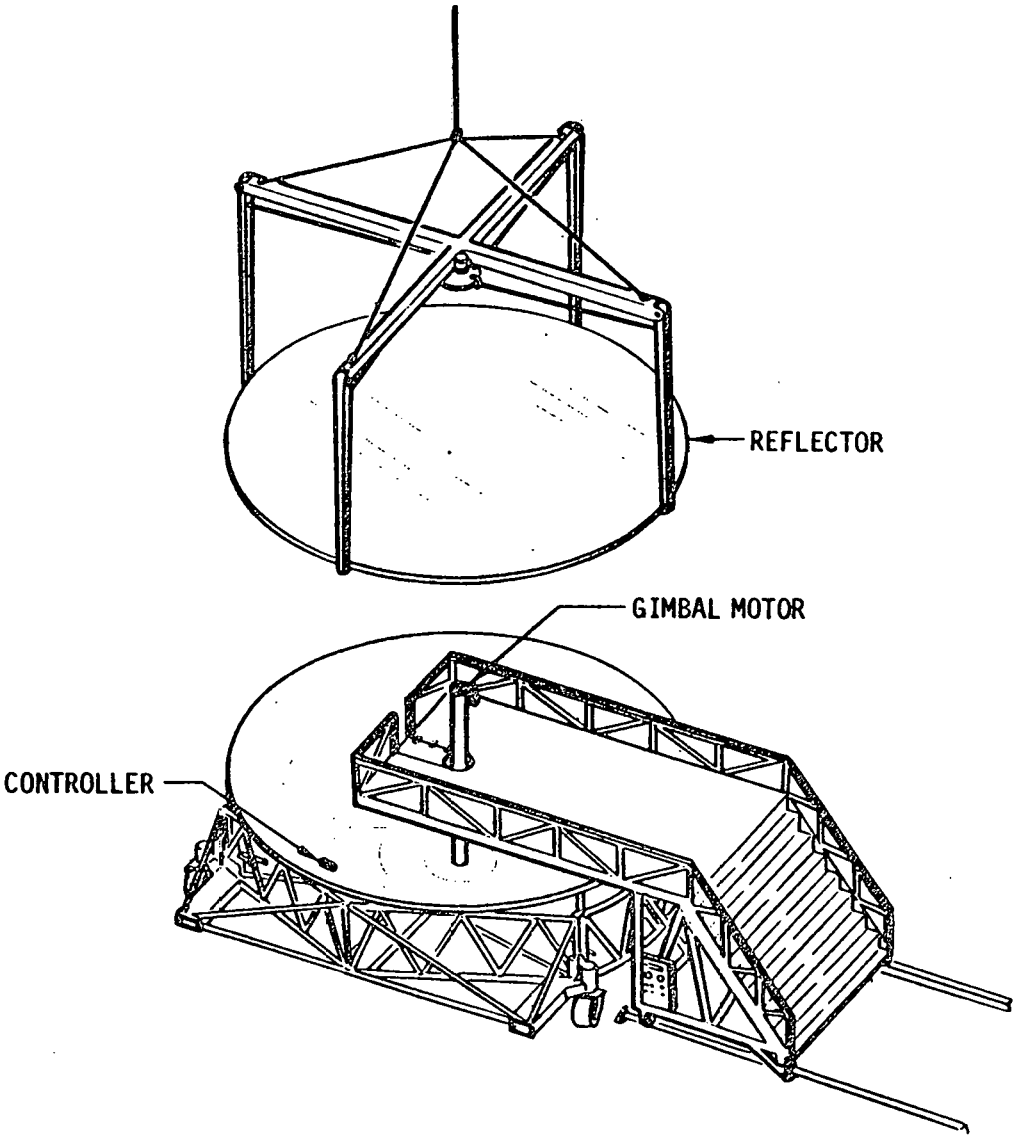

Figure 3.1-10 Reflector Installation

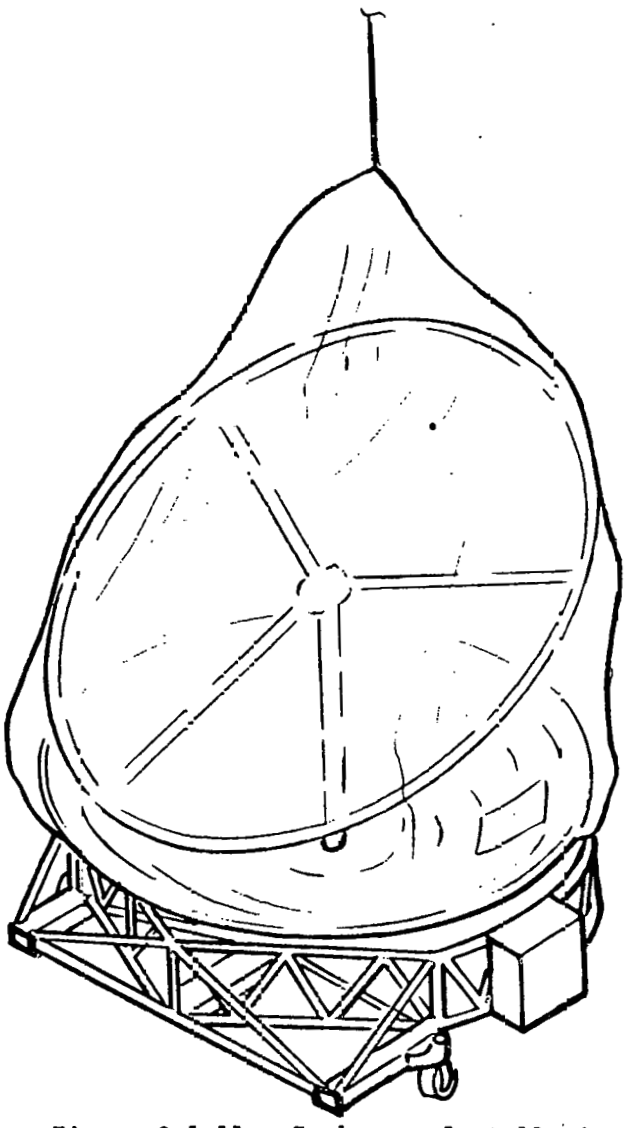

Figure 3.1-11 Enclosure Installation

3.2 HELIOSTAT INSTALLATION CONCEPT

Heliostat foundations are installed at the surveyed locations in the field. The foundations consist of reinforced augercast concrete piling. Three pilings interface with the base stanchions and a center piling interfaces with the pedestal. The Lee Turzillo Contracting Company has provided an analysis and design of the automated equipment for installing the piles. The equipment consists of a drill platform mounted on a motorized tractor vehicle, and a companion vehicle which carries the grout mixture and provides the pumping capability. This equipment is illustrated in Figure 3.2-1. One set of this equipment, drilling and grouting four piles simultaneously, is capable of installing 40 heliostat sets of piling in an eight hour shift. A follow up vehicle will install and level the reinforcing steel and capping plates. (Figure 3.2-2). This foundation concept is adaptable to varying soil conditions and requires a minimum of site preparation. The 1/4 to 1/3 yard of soil drilled from each pile will be spread over an approximate six foot circle, requiring no removal of excess soil. After appropriate cure, the pilings are ready for heliostat installation.

The factory assembled, functionally checked, and internally clean heliostat arrives at the site from the production/assembly facility over plant dedicated roads. This vehicle and transport fixture is shown in Figure 3.2-3. The fixture is that utilized in the plant assembly process. It provides a clamping support to the pedestal for support during transit and installation. The speed of this vehicle should be in excess of 20 mph on prepared interconnecting roads, and approximately 5 mph over the rough graded site. The transporter vehicle provides axial movement up to 18 inches in the horizontal plane to precisely interface the heliostat with the piling. A vernier control in the vertical plane will provide a shock free lift power capability. The heliostat and fixture is lowered until contact is made between the pedestal, stanchions, and the four steel piling caps. A verticality check is made

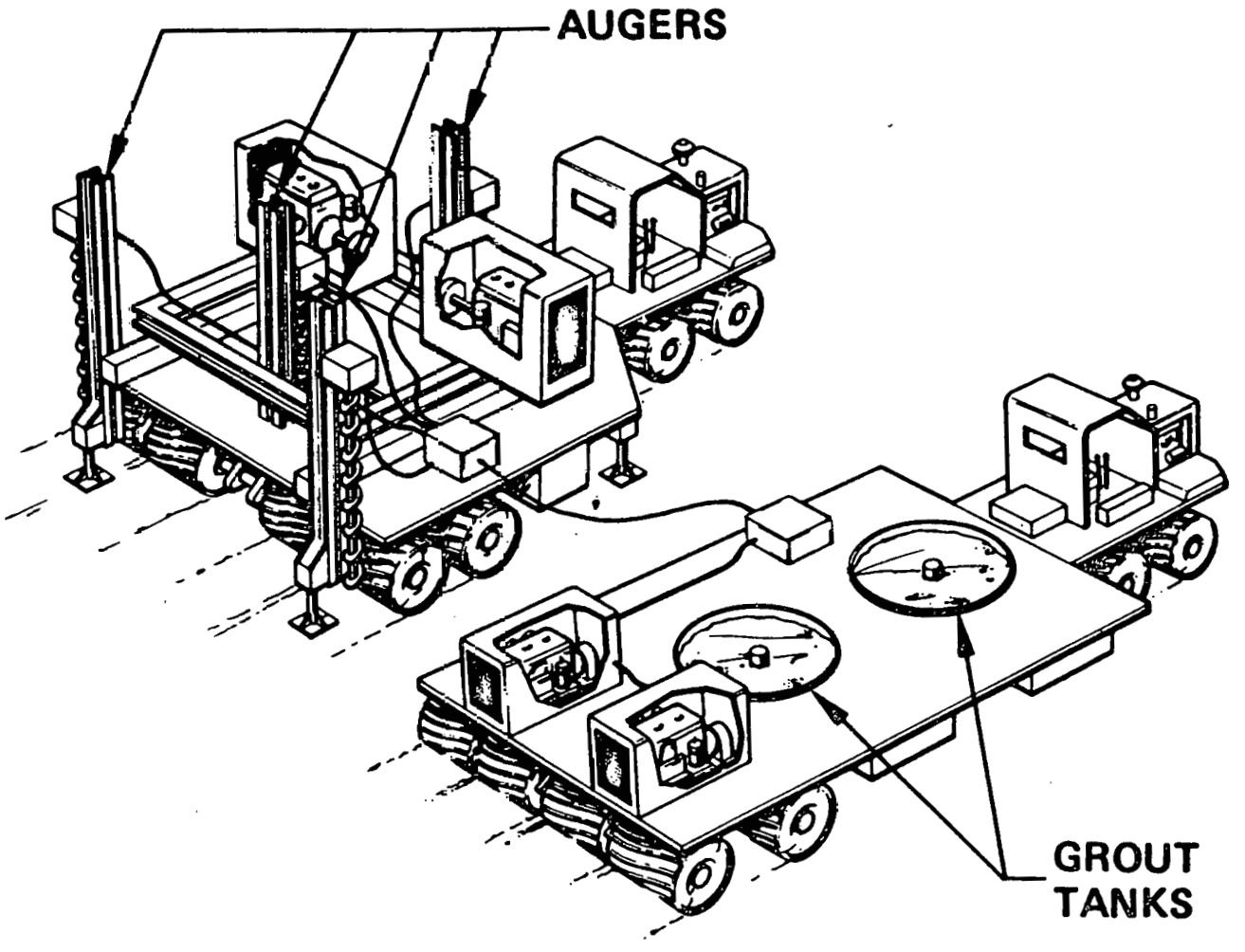

Figure 3.2-1 Auger cast Piling Installation Equipment

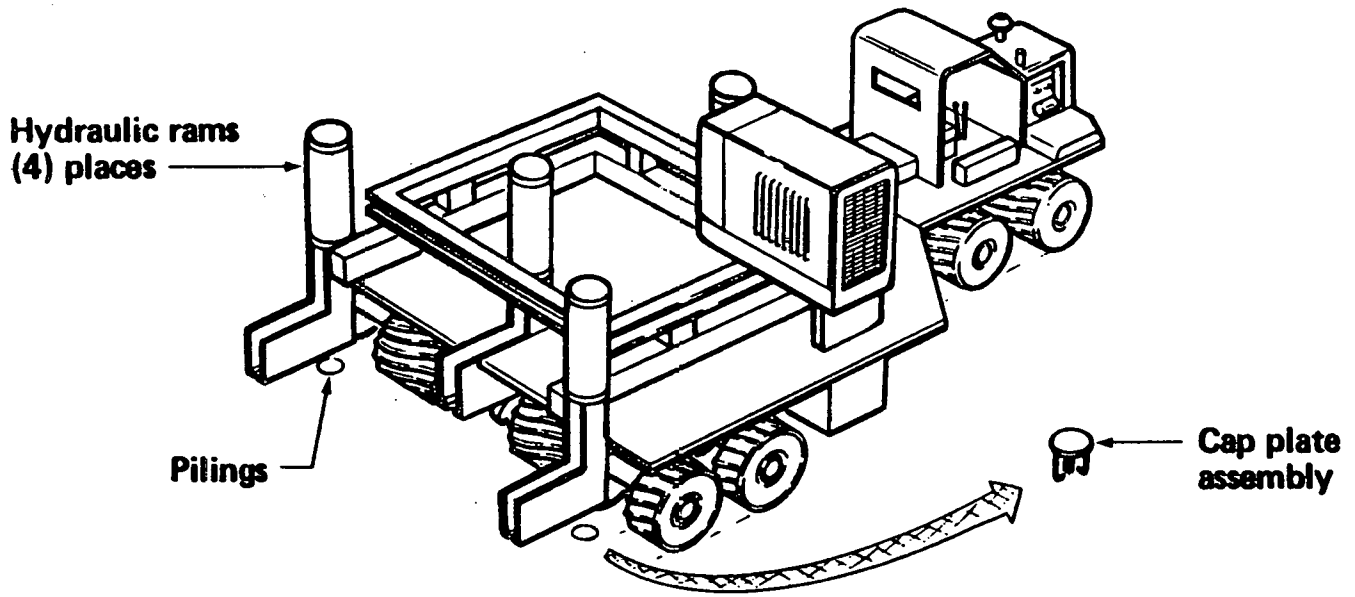

Figure 3.2-2. Cap Plate Placement & Leveling Station

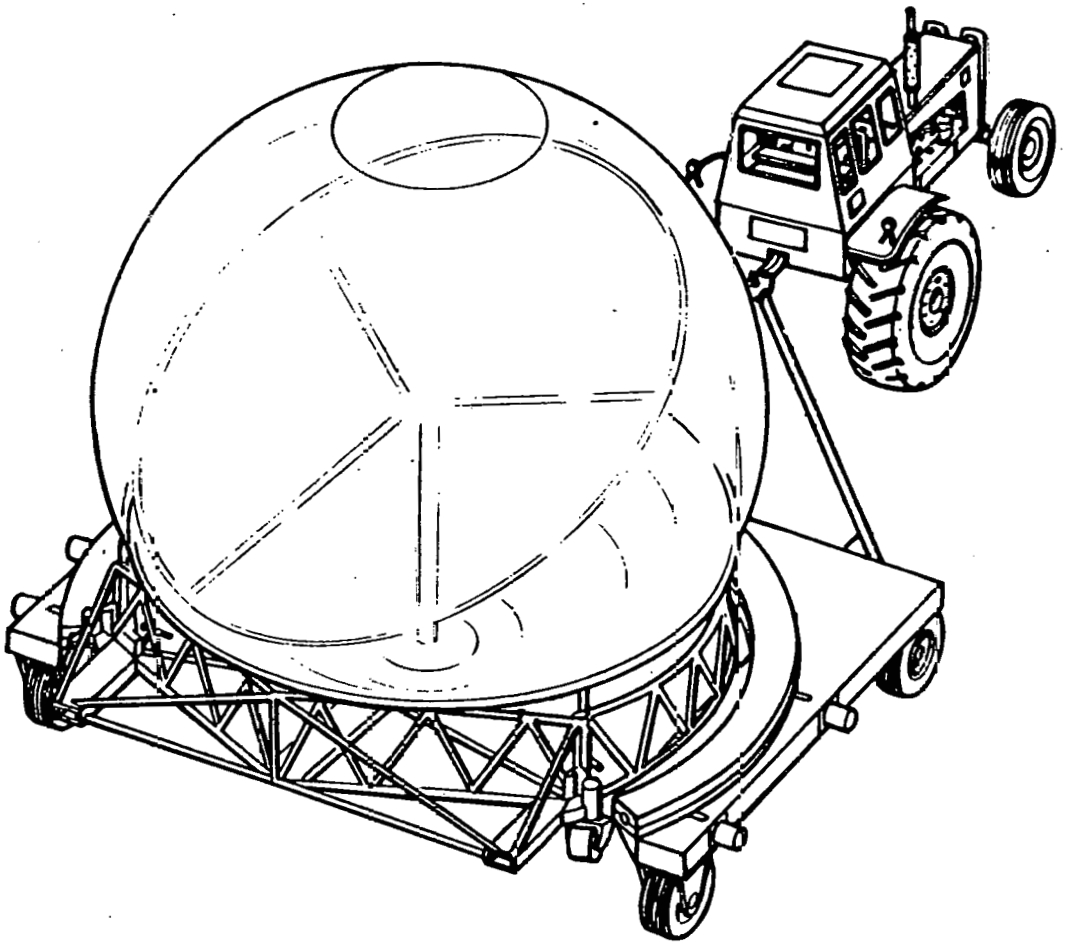

Figure 3.2-3. Heliostat Transporter

to assure the pedestal is properly aligned before arc welding the pedestal to the piling cap plate. The three stanchions are now welded to their cap plates. The power connection to the blower is transferred from tractor power to field power. The assembly fixture is now removed from the heliostat, returned with the transporter vehicle to the factory, and recycled into the production line.

The power and signal wiring connection is now made to the heliostat controller, the ground connection made, and the heliostat is ready for functional checkout and alignment processes.

4.0 MAINTENANCE CONCEPTUAL DESIGN

This section describes the conceptual design of key maintenance processes and equipment, and provides details of the supporting cost trade studies which were conducted to select the preferred designs. Table 4.0-1 presents the analyses performed by major heliostat assembly.

TABLE 4.0-1

ASSEMBLY	A N A L Y S I S
Enclosure	Evaluation of cleaning approaches. Water cleaning assumed for all concepts. Four concepts in current trade study: (1) Self-contained mobile washing machine. (2) Centrally supplied mobile washing machine. (3) Overhead sprinkler system with central supply. (4) Individual enclosure wash units (flood type) with central supply. (5) Combination of (2) and (3) above. Scheduled replacement. Time/motion analysis to estimate man and machine requirements based on a 15-24 year replacement cycle.
Reflector	Analysis of dust accumulation over heliostat lifetime to determine need for cleaning. Near zero leakage heliostat.
Gimbal	Equipment concept for gimbal maintenance: (1) Van with airlock/ladder modifications. (2) Temporary reflector support used during gimbal replacement.
Controls	Cost/technical trade to assess increasing high maintenance component MTBF's. Study to determine location of heliostat controller (HC) outside or inside heliostat. Equipment concept for replacement of HC, if located inside.
Air Supply	Low leakage rate 0.006 m^3/min (.2 CFM) heliostat design has been selected. Ultra-high filtration system used to assure cleanliness of reflector has been studied. Individual heliostat blower versus central air supply system was evaluated for technical feasibility and cost benefits. Air bearings and other long life bearings for blower were considered to increase blower MTBF.

4.1 PROTECTIVE ENCLOSURE CLEANING

Experience has shown that the external surface of the enclosure will gradually become contaminated to the extent that a reduction in specular transmittance will be realized. Analytical and experimental work has been performed in an attempt to quantify the extent of reflectance loss with time and determine acceptable ways to clean the surface.

A literature search was conducted to seek out ways to clean plastic films utilizing techniques other than with water. No techniques were found that appeared applicable to the enclosure concept at this time.

Experience by Boeing with the research experiments heliostats and others with glass mirrors (Ref. 4.1-1) were utilized in the selection of the four cleaning techniques and preparation of parametric charts.

Work performed at the Solar Thermal Test Facility (STTF) and at Triton Corporation of Houston, Texas, reported by R.S. Berg (Ref. 4.1-1), showed that high pressure water spray (above 500 psi at nozzle) successfully cleaned glass mirrors. The high pressure sprays recovered up to 95% of the reflectance loss from dirt accumulation. Washing experiments by Boeing on the research experiment heliostats at Boardman, Oregon using a John Deere Model A18, 500 psi commercial spray machine produced visually clean heliostats. The same machine used on a coupon of Tedlar exposed in the desert, produced complete transmittance recovery (measured on Boeing Beckman DK-2 Specular Transmittance Instrument).

Preliminary tests on Research Experiment heliostats showed that approximately 50 gallons would be required to pressure wash a 5.18m (17 ft.) diameter enclosure. This suggests that about 200 gallons may be required for washing 9.7m (31.8 ft.) enclosures.

Berg suggests that frequent rinsing (possibly with detergents) at intervals less than two weeks may be effective in removing contaminants from glass. Frequent rinsing removes dirt before strong chemical or mechanical bonds can develop. It is believed, based on observations of domes exposed to occasional rains, that rinsing will be effective on plastic as well as glass. Rinsing of a 30 foot enclosure is estimated to require about 50 gallons if low pressure top to bottom spraying or flooding is employed.

Four water cleaning equipment concepts were selected for evaluation and are discussed below. These concepts are shown in Figure 4.1-1. Cost trade studies of labor and equipment have been performed and are presented parametrically.

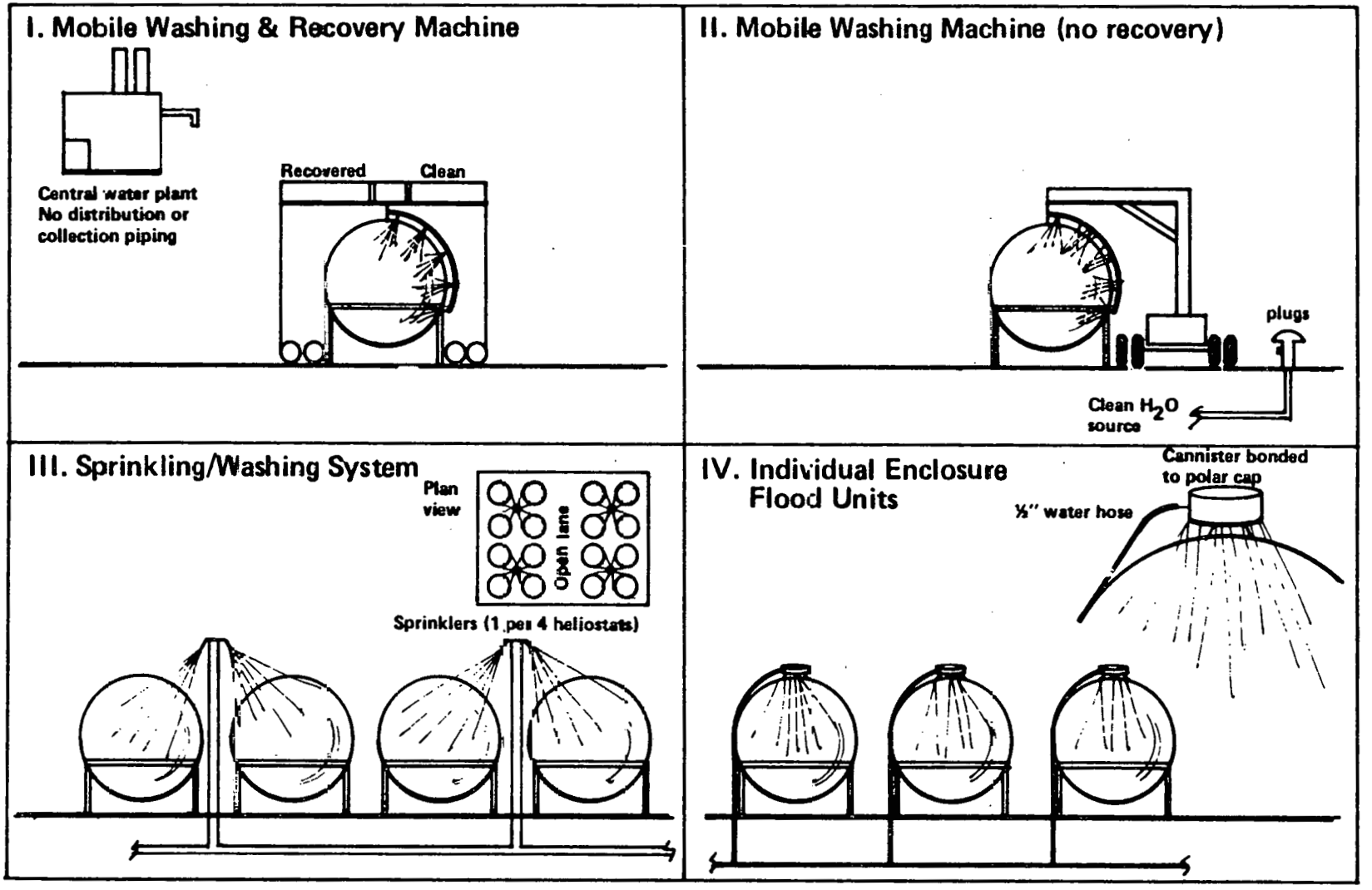

Figure 4 1-1. Heliostat Washing Evaluation Concepts

4.1.1 Self Contained Mobile Washing Machine (Concept I)

The mobile washing machine as shown in Figure 4.1-2 is considered for dome cleaning. When used for cleaning it would be equipped with hemispheric arms containing rows of nozzles which sweep around the dome and clean the surface. Self contained tanks would provide water and/or cleaning solution if required, and recover residue for later filtering and reuse. This machine requires two men to operate. Cleaning experiments at Boeing were conducted on a Boardman heliostat enclosure to obtain data on nozzle-to-enclosure configuration, nozzle sweep rate across dome surface and water consumption.

The analysis of the test data leads to the following:

3 minutes to wash one heliostat
5 minutes to move and set up between heliostats
2 minutes/heliostat for tank draining and filling

10 minutes/heliostat cleaning time.

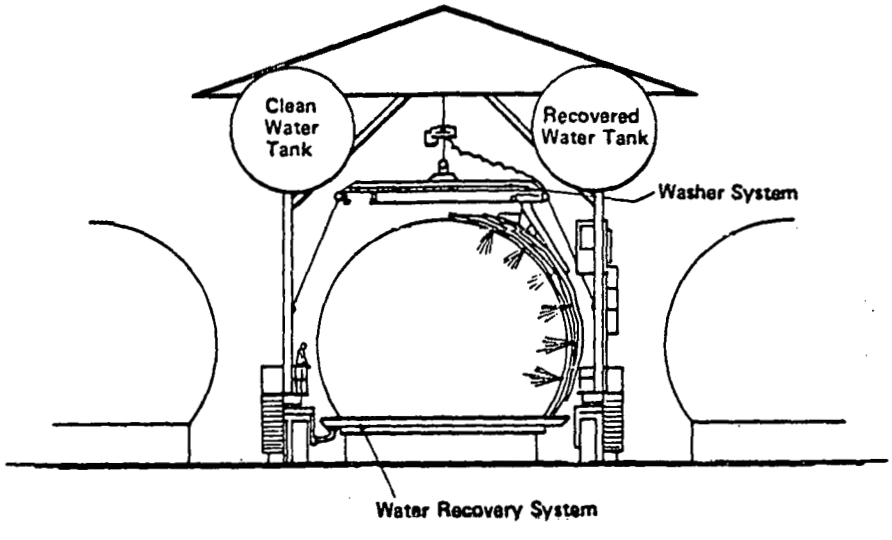

Figure 4.1-2. Self-contained Mobile Cleaning Facility (Concept I)

4.1.2 Centrally Supplied Mobile Washing Machine (Concept II)

This concept employs the same basic approach to cleaning as Concept I; i.e., hemispherical rotating arm with pressure spray nozzles. However, a simpler basic chassis is involved and no water storage tanks are included (Figure 4.1-3). Wash water is supplied from a central supply through piping and hydrants in the heliostat field, or a water trailer towed behind. Long hoses are used between the hydrant or trailer and washer. No provision for water recovery is included.

The washing time per heliostat, hence annual labor cost of this machine is expected to be about 80 percent that of Concept I because of no tank empty and fill cycle. The cost per machine is expected to be considerably less.

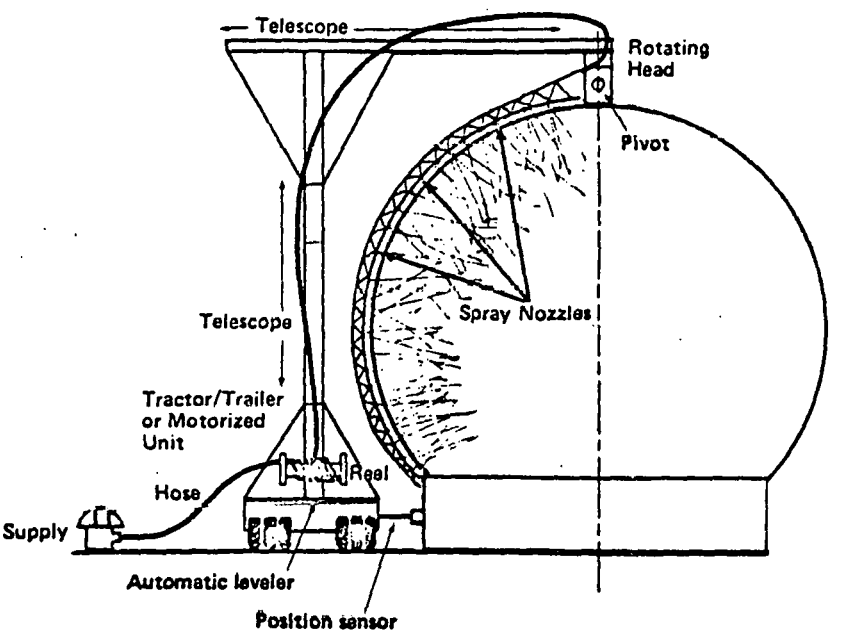

Figure 4.1-3. Washing Concept II

4.1.3 Sprinkler Washing System (Concept III)

This concept is based upon experience and studies (Reference 4.1-1) that indicate frequent rinsing may provide satisfactory cleanliness. The approach employs a high standpipe located centrally between four heliostats. At the top of the standpipe is a set of four spray nozzles that direct rinse water onto four enclosures. The water runs down the side walls of the enclosure carrying away dust contaminants. It is assumed that because of the short duration between rinsing cycles, bonding between dust particles and the enclosure is weak and easily overcome.

The actual rinsing frequency will have to be determined by experimentation. The concept has the additional feature of being able to rinse immediately after dust storms or light rains, thus, maintain high plant availability. It would likely have higher water usage than concepts I and II but be much less labor intensive.

4.1.4 Individual Flood Units (Concept IV)

The approach described here is quite similar in most respects to the sprinkler system of Concept III, except that water is dispensed directly on the polar cap of each enclosure. The water and labor requirements are essentially the same. It would also employ the principle of frequent rinse. The potential advantages over the sprinkler system are; slightly lower water usage due to over-spray losses, and no access lane blockages for sprinkler risers. A feasibility test would be required.

4.1.5 CLEANING CONCEPT SELECTION

Recognizing that further cleaning and contamination accumulation experiments need to be conducted on heliostats in a typical environment before final choices are made, it was necessary to make a preliminary selection to develop commercial plant cost estimates. To aid in the selection process, two sets of parametric curves were constructed. The purpose of these curves was to provide cost and water consumption comparisons of the various cleaning concepts or possible combinations of any two concepts.

Figure 4.1-3 shows water usage per year versus rinsing frequency for various washing frequencies. From this chart one can compare washing methods I and II and rinsing method III, or a combination of washing and rinsing. (Method IV although not shown closely approximates method III in water consumption.) The cost of water will be largly site dependent and was not included in this analysis or the cost analysis in Volume III.

Figure 4.1-4 shows relative equipment and labor cost versus rinsing frequency for various washing frequencies. Again, comparisons can be made for concepts I, II and III or a combination of two concepts.

From Figures 4.1-3 and -4, one can select equipment and labor costs and water requirements for 0 to 6 washes per year (by either of 2 methods), up to 52 rinses per year or any combination of wash and rinse frequencies. Since it is not known which of these methods or combinations will be technically and economically preferred, sample cases of concepts I, II, III and a combination of II and III were taken from Figures 4.1-3 and -4 and shown in Table 4.1-1.

The washing concept cases selected for comparison assumed six washes per year. For the sprinkler system case, weekly rinsing was assumed. The selected combination case was for a weekly rinse and an annual wash. (This latter case is based upon uncertainty as to whether sprinkler cleaning alone can prevent long term build-up of contaminates.) From Table 4.1-1, it can be seen that washing machines are labor intensive while sprinkler (or flood) systems are capital cost and water intensive.

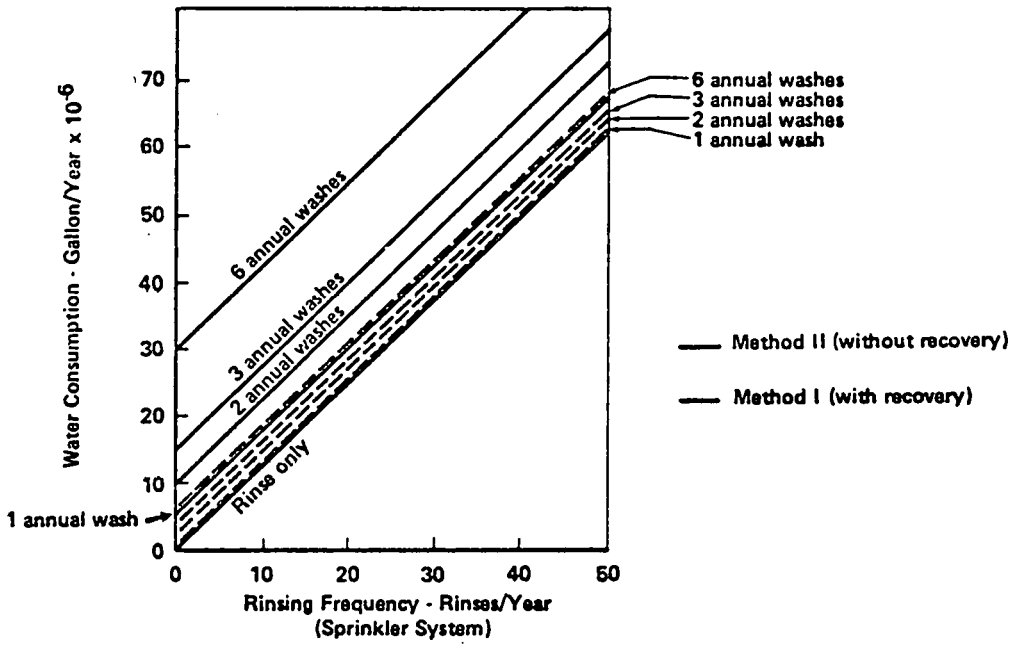

Figure 4.1-3. Water Consumption vs Washing/Rinsing Frequency

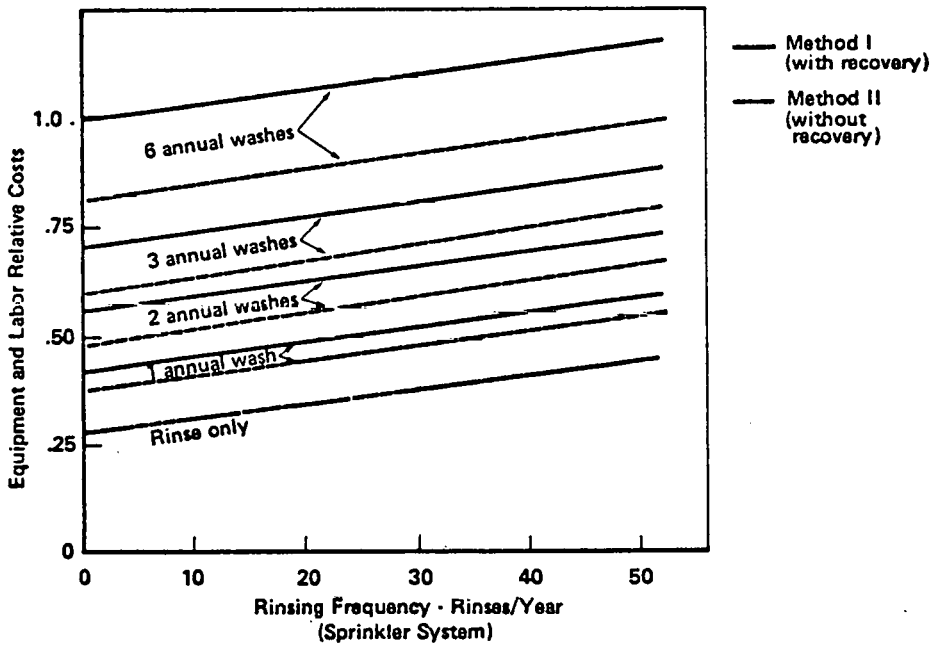

Figure 4.1-4. Relative Equipment & Labor Costs vs Washing/Rinsing Frequency

TABLE 4.1-1

ENCLOSURE CLEANING COST ANALYSIS

Concepts	Relative Costs Normalized to Concept I			Cleaning H_2O Usage Gal/Yr.	Concept Merit	Comments
	Special Equip.	Labor	Total			
I Mobile Unit w/Recovery	.05	.95	1.0	$5x10^6$	1	6 washes/year, 3 machines, 2 operators.
II Mobile Unit w/o Recovery	.03	.76	.79	$30x10^6$	1	Same as above, but fewer labor hours because of no recovery operations.
III Sprinkler System	.19	.06	.25	$65x10^6$	2	Weekly rinse; piping, sprinklers, installation and one man full time maintenance.
V Combination of II & III	.20	.18	.38	$70x10^6$	Selected	Weekly rinse, annual wash. Sprinkler system one man full time one washing machine, 2 operators.

1 Cleaning concept proven; frequency expected to be adequate.

2 Concept requires minimal development, may have long term residue build up.

The combination approach was selected for pricing purposes, and as the preferred method until more data and experience is available. The approach is technically appealing because it provides the ability to rinse the entire field immediately after dust storms or light rains; inhibits graduate dust accumulation; and provides for a thorough wash annually with a single machine in the event it is required. Economically, the combination approach provides lower maintenance costs than the washing machines, but somewhat higher costs than the sprinkler system alone.

4.2 PROTECTIVE ENCLOSURE REPLACEMENT

Previous analysis of enclosure material life indicated that enclosures would have to be replaced once in 30 years. The replacement would start near the 15th year and require completion by at least the 24th year. Two concepts were considered for enclosure replacement:

(1) return of each heliostat to a factory building

(2) use of a mobile facility that straddles the heliostats, removes old enclosures and installs new ones on site.

Replacement of enclosures in the factory building would involve the following operations:

(1) Serially remove a row of approximately 125 and transport to factory for enclosure replacement.

(2) Transport refurbished unit to field.

(3) Locate and place unit.

(4) Pick up old unit from adjacent row.

(5) Transport old unit factory.

(6) Offload old unit and pick up refurbished unit.

Mechanical and electrical disconnection and reinstallation operations, as well as factory refurbishment work, would be performed in parallel with the above transporter functions. Welder, electrician, mechanic, operator and possibly alignment technician skills would be required.

Figure 4.2-1 is a conceptual schematic of the specialized mobile facility required to move through the field, remove old enclosures and install new ones. The facility straddles a heliostat, encloses it for wind protection, while removal and installation operations

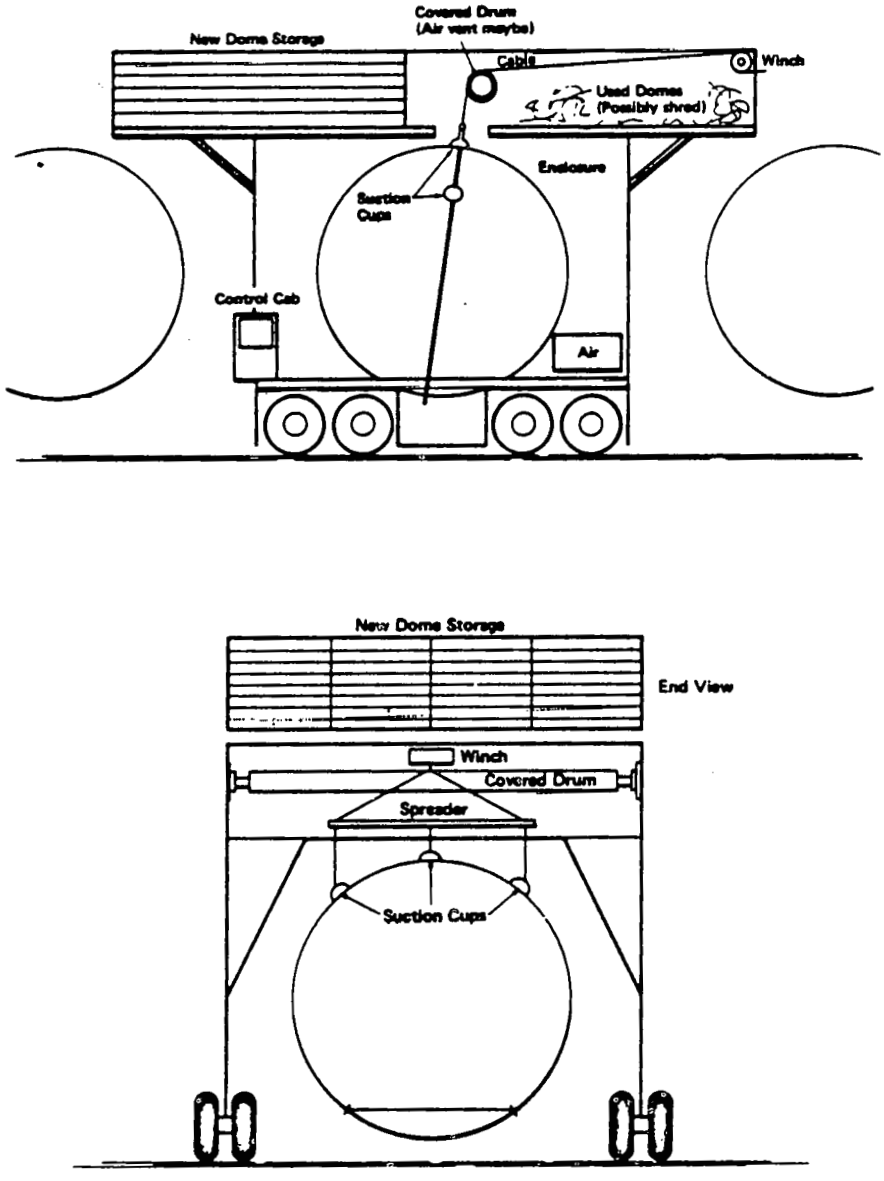

Figure 4.2-1. Enclosure Replacement Facility

proceed. Twenty to thirty new enclosures are stored folded in a storage loft on top of the unit. A winch and roller system are used to move enclosures about. The enclosure is lifted with a multiple suction cup and spreader array attached to the winch cable. Used enclosures are compacted or shredded to minimize spacial requirement in the loft. Two such machines would complete the enclosure replacement in about 5 years. This machine would also be useful for replacement of the small number of accidentally failed enclosures randomly occurring during the 30 year plant life.

A cost analysis of these two approaches was made. Replacement in a factory building is considerably more labor intensive but requires no new equipment. The in-field approach is less labor intensive but requires 2 specialized machines. The analysis results showed that the factory approach would be the more expensive by 32%. Accordingly, the mobile facility approach is recommended as the commercial plant concept.

4.3 REFLECTOR CLEANING AND REPLACEMENT

The enclosure design provides for near-zero air leakage. A flow rate of 0.0006 m^3/min (0.2 cfm) is predicted. An analysis of the particulate contamination transport into the enclosure and the subsequent selection of ultra-high quality filtration provides assurance that reflectance losses will remain less than 5% in 30 years. (See Section 2.3.3). If the reflectance loss after 15 years has reached an unacceptable amount, cleaning of reflectors can be accomplished during enclosure replacement operations. Experience gained during previous research showed that distilled water rinse, pressurized water spray and air wash all provided considerable cleaning effect.

4.4 GIMBAL ASSEMBLY MAINTENANCE

A design goal was established early in the program to eliminate the requirement to enter the heliostat for maintenance purposes. As a result of this goal, a gimbal/actuator design was selected which allowed placement of associated electronics on the base shell for ease of maintenance. For unscheduled maintenance on gimbal/actuator mechanical components, an access hatch has been included in the base shell design. Figure 4.4-1 illustrates the heliostat maintenance van which has been designed to perform gimbal maintenance, heliostat controller replacement and enclosure repairs. The cargo section is sealed and equipped with a blower for pressurization. The rear entry is equipped with an air bag that can be extended and connected to the heliostat base door penetration. When the cargo section and air bag are pressurized to 0.067 N/cm^2 (0.1 psi) the door can be removed. Heliostat electronics, which are mounted on the inside of the door, can be serviced without entrance to the heliostat. Gimbal mechanical component maintenance is performed via the boom/ladder apparatus shown in Figure 4.4-1. This apparatus allows the worker to enter and climb up to the gimbal without any contact with the enclosure, base shell, or pedestal. The vehicle is a standard utility van with modifications to make it reasonably airtight, blower unit w/filter, hydraulic controlled extension boom, 8-10 foot extension ladder with special attachment fittings, and possibly some ballasting and suspension stiffening.

Maintenance of mechanical components will be performed by removal of the unit, replacement and then repair of the malfunctioning unit at the maintenance depot. Figure 4.4-2 shows the tool used to support the reflector while the exchange takes place. The tool simply grips the pedestal directly below the gimbal, supports the reflector by its spokes near the center hub, and lifts the reflector upward a fraction of an inch when support arms are rotated to an off-center lock position. The fasteners at both interfaces have been loosened several turns prior to the lifting step. Removal and replacement of the gimbal is now accomplished.

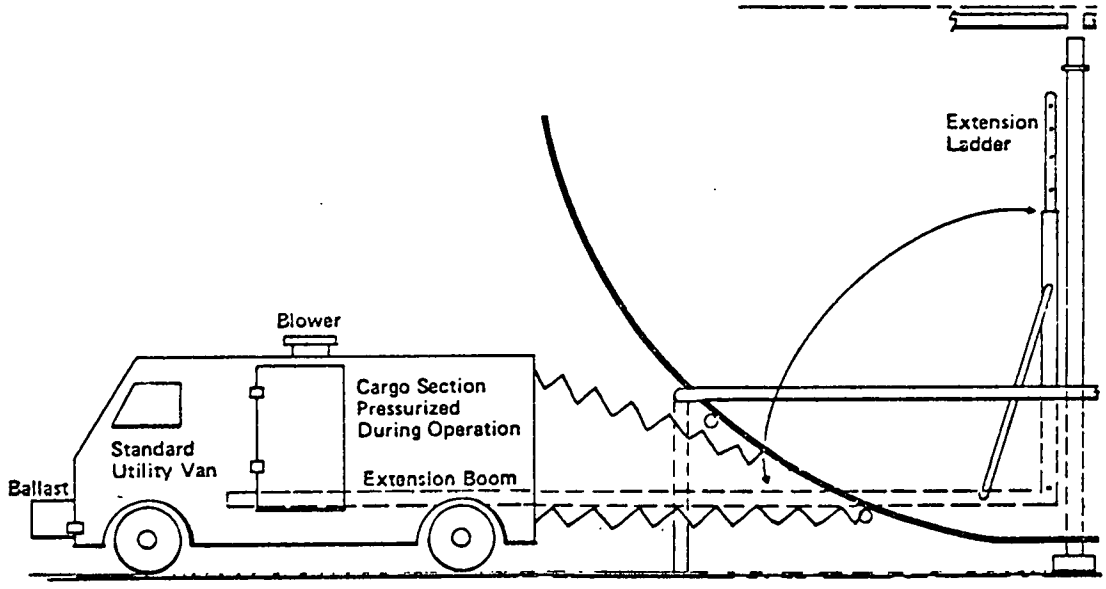

Figure 4.4-1. Heliostat Maintenance Van

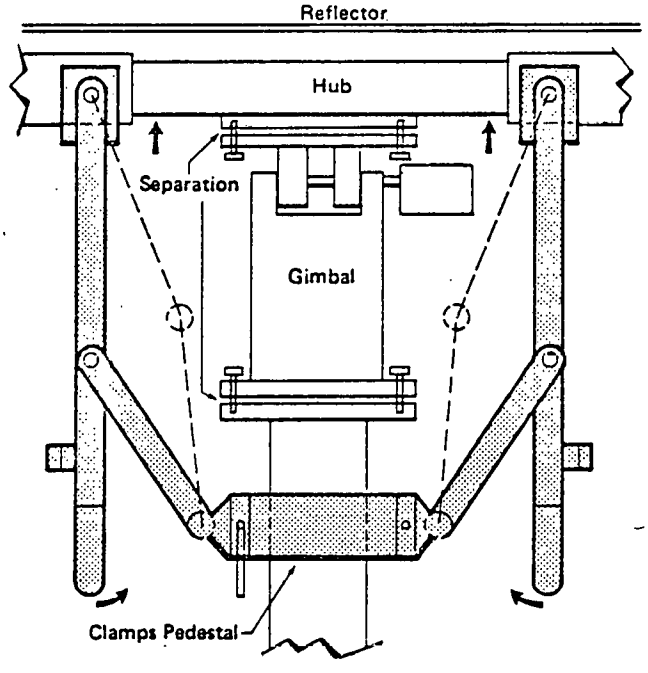

Figure 4.4-2. Gimbal Removal Tool

4.5 CONTROL SYSTEM MAINTENANCE

A cost trade study was performed to assess the possibility of increasing electronic component MTBF's. The heliostat controllers are of particular interest by virtue of their large number. Table 4.5-1 lists components of the heliostat controller, the failure rates determined in previous work and failure rates recently determined for higher quality equivalent components. As can be seen, the net effect is an overall failure rate decrease of 26 failures per million operating hours (MTBF improvement of 16.2 years) is realized. This improvement is at a cost which was traded off against labor savings. The cost analysis revealed that the high reliability parts were more cost effective than the commercial parts by a ratio of 3.9.

A study was made to determine whether the heliostat controller should be placed inside the enclosure with minimal packaging, or outside the enclosure with weather-proof packaging and forced cooling provision. Inside placement would rely upon natural convection cooling. To perform this analysis, the costs associated with the outside packaging and cooling blower had to be traded against the added labor costs due to opening and entering the enclosure. By mounting the controller on the inside of the hatch and utilizing the maintenance-van airlock system described earlier, it was found that the time for removal was only slightly greater than for removing the components from an outside-mounted weather-tight sealed box. The cost of the weather-tight sealed box would outweigh the few minutes labor savings, especially in view of the low number of replacement operations performed over the plant life.

4.6 AIR SUPPLY MAINTENANCE

Selection of a low-leakage enclosure design significantly decreased air supply maintenance costs. The reduced air flow resulted in extending replacement intervals to five years for the pre-filter, and once in 30 years for the primary filters. These filter replacement intervals are based upon the contamination analysis described in Appendix C.

TABLE 4.5-1

FAILURE RATE/MTBF HELIOSTAT CONTROLLER

COMPONENT	NO. REQ.	COMMERCIAL PARTS PART NUMBER	FAILURE RATE $X10^{-6}$ (F/MOH) EACH	TOTAL RATE $X10^{-6}$ (F/MOH)	HIGH RELIABILITY PARTS PART #	FAILURE RATE $X10^{-6}$ EACH	TOTAL	SOURCE OF INFORMATION
Integrated Circuits	12	CD4000 AD	.145	1.74	M98510/05503BEX	.036	.472	(1) B-1
Integrated Circuits	5	SN 5400	.145	.725	MS8510/00302BCB	.0185	.0925	(1) 206,B-1 Q
Capacitor-Ceramic	13	CK	.22	2.86	M39014/01-13--	.00013	.002	(1) 411,C-2-4
Capacitor-Electrolytic	2	CE	.41	.82	M39003/01-2977	.002	.004	(1) 401,C-2-6
Resistor	1	RN	.017	.017	-	-	.017	
Resistor	75	RC	.01	.75	-	-	.75	
Transformer	1	182-11380-2	.066	.066	-	-	.066	
Inductors - Filter	2	P53-4, -10	.063	.126	-	-	.126	
Zener - Diode	4	IN971B,IN746A	.8	3.2	Like JANTXIN78286	.03	.12	
Voltage Comparator	2	LM 111	.24	.48	-	-	.48	
Triac	1	T2300B	.8	.8	-	-	.8	
Diac	1	D32024	.8	.8	-	-	.8	
Transistor	8	80278	.9	7.2	JANTX2N3741	.006	.048	(1) 309,C-5
Crystal OSC	1	20A0111	.2	.2	-	-	.2	
Relay	1	1A012	.6	.6	-	-	.6	
*Switch	1	PIP-8	.57	.57	-	-	.57	
Micro Processor	4	8000 Series	.2	.8	-	-	.8	
Power Supplies	2	-	5.0	10.0	-	-	-	
Fuse	1	-	.1	.1	-	-	.1	
Power Supply	-	-	-	-	-	-	-	
Transformer	1	-	-	-	Similar to B-1 C & D	.1	.1	
Capacitor-Electrolytic	-	-	-	-	M39006/01-3037	.064	.195	
Capacitor-Ceramic	3	-	-	-	M39014/01-13--	.00013	.00039	
Transistor	1	-	-	-	JANTX2N3741	.012	.012	
Zener	1	-			JANTXIN38286	.03	.03	
Diodes	6	-				.03	.12	
Resistors	5	-				.017	.085	
	TOTAL FAILURE RATES			31.854			5.77	
	MTBF			3.59 Yrs.			19.8 Yrs.	

The blower selected is a positive displacement rotary-vane compressor, equipped with 30-year-life sealed self-lubricating bearings. The only parts that will require replacement are the compressor vanes which have an estimated MTBF of 20 years. This results in the requirement to replace the vanes in all blowers once in the plant life. This approach was the least expensive in terms of initial cost, maintenance labor and parts, of the concepts studied.

A cost and technical evaluation of a central air supply system was conducted for comparison against the individual blower concept described above and in Section 2.3.3. This central system would employ a compressor station (or stations) with filtration and humidity control also centralized. The clean dry air would be fed to the individual heliostats through a system of piping laid in the same trenches provided for power and signal wiring. The low flow rate requirements make possible the use of small diameter and low-cost piping which is the primary capital cost driver of such a system. The attractiveness of this system lies in the maintenance of a single large blower and filter facility instead of a large number of individual air supplies.

Results of the labor and materials analysis of the two air supply systems show that the central system would cost about 22 percent more than the individual blower approach. The primary source of higher cost in the central system is the large quantity piping required. Therefore, the individual blower approach was selected for the commercial plant design.

5.0 REFERENCES

2.3.2.2-1 D277-10022-1, Collector Subsystem Detail Design Report, ERDA Contract EY-76-C-03-1111, Dated February 24, 1976

2.3.2.3-1 Design Manual for Spherical Air Supported Radomes (Revised), W. W. Bird and M. Kamrass, Cornell Aero Laboratory Report No. U. B. - 909-D-2 Rome Air Development Contract No. AF 30 (602)-976.

2.3.2.3-2 Heliostat Enclosure Wind Tunnel Test Performed At The University of Washington Aeronautical Laboratory (U.W.A.L.) See Collector Subsystem Final Report P.121.-135.

2.3.2.3-3 Uniform Building Code, International Conference of Building Officials, Whittier, California, 1976 Edition.

2.3.2.3-4 Hailstone Test Report, dated February 15, 1978 Performed under Contract EY-76-C-03-1111 (Modification No. A006)

2.3.4.2-1 D277-10047-1, Collector Subsystem Final Report SAN-1111-76-7 ERDA Contract E-(04-3)-1111, Dated August 15, 1977.

2.3.4.3-1 Design Response Spectra For Seismic Design of Nuclear Power Plants Regulatory Guide 1.60 U. S. Nuclear Regulatory Commission, December 1973

2.3.4.3-2 Strong Motion Earthquake Accelerograms; Digitized and Plotted Data; California Institute of Technology, Pasadena, California, September 197?.

2.3.6-1 D277-10053-3, Volume 3, Central Receiver Solar Thermal Power System Pilot Plant Preliminary Design Report. SAN-1111-76-8 Collector Subsystem, April 29, 1977 Reference Contract EY-76-C-03-1111.

4 1-i Heliostat Dust Buildup and Cleaning Studies;
R. S. Berg, Sandia Laboratories, Albuquerque, New Mexico.
Presented At Solar Central Power Systems Semi-Annual
Review Conference, March 2, 3, 1978
San Diego, California.

APPENDIX A

ALTERNATIVE GIMBAL/ACTUATOR DESIGNS

APPENDIX A

Berger-Lahr Concept

The Berger-Lahr concept is shown in Figure A-1. Both azimuth and elevation actuation assemblies are identical. Drive torque is provided by a 5 phase mini-angle stepping motor with bi-level drive control to reduce power consumption. Gearbox utilizes a 500 to 1 torsionally loaded spur gear system with zero backlash. The actuator outer housing with a compression coupling rigidly fixed to the actuator shafts provides a simplified gimbal design. A conventional optical shaft encoder provides position information. The Berger-Lahr concept has many good features but was eliminated from the present effort on the basis of cost and failure to meet encoder specifications.

Boeing Concept

The Boeing conceptual design shown in Figure A-2 is based on injection-molded filled-plastic technology. The design is executed using glass reinforced nylon (6-6) except for the drive motors and necessary wiring and bearings. This selection minimizes fabrication cost while providing excellent environmental qualities. The properties of nylon are used to advantage by eliminating lubrication requirements for the final drive assembly. This structure has good aging and stiffness characteristics with insignificant creep over long periods of time. Water absorption by nylon is not considered to be a concern for this application.

To minimize power, permanent magnet stepper motors were selected. This motor type does not require power unless it is in the process of moving to a new position. The holding torque is sufficient to maintain the mirror in the last commanded position. The motors are 24 VDC and were selected to minimize the operational power requirements.

All components were selected from commercial stock with MTBF comparable to state-of-the-art reliability.

Berger-Lahr Corporation

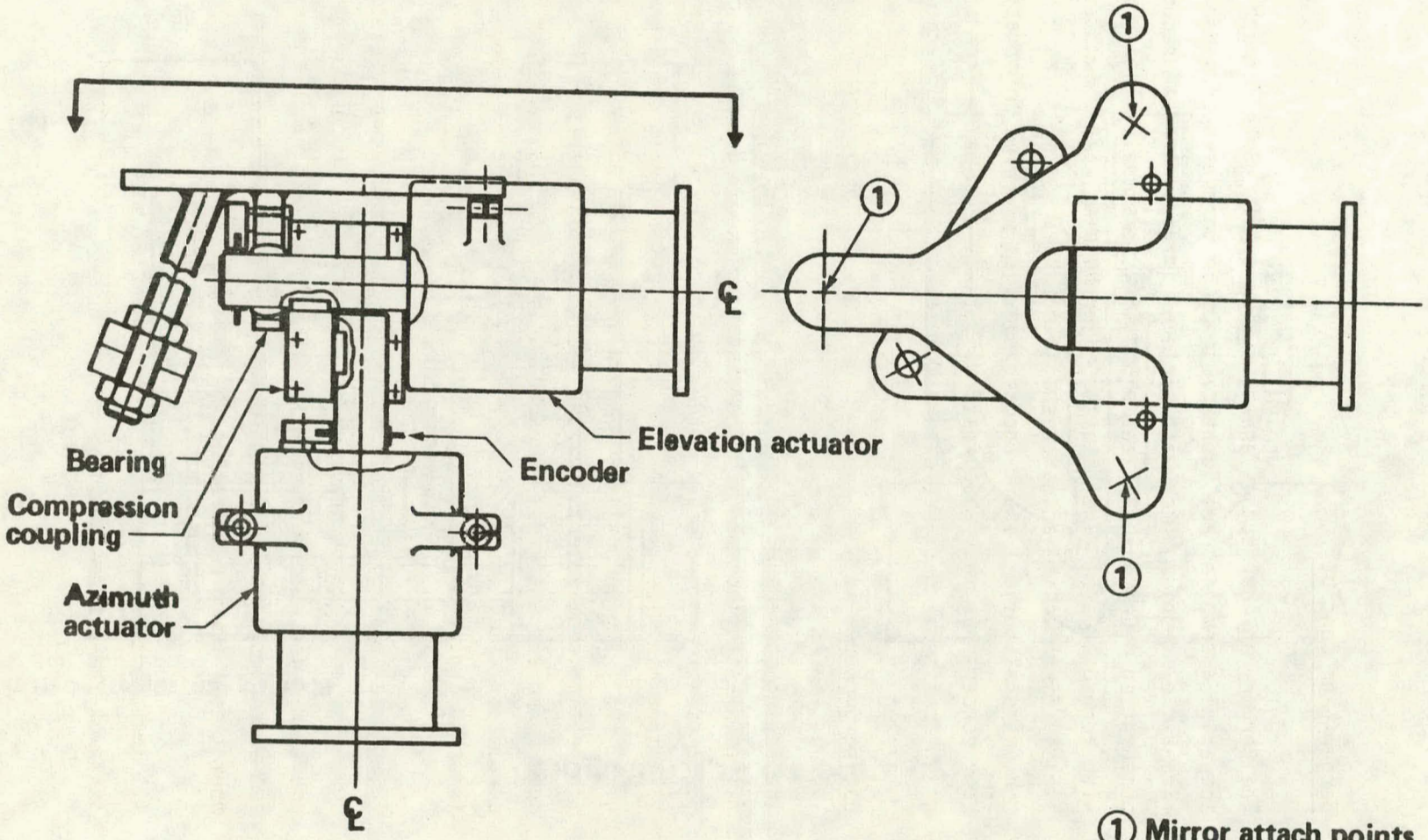

Figure A-1. Heliostat Gimbal/Actuator

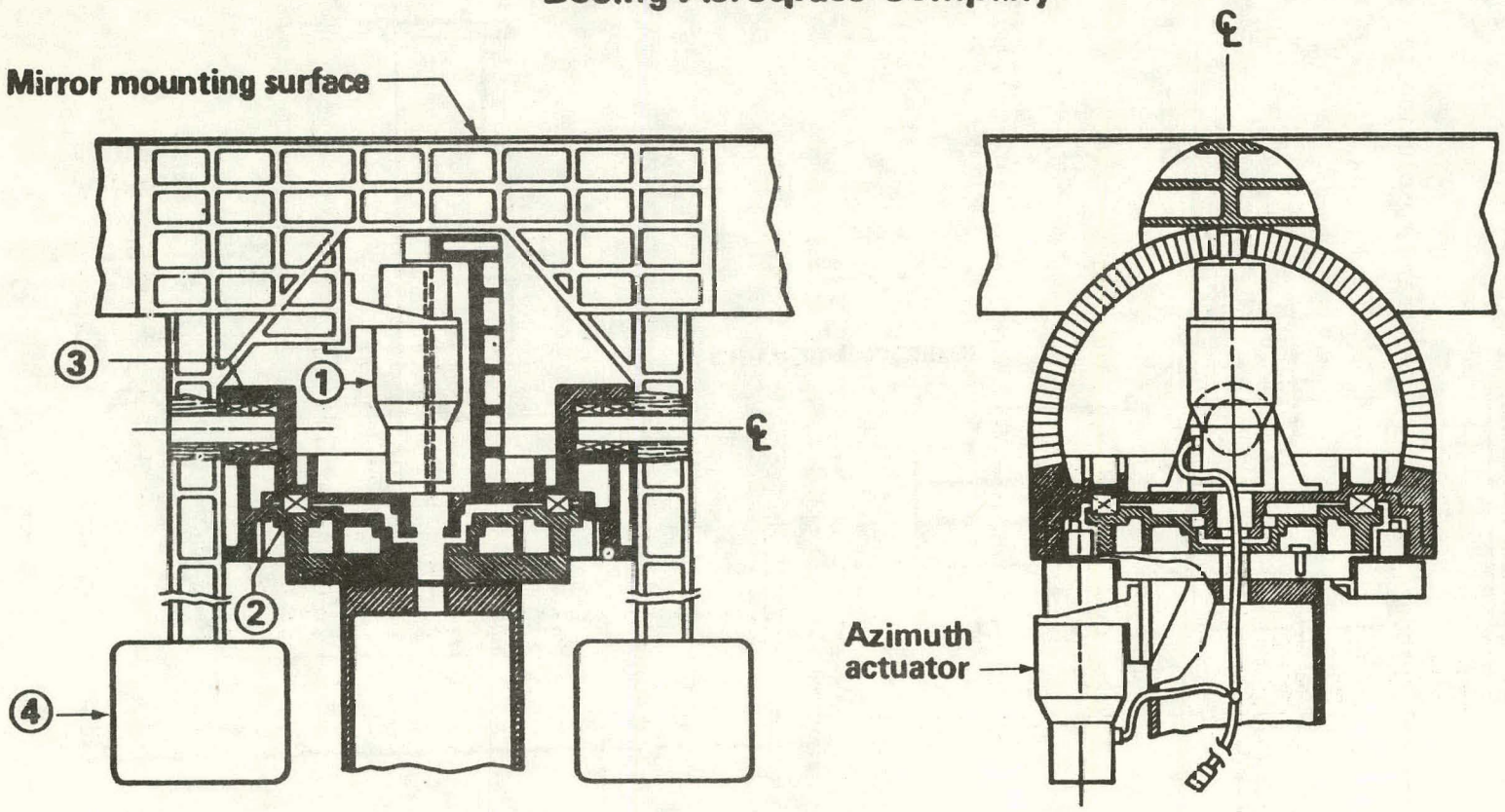

① Elevation actuator
② Azimuth bearing
③ Elevation bearing (typ.)
④ Counter weight

Figure A-2. Low Cost Injection Molded Heliostat Pointer/Tracker

The problems of perpendicularity and axis orthogonality are handled by shims and by trunion bearing adjustment. The current state-of-the-art in precision molding, is such that only minor misalignment problems are anticipated.

A low-cost 5 bit optical encoder provides the necessary resolution to provide a signal which is used by the controller to determine if the commanded step was implemented in the required time and in the proper direction. If the command was not implemented properly, the controller would reissue the command and again monitor the response. If this procedure is repeated a predetermined number of times without success, the tracker is declared inoperable, and a signal is provided to the main controller if necessary.

This design concept potentially could be very low cost and should be investigated in the future. The concept was not selected because of unknowns associated with performance, life expectancy, and rotational stiffness. Also, there are no provisions for mounting position indicating devices directly on gimbal shafts.

Sigma Instruments Concept

As an alternative to gear systems, Sigma proposed direct-drive stepping motors for elevation and azimuth (see Figure A-3). The proposed motor is an extrapolation of existing designs, with the following tentative specifications:

Steps/Revolution:	2,000 (microstepped to 64,000 steps/ revolution)
Torque:	10,000 oz. in.
Size:	15" D x 4.5" L
Weight:	200 lbs.
Power Consumption:	35 watts
Rotational Stiffness:	400 ft./lb/degree

The proposed motors would directly drive both axes.

Basically, the proposed motor achieves the desired accuracy by means of magnetic averaging; the structure would involve 500 rotor segments and 400 stator segments. With reasonable manufacturing control, the angular accuracy of such a system is far in excess of the individual mechanical accuracies of the rotor and stator segments.

In order to provide the required resolution, as well as extremely smooth motion, the motor is advanced by electrical division of each 0.18^{0} step into 32 increments. This technique is known as microstepping and requires electronic current control of the motor phases. Essentially, the logic drives operate a D/C converter to control the current ratio in the windings. In general, this technique results in very linear operation, but small errors in linearity due to motor characteristics can be compensated easily in the electronic system. The motor construction lends itself to the addition of a Hall effect incremental encoder, and this, plus a reference point, should satisfy the requirements of position information.

This "actuator" is not compatible with the current Boeing design. However, because of its inherent simplicity, it merits future consideration.

Sigma Instruments, Inc.

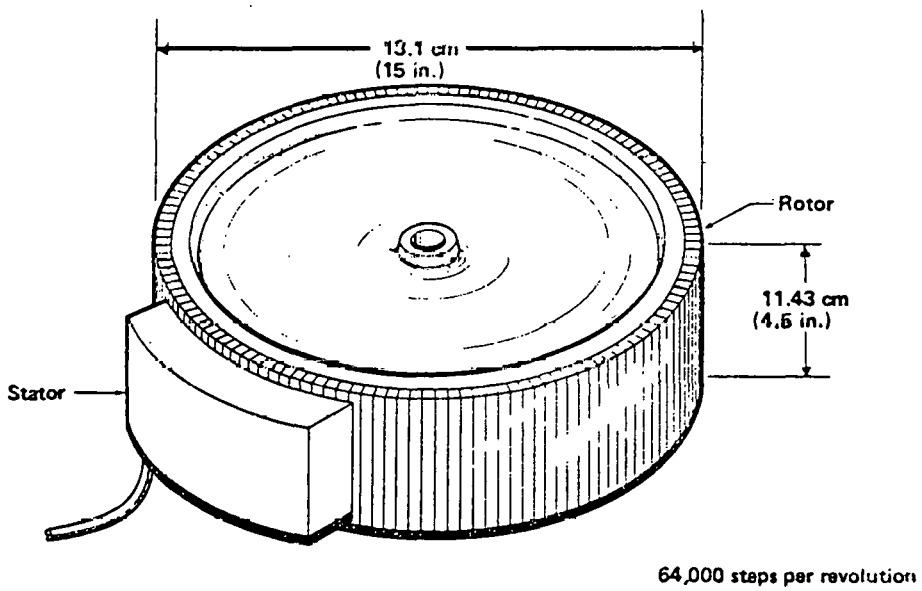

Figure A-3. Direct Drive Stepping Motor

APPENDIX B

AUGERCAST PILE STUDY

LEE TURZILLO CONTRACTING COMPANY

P. O. BOX 155 • BRECKSVILLE, OHIO 44141 • TELEPHONE 216/659-3141 • TWX 810-427-9101

"Our Experience Makes The Difference"

February 22, 1978

Boeing Engineering and Construction
P.O. Box 3707
Seattle, Washington 98124

Attention: Mr. Doug McDonald

Subject: AUGERCAST® Piles, Heliostat Foundations

Gentlemen:

In accordance with your request at a meeting with Mr. L. J. Koss and the writer of the Lee Turzillo Contracting Company we are enclosing the following information, which I trust will answer the questions that you put forth regarding the above referenced job.

(1) We are enclosing copies of our design for required reinforcement to accommodate the design criteria that you furnished to us.

(2) We are enclosing conceptual drawings showing the grout plant for the automated equipment for the above referenced project and our drawing for the pile rig or drilling rig for the pile installation for an automated basis for the above referenced job.

(3) The time required to design, develop and fabricate these two prototype machines referenced above we estimate to be nine months.

(4) The cost of development and prototype demonstration for said equipment we estimate to be

(5) The estimate of installation rate that could be achieved by the equipment is 40 pads per 8 hour day per rig unit.

(6) The quantity of automated equipment required to support the installation rate of 15 heliostats per hour is three rig units; the quantity of equipment required to support the installation rate of 70 heliostats per hour is 14 rig units; and the quantity of equipment required to support the installation rate of 450 heliostats per hour is 90 rig units. This is in accordance with the format of your Table I.

LEE TURZILLO CONTRACTING COMPANY

The replacement life for the basis of 15 heliostats installed per hour over the life span of 30 years for the job would require the replacement of 18 rig units; the replacement life predicated on the installation rate of 70 heliostats per hour for a life span of 30 years would require 126 replacement units; and the life span of replacement predicated on the installation of 450 heliostats per hour over the 30 years period would require 1,080 replacement units.

(7) Our estimate of unit cost of equipment for quantities required at the three indicated installation rates, including spares and refurbishment is as follows:

would be required for the installation rate of 15 heliostats installed per hour; would be required to maintain the installation rate of 70 heliostats per hour; would be required to maintain the installation rate of 450 heliostats per hour, over the life span of 30 years.

(8) Our estimate of the current foundation costs, materials and labor, per heliostat, is each. This estimate is predicated on a foundation of four piles per heliostat at present material and production costs.

I trust the information set forth will meet with your requirements and if you need any added refinement or additional assistance, kindly do not hesitate to contact the writer.

Very truly yours,

LEE TURZILLO CONTRACTING COMPANY

H. Bachmeier

H. Bachmeier, Regional Manager

HB:h
Enclosures

APPENDIX C

ANALYSIS OF AIR FILTRATION

THE BOEING COMPANY.

LABORATORY REPORT

NO. 2-4809-0001-048

Purpose _____ Model _____ Date 2-9-78

To: Roger Gillette M/S 8K-20 Org'n. K-6160 Part No. _____

Subject: Model for Predicted Light Scattering as a Result of Dust Accumulation

Source Heliostat Program Reinsp. Req. _____

Purchase Order _____ R.R. _____ Date Rec'd. _____ Quan. _____ Acc. _____ Rej. _____

Material _____ Spec. _____

☐ Chem. Lab. _____ ☐ Sonic _____ ☐ Met. Lab. _____ ☐ Mechanical _____

☐ X-Ray _____ ☐ Mag/Penetrant _____ ☒ Particle Identification Laboratory

Reference: C.C. to:

D277-10046-1, Volume #1, Technical Proposal
Solar Central Receiver Prototype Heliostat, July 15, 1977
(Other technical references at end of report)

SUMMARY: The task of this assignment was to determine make-up air filtration requirements for a heliostat unit in Arizona such that dust accumulated on the reflector surface over the proposed 15 year life cycle would not degrade reflective efficiency by more that 5%. There were three separate problems associated with this task:

1. A mathematical model of the dust accumulation rates for the reflector had to be prepared,
2. A model for relating dust accumulated on a surface to light scattering efficiency was needed, and
3. A filtration system which was inexpensive but could handle both the loading and the high efficiency requirements for the make-up air had to be selected.

A full mathematical model for the dust accumulation rates was outside the scope/budget requirements but a simplified model was constructed and used to determine essential system requirements. This model indicates that most of the airborne dust in the dome would sediment out in the first 24 hours of operation. Following that period, the dust in the air would be from the make-up air or resuspended dust from the lower part of the dome.

By minimizing air flow velecities the amount of resuspended dust can be minimized. Figure #1 in the following report indicates the areas of the dome that will deposit particles of a given size range on the reflector surface in eight hours.

The relationship between particle diameter and light scattering efficiencies is indicated by figure #2 in the following report. It can be seen that the critical size range is from 0.1μm to 1.0μm diameter particles, Most of these particles sediment from a height of not more than 128 cm above the surface of the reflector. (1σ from the mean radius of the small particle log normal mode of r = .2 um).

Prepared by E. R. Crutcher Approved by R. H. LeDoux Org'n. 2-4809

F. R. Crutcher R. H. LeDoux

DD 5000 2100 ORIG.3/71

This reduced sedimentation volume was still large enough to collect particulate from the total volume, including all make-up air, over the 15 year life of the reflector. For these reasons it is important to keep the total airborne particulate levels low for the make-up air.

The filtration system recommended consists of a Gelman Type E/8" x 10" glass prefilter followed by a Gelman Acropor pore size 0.45 μm 8" x 10" filter or their equivalence. The Type E prefilter is a depth filter which will tolerate high loading (up to a gram of material). It is relatively efficient collecting approximately 99.7% of the total mass of airborne particulate. The acropor filter following the prefilter stops 99.99% of the particulate remaining. Assuming the filters were directly exposed to the atmosphere they would remove the particulate from 45,000 m^3 of air. Using the peak monthly average for Phoenix of 300 $\mu g/m^3$ as one extreme and the minimum monthly average for the Grand Canyon of 20 $\mu g/m^3$ for the other the following loadings would result:

Prefilter	Loading in 15 Years	Result
a. 300 $\mu g/m^3$	13.46 grams	Yearly change of filter
b. 20 $\mu g/m^3$	.9 grams	15 year life
Membrane		
300 $\mu g/m^3$	.04 grams	15 year life
20 $\mu g/m^3$	.003 grams	15 year life

With some intake air impingement both filters should last for the full 15 years.

Less than 5% loss of reflector efficiency can be expected due to external sources of particulate with this filtration system and a make-up flow rate not significantly exceeding 0.5 cfm. The interior of the dome, representing 1% of the total air exposure for the reflector will carry 99.99% of the particulate exposed to the reflector surface. An initial rest period after installing the reflector of 48 hours with the reflector stored in a vertical position should minimize the effect of this original particle burden.

(NOTE: Leaks will function as concave impactor orifices. This will result in a local accumulation of dust on the surface near the leak. The accumulation of dust at a point can be used to locate leaks and to act as a "typical" dust collection to evaluate the types of dust in the dome environment (i.e., wear metal from reflector rotation machinery, external dusts, etc.)

APPENDIX D

PHASE I TEST PLANS

SOLAR CENTRAL RECEIVER
PROTOTYPE HELIOSTAT

MATERIALS TEST PLAN

1 December, 1977

Prepared for
United States
Department of Energy

under Contract Number
EG-77-C-03-1604

Boeing Engineering & Construction
A Division of The Boeing Company
Seattle, Washington 98124

TABLE OF CONTENTS

1.0 INTRODUCTION

This document describes the material - level tests planned for the Solar Central Receiver Prototype Heliostat Program. It provides a list of candidate materials, a general description of the tests, states the test objectives and shows the sequence of testing and schedules for test performance.

2.0 SUMMARY AND OBJECTIVES

The tests are planned for candidate enclosure and reflective surface coating materials and are intended to furnish as-manufactured properties of several standard and derivitive plastic films and coatings. The effects of environmental exposures on mechanical and optical properties will be measured. In addition to testing standard film specimens, tests will be performed on specimens containing seams simulating those that would be used to manufacture heliostat enclosures and reflecters.

The overall objectives of these tests are to support design with mechanical, optical, and life properties of candidate materials sufficient for material selections.

Individual test objectives are listed in Table 1.

TABLE 1

INDIVIDUAL TEST OBJECTIVES

TEST DESCRIPTION	NUMBER OF SPECIMENS PER DATA POINT (Min.)	SPECIMEN DESCRIPTION	OBJECTIVE OF TEST
Tensile & Elongation (Macro)	3	Fig. 4 (1 x 12)	- Comparison of Candidate Material - Test for Anisotropy - Control Properties for Environmental Exposures - Design Properties for Derivative Films
Tensile (Micro)	3	Fig. 3	- Control for Environmental Exposure where Exposed Sample Size is Limited
Tear	3	Fig. 5	- Comparison of Candidate Material - Design Properties for Derivative Materials
Joint	3	Fig. 4	- Comparison of Candidate Joining Methods - Joint Design Properties - Control Properties for Environmental Exposure
Creep	3	Fig. 3 or Fig. 4	- Design Life Studies - Comparison of Candidate Materials and Joining Methods
Solar Transmission	1	1-1/2 In. Dia.	- Comparison of Candidate Material - Control Properties for Environmental Exposure - Design Properties for Derivative Films

Table 1 (Cont.)

TEST DESCRIPTION	NUMBER OF SPECIMENS PER DATA POINT (Min)	SPECIMEN DESCRIPTION		OBJECTIVE OF TEST
Solar Reflectance	1	3-1/2 In. Dia.		- Comparison of Candidate Coatings - Control Properties for Environmental Exposure - Design Properties for Derivative Coatings
Flammability	1	1 x 18 In.		- Comparison of Candidate Materials
UV Exposure				
Accelerated				
Transparent Dome:				- Predict Long Term Exposure Effects - Mechanical Properties Degradation - Solar Transmission Degradation
Tensile	1-3	Fig. 3		
Transmission	1	1-1/2 In. Dia.		
Reflective Surface:				
Reflection	1	3-1/2 In. Dia.		- Predict Solar Reflection Degradation
Real Time				
Transmission	1	1-1/2 In. Dia.		- Predict Real Life - Predict Change in Optical Properties
Reflectance	1	3-1/2 In. Dia.		
Tensile	3	Fig. 3		

Table 1 (Cont.)

TEST DESCRIPTION	NUMBER OF SPECIMENS PER DATA POINT (Min.)	SPECIMEN DESCRIPTION	OBJECTIVE OF TEST
Washability Exposure Transmission	 1 1	 4 x 4 1-1/2 In. Dia	 - Compare Cleaning Methods - Predict Reduction in Solar Optical Property - Develop Techniques for Assembly Level Cleaning
Thickness Measurement	measure all types of specimens at several locations	not critical	- Document material thickness - Predict thickness to be used for design analysis - Verify compliance with specified thickness

3.0 GENERAL TEST PLAN

Figures 1 and 2 illustrate the general test plan for transparent dome and reflective surface candidate materials, respectively. Candidate materials will first be screened by macro-tensile, tear and optical properties. Remaining viable candidates after screening will continue thru remaining control tests, environmental exposures and joint studies. Upon completion of environmental tests, plots of property values versus exposure time will be prepared.

3.1 Candidate Materials

3.1.1 Transparent Dome

Candidate dome materials are shown in Table II. It can be seen that several optional forms of films can be obtained due to possible variations in formulation and processing. The materials shown allow independent comparisons of any of the available optional forms of the materials. From the resulting data, films identified as serious contenders will be carried into environmental test.

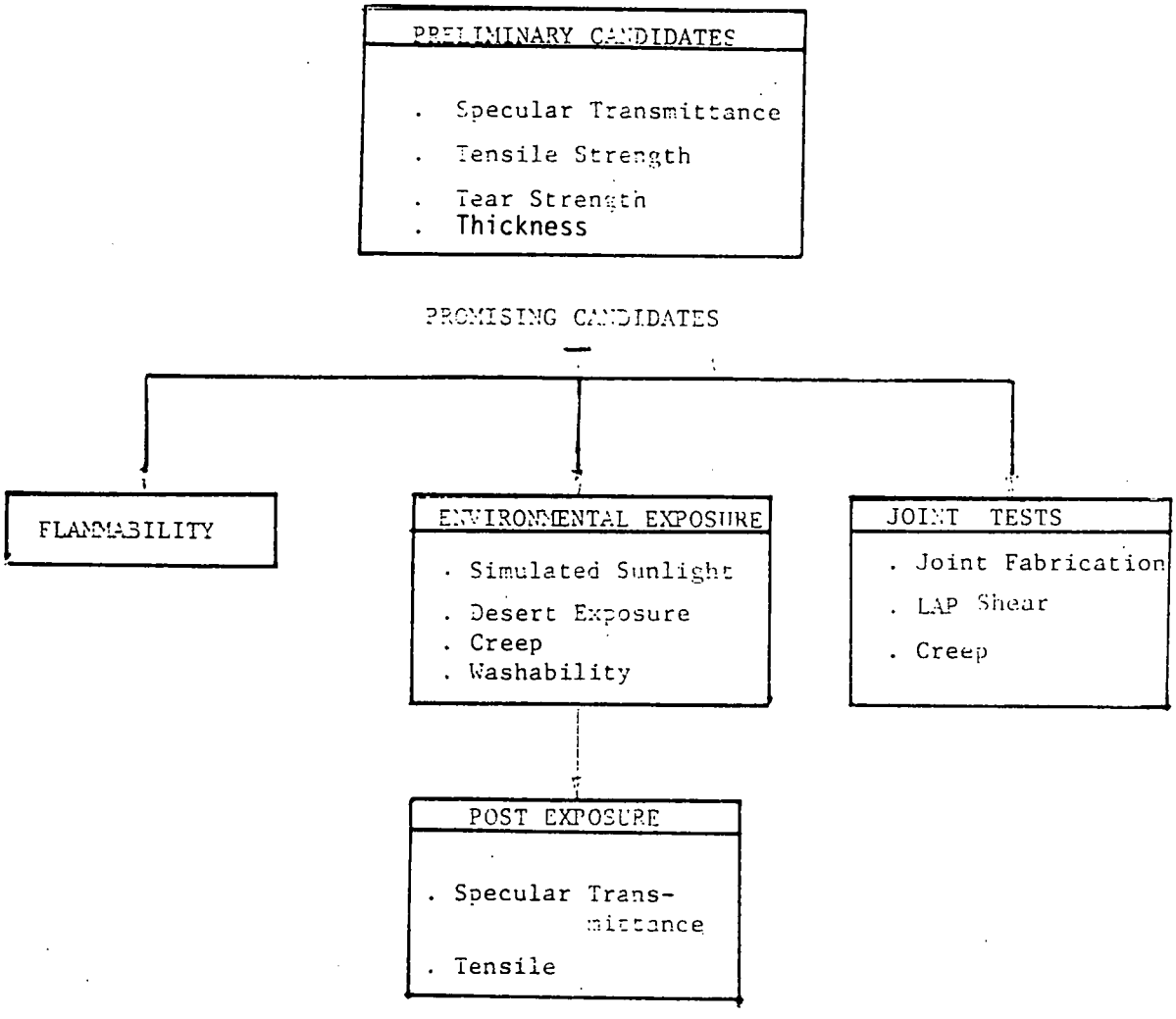

Figure 1
Enclosure Material Test Plan

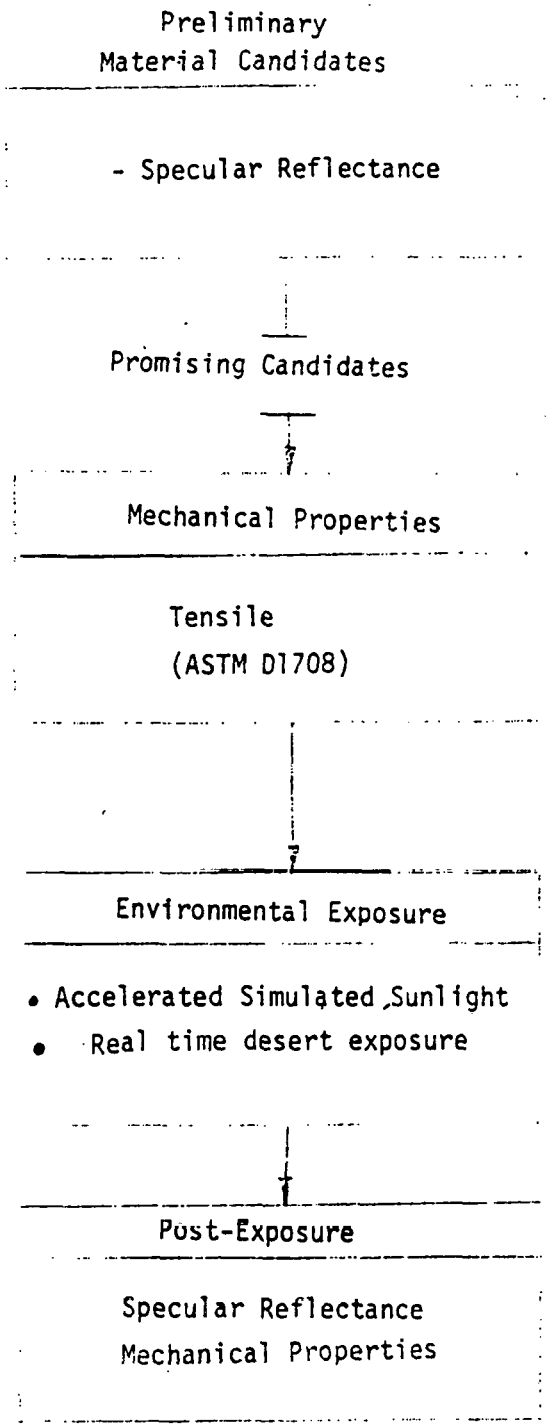

Figure 2
Reflector Coating Test Plan

Table II

Dome Material Candidates

MATERIAL	SUPPLIER
Polyethylene Terephthalate (Melinex "O" , Mylar "D" and Celanese 4000)	Martin Processing
Vinylidine Flouride (Kynar 900)	Pennwalt -
Polypropylene w/UV additive	Hercules
Polypropylene, Polyethylene, or PVC w/UV additive	Ethyl Corp.
Polyester w/UV additive in extruded film (Petra "A")	Allied Chemical
Polyester w/UV additive in extruded film	Celanese
Polyester or Cellulose Acetate	Eastman (Tennessee)
Acrylic and Urethane	Desoto
Reinforced Films	Air Tech. Industries
Material not yet defined	Amoco

3.1.2 Reflective Surface

Materials testing for the reflector will consist primarily of effort toward developing a suitable coating for the baseline material (Aluminized Melinex 0). Reflective surface coatings developed cooperatively with other companies will be screened first optically for suitable reflectivity, then the promising coated specimens will be life tested. Figure 2 is a flow chart of the proposed coating evaluation test plan. The proposed tests are: Specular reflectance measurements with the Boeing Bi-Directional Reflectometer (628 nanometer lasor source), mechanical properties tests (yield, ultimate, elongation), accelerated ultraviolet exposure testing and real time desert exposure testing. Optical and mechanical property tests will be performed on exposure coupons periodically to obtain degradation vs time profiles:

3.2 Test Descriptions

3.2.1 Tensile Strength and Elongation

Tensile strength tests will be performed according to the methods shown in Table III at maximum and minimum design and ambient temperatures. Specimens are shown in Figures 3 and 4. The choice of micro or macro sized specimen will be dictated by 1) the amount of sample material available, 2) the requirement for modulus measurement (Modulus can only be measured on macro-specimens), and 3) the type of long term exposures involved (accelerated UV exposures are area-limited). Control tests will be run on a minimum of 3 replicate specimens. Test run on exposed specimens will use a minimum of 3 replicate specimens per exposure period except for area-limited exposures such as accelerated UV. Since some of the stretched films are anisotropic, tensile properties will be determined at 0° and 90° to the roll length direction.

3.2.2 Seam Strength

Seam strength of joints will be run in the same manner as the tensile tests above. Specimens will be sampled so that the seam is centered in the reduced section of the microtensile specimen and within the gage area of the macro-tensile specimen.

Table III

Standard Test Methods

TEST TYPE	TEST METHOD	SPECIMEN (Overall Dimensions) inches
TENSILE (MACRO)	ASTM D882	(1 x 12)
TENSILE (MICRO)	ASTM D1708	(.625 x 1.5)
FLAMMABILITY	ASTM D568	(1 x 18)
TEAR	ASTM D1004	(1.25 x 4.00)
TENSILE CREEP	ASTM D2990	(1 x 12)
THICKNESS	MICROMETER	not critical

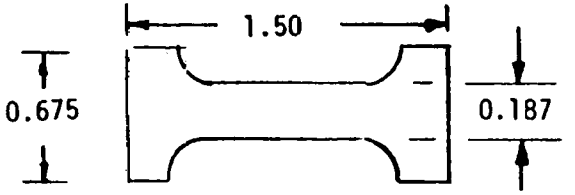

FIGURE 3 MICRO TENSILE SPECIMEN

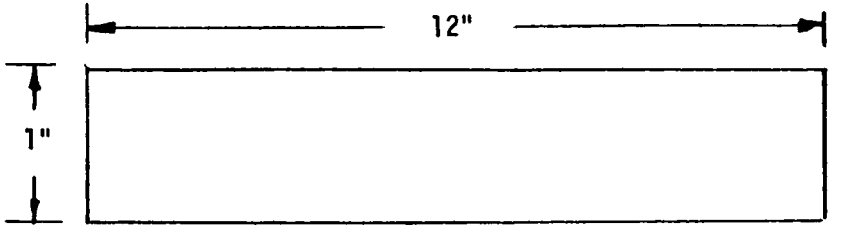

FIGURE 4 MACRO TENSILE SPECIMEN

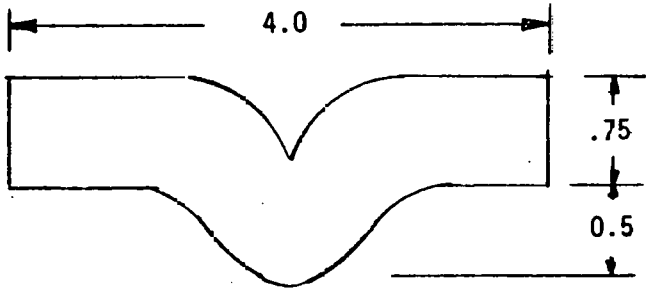

FIGURE 5 TEAR SPECIMEN

3.2.3 Tear Strength and Flammability

Tear strength and flammability tests will be conducted per methods indicated in Table IV. These tests will aid in evaluating risks due to hazards of flame and tear. The tear specimen is shown in Figure 5. No flammability or tear tests will be performed on materials where supplier data is already available.

3.2.4 U/V Exposure

A Spectrolab X-200 solar simulator with special filtering will be utilized to provide ultraviolet radiation at a 10 to 20 sun level in the wavelength region less than 400 nanometers (based on an air mass 2 spectrum). Microtensile, transmittance and reflectance specimens will be exposed and periodically withdrawn during exposure. Data obtained here will be used primarily to screen samples on a comparative basis rather than to predict ultra violet lifetime. The microtensile will be tested to destruction and the transmittance and reflectance specimen tested and returned to exposure.

Real time exposure to sunlight at desert conditions will be performed on microtensile, transmittance and reflectance specimens of all film candidates. These exposures will run concurrent with the other tests and will continue throughout most of the Phase I program and will extend on through Phase II. Samples mounted on a test rack at a location in the Southwest (TBD), will be removed at 6 month intervals for mechanical and optical evaluation. Data obtained here will be useful in the correlation and validation of accelerated U/V test data as in addition to the actual estimation of material outdoor life.

3.2.5 Creep

Transparent dome and reflective surface candidate material will be evaluated for creep resistance. Tests will be conducted per Table III, at maximum design and ambient temperatures and design stress, using a hanging weight tension system (weight per-determined). Changes in length will be determined optically. Creep data is required for transparent dome design.

3.2.6 Washability

A specimen of each candidate material will be exposed to water, dust and smoke residue contamination. Cleaning techniques shall be evaluated utilizing water and/or cleaning solutions. Transmittance or reflectance measurements shall be taken on each specimen following contamination exposure and cleaning. Cleaning techniques for the specimens will be scalable to the assembly level.

3.2.7 Specular Reflectance Measurements

The objectives of specular reflectance tests will be to determine: which membrane surface coatings provide the smallest loss in reflectance and effects of various environmental/developmental tests on surfaces. Specular reflectance tests will be performed with a modified bi-directional reflectometer utilizing a 628 nanometer wavelength laser light source (Figure 6). Apertures defining various solid angles are placed at the entrance port to the integrating sphere/detector to determine the distribution of energy in the reflected beam.

3.2.8 Specular Transmittance Measurements

Special specular transmittance appartus assembled for these measurements (Figure 7) utilizes an existing Beckman DK 2A spectrophotometer and a Gier-Dunkle integrating sphere to provide specular transmittance within an acceptance cone angle of 0.5^{o}, as a function of wavelength from 250 to 2500 nanometers. Selected specimens will be tested on the bi-directional instrument described in 3.2.7 at scattering cone angles ranging from 0.08 to 0.5^{o} (628 nm only).

4.0 SCHEDULE

Figure 8 shows the test schedule. All tests will begin as indicated on materials available at that time. Later arrivals will be processed as they come in. Most environmental exposure tests are subject to periodic inspection in order to develop a projectable life curve.

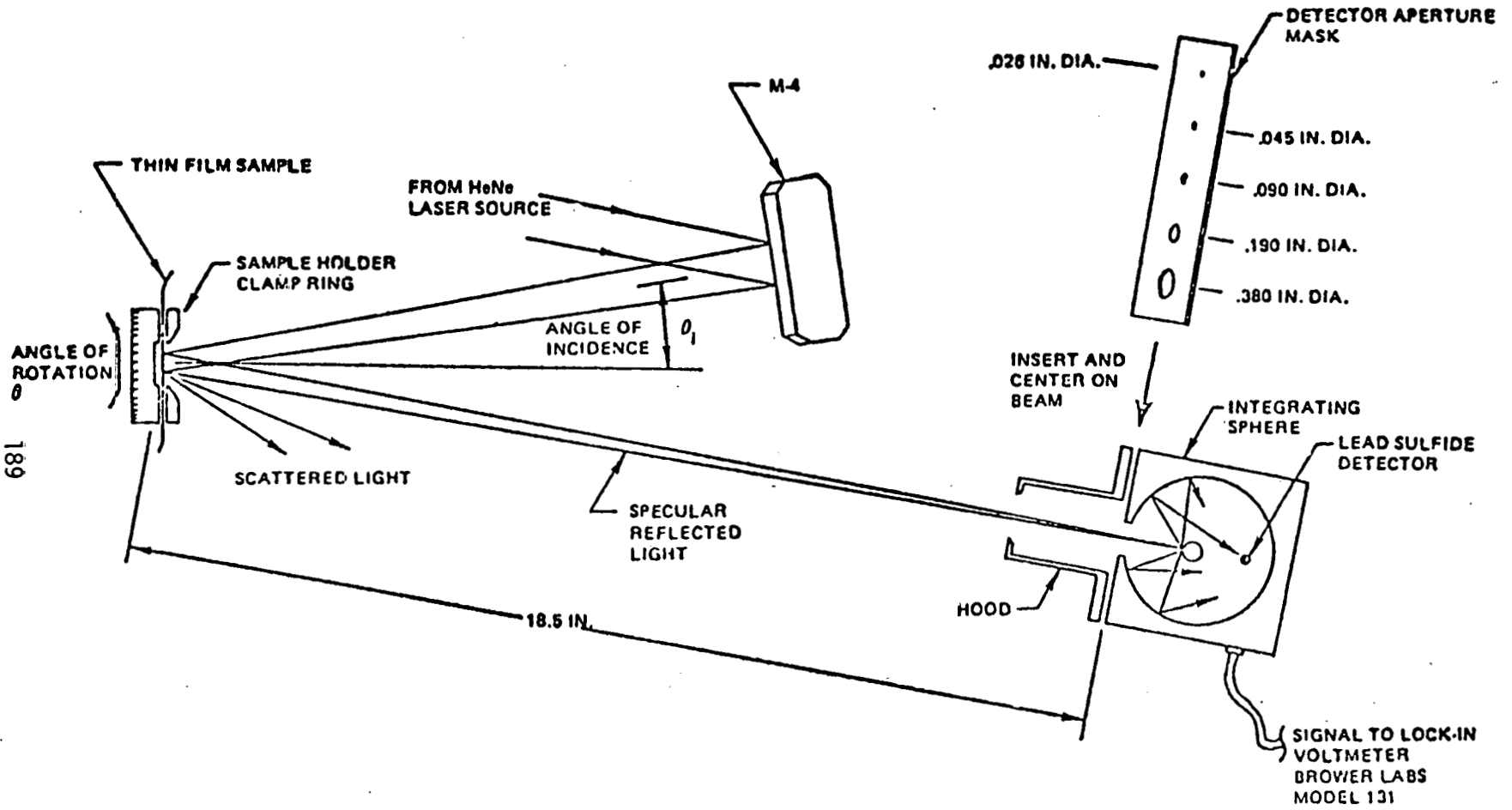

Figure 6 Schematic of Specular Reflectometer Optical System

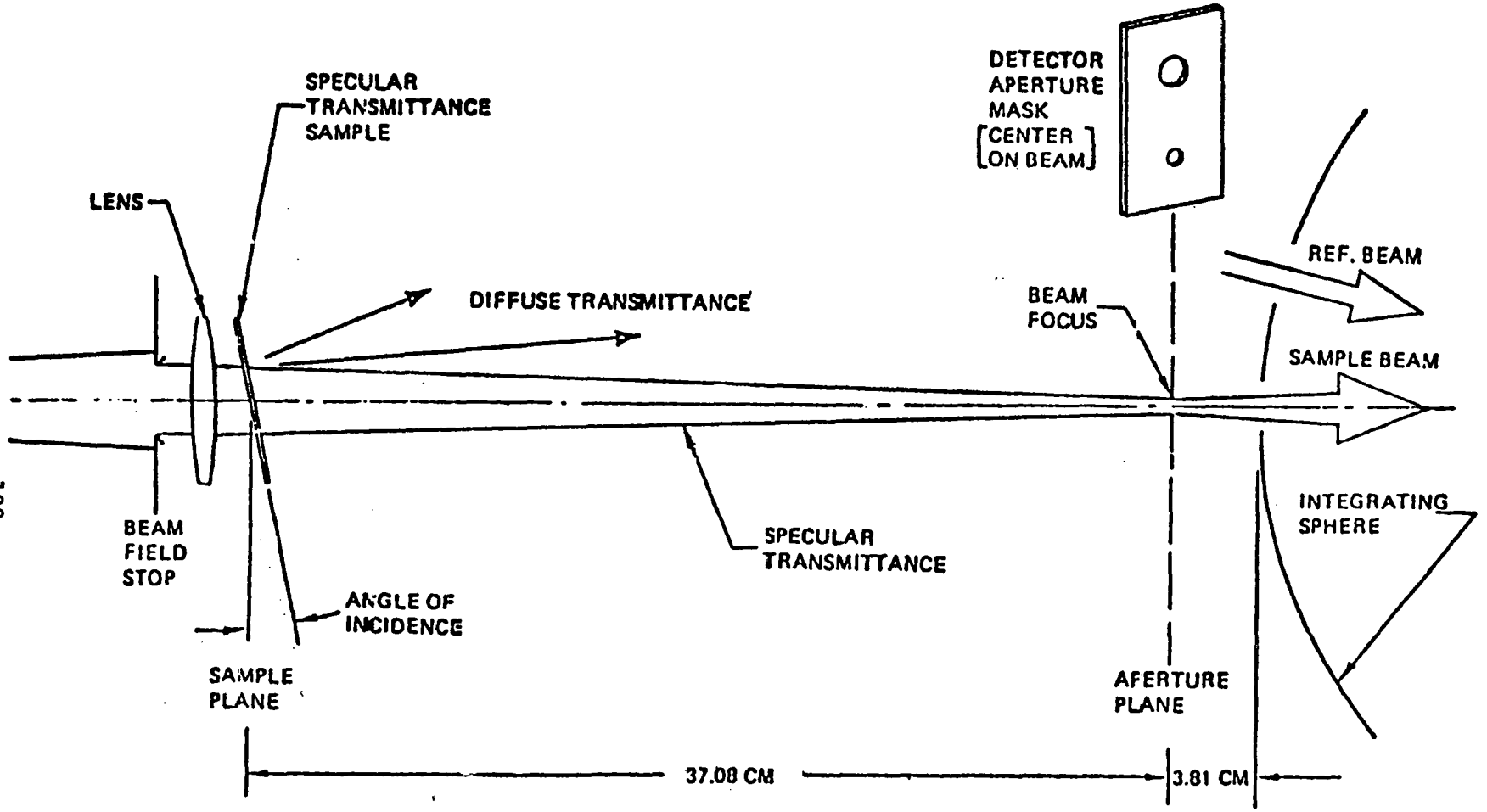

RESOLUTION OF SYSTEM

0.32 CM DIA. APERTURE PASSES 93 PERCENT OF BEAM (WITHOUT SAMPLE), 0.5° CONE

Figure 7 Specular Transmittance Test Set-up

Figure 8

Materials Test Schedule

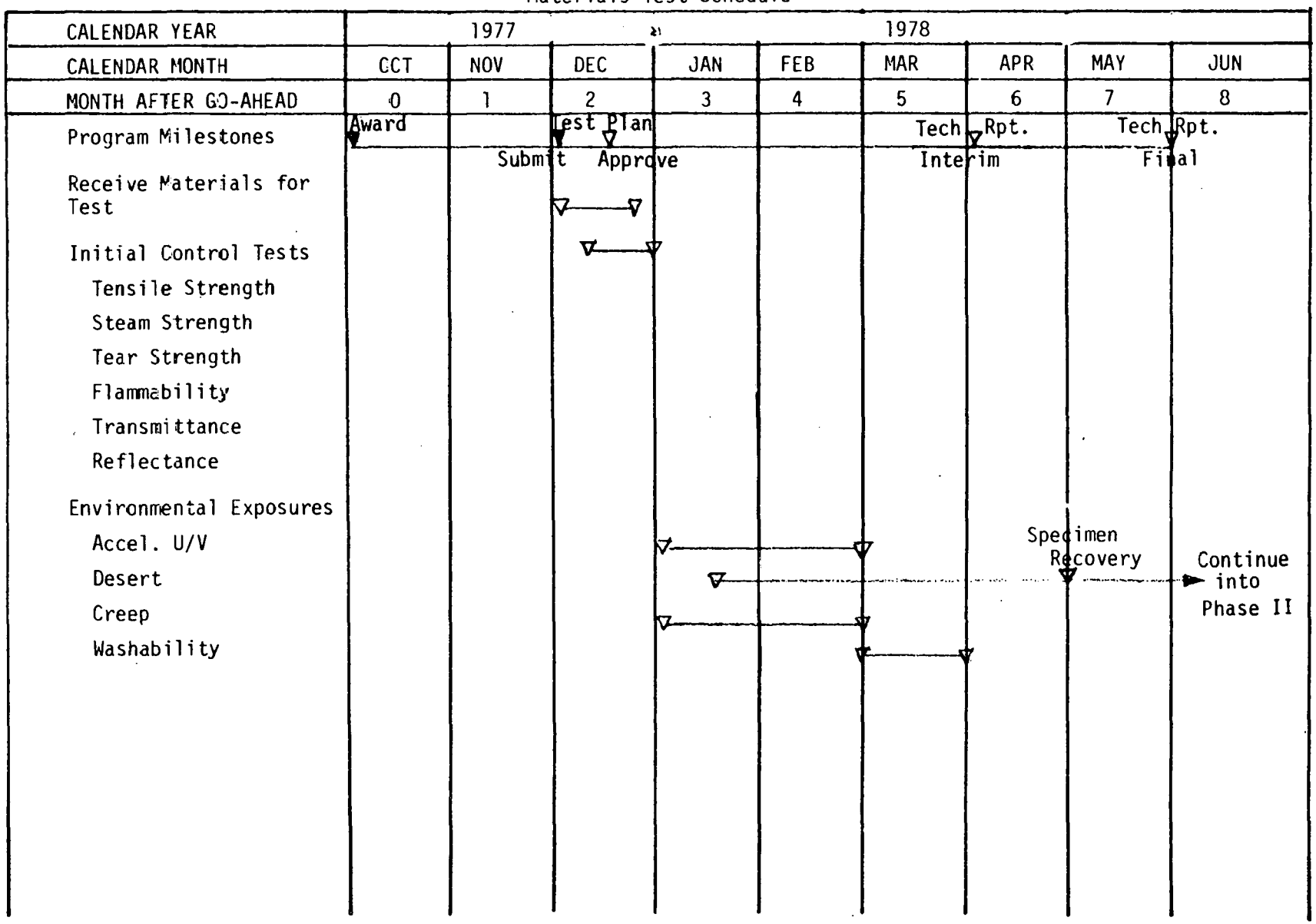

APPENDIX E

ATTACHED DRAWINGS

(DRAWINGS UNAVAILABLE)

A P P E N D I X F

TEST DATA AND RESULTS

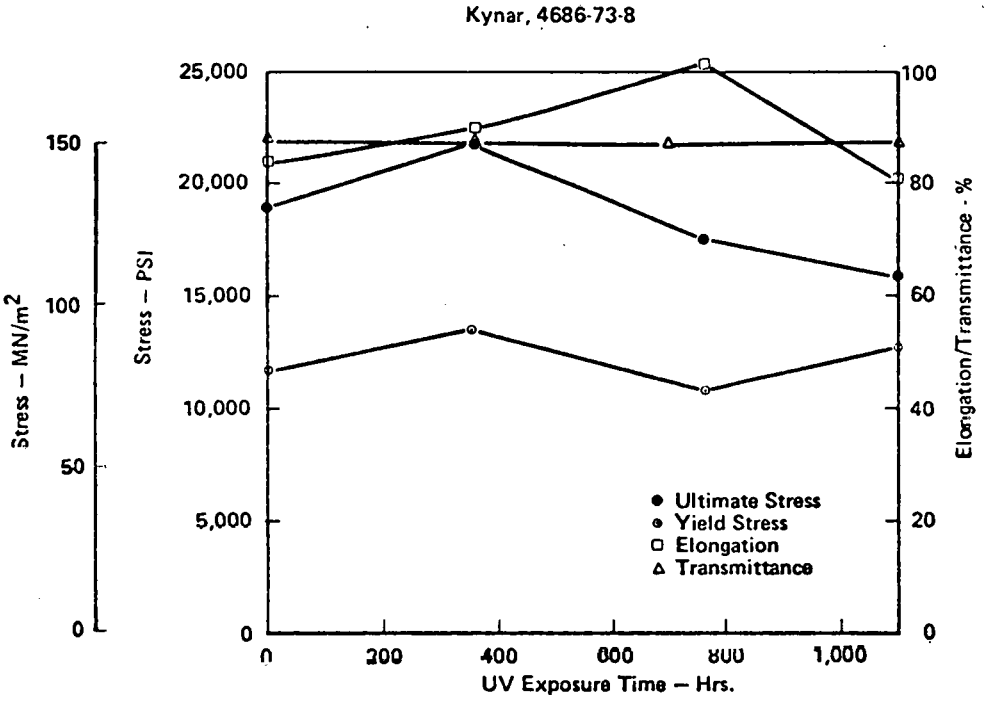

Figure F-1 *Kynar A U/V Exposure Data*

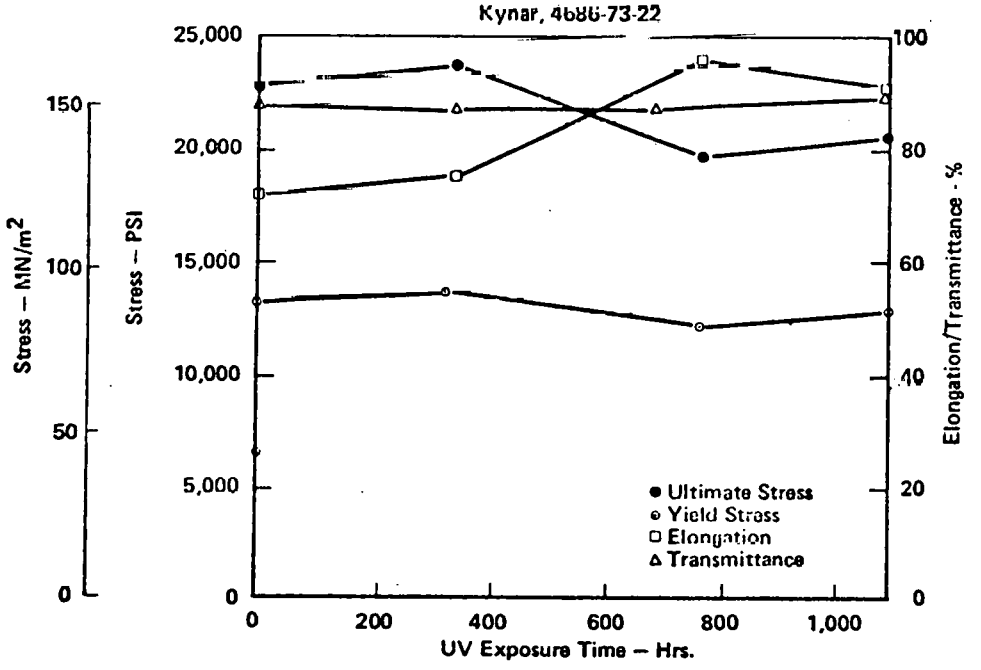

Figure F-2 *Kynar B U/V Exposure Data*

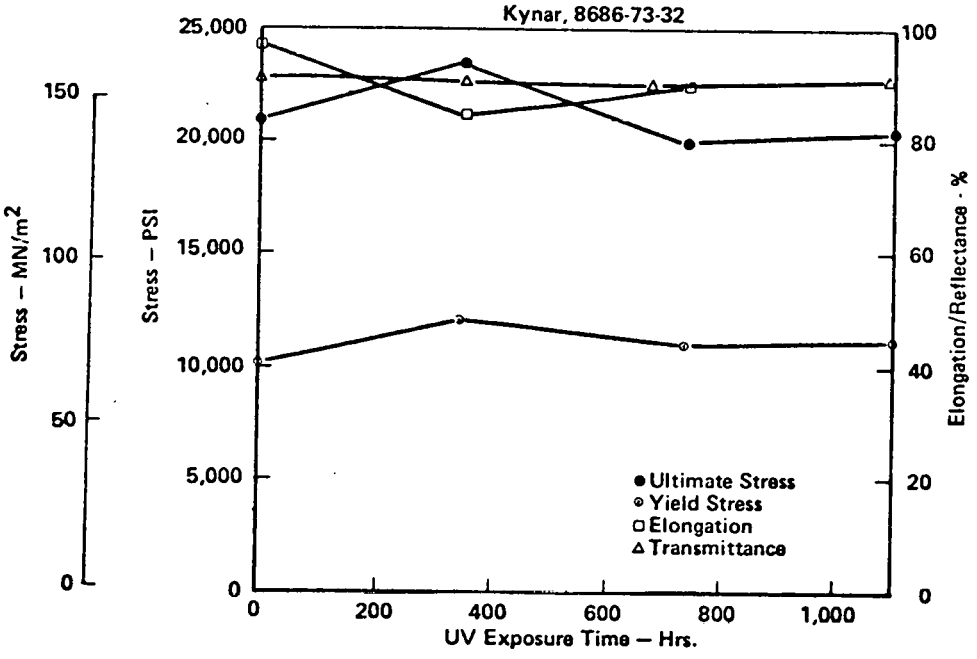

Figure F-3 *Kynar C U/V Exposure Data*

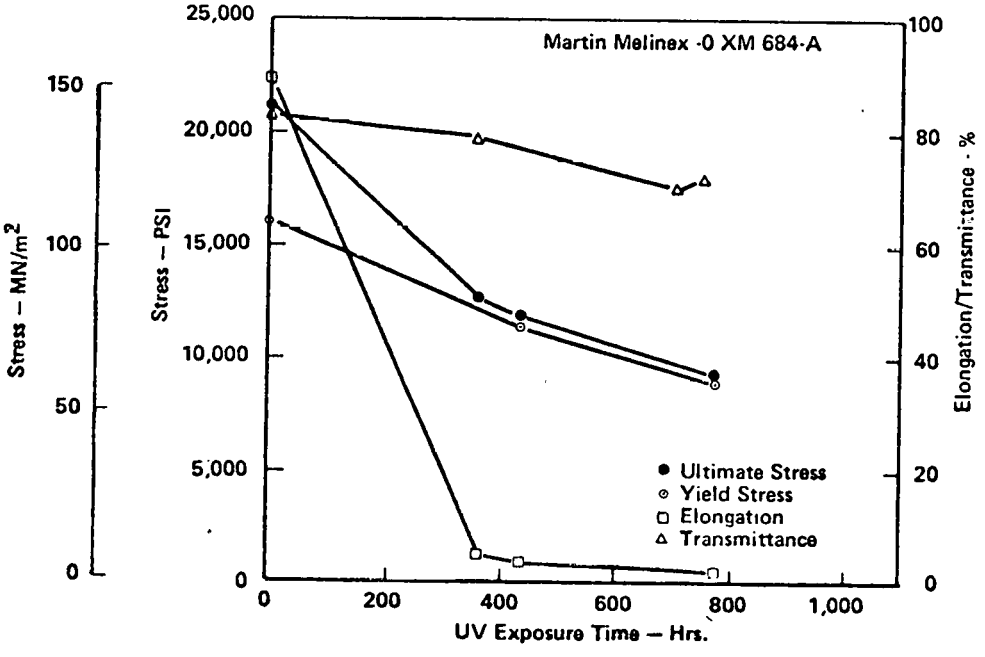

Figure F-4 *Martin Weatherable Polyester U/V Exposure Data*

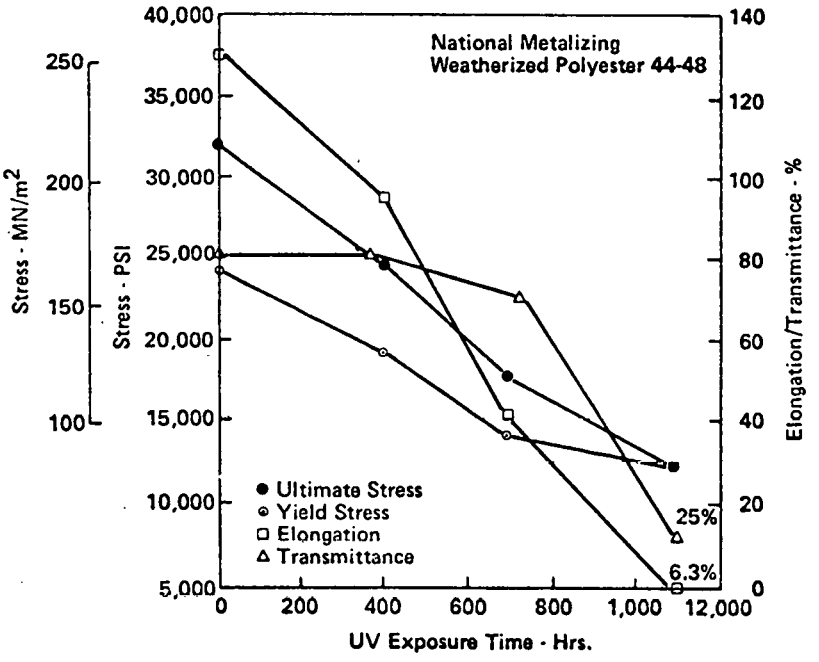

Figure F-5 *National Metalizing Weatherable Polyester U/V Exposure Data*

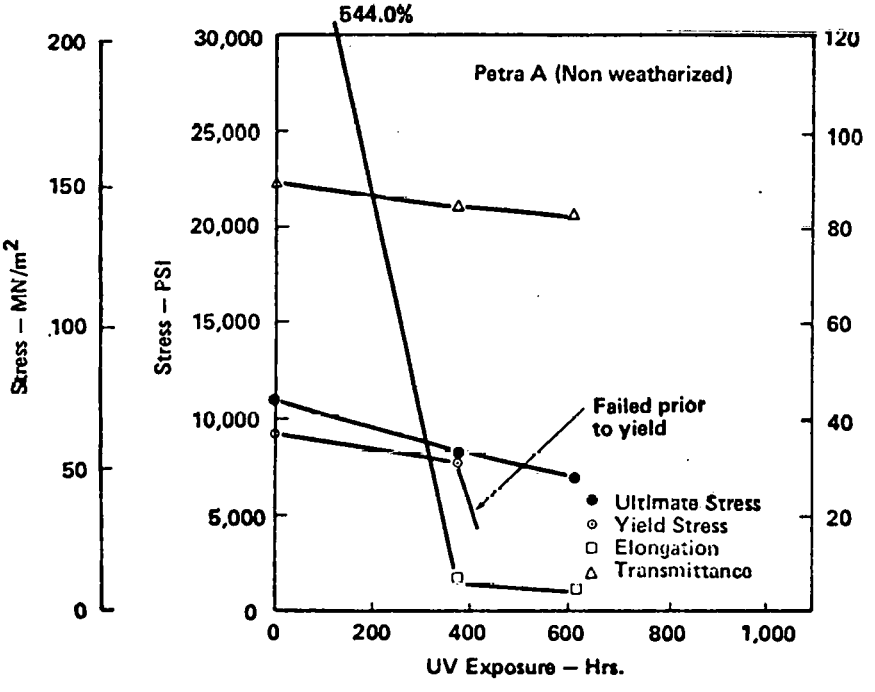

Figure F-6 *Petra A U/V Exposure Data*

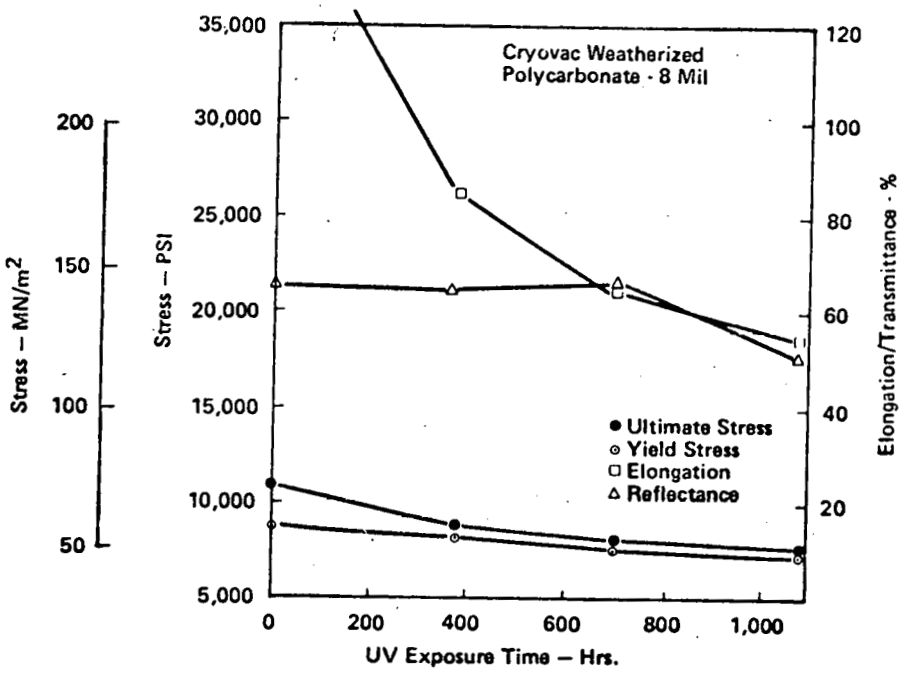

Figure F-7 *8 Mil Weatherable Polycarbonate U/V Exposure Data*

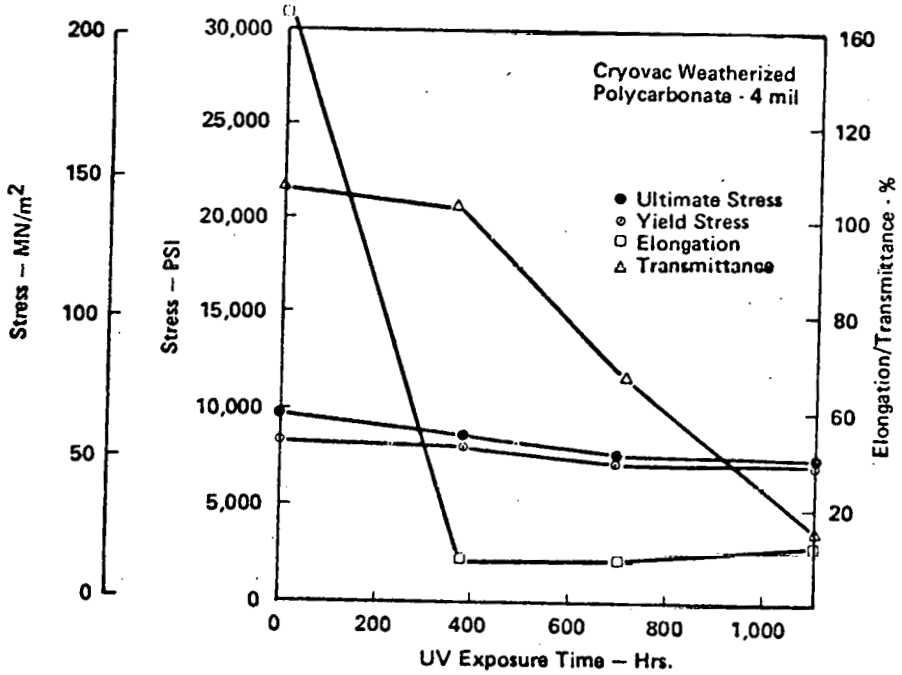

Figure F-8 *Weatherable Polycarbonate U/V Exposure Data 4 Mil*

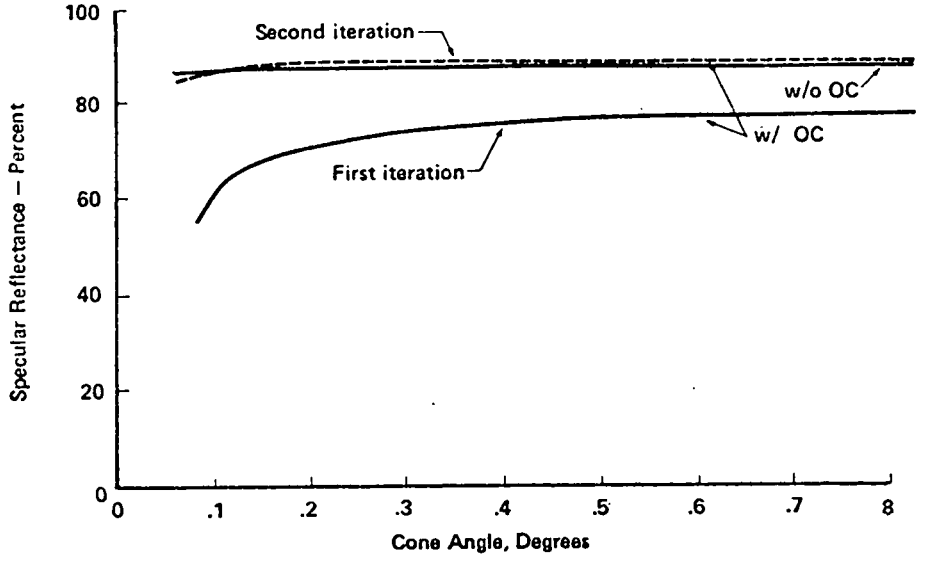

Figure F-9 *Specular Reflectance vs Cone Angle for Mylar Aluminized by National Metalizing*

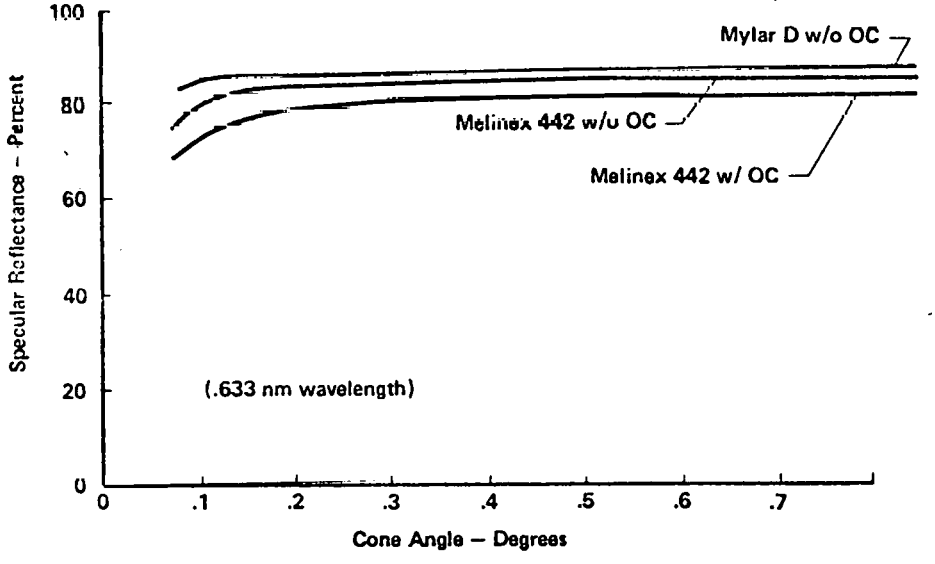

Figure F-10 *Specular Reflectance vs Cone Angle for Mylar and Melinex 442 Films Coated by Dunmore*

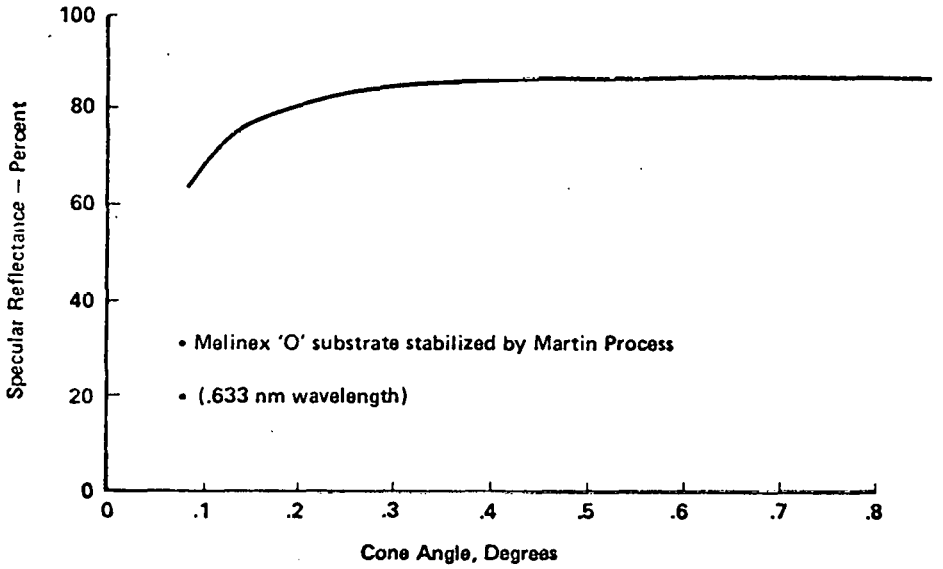

Figure F-11 *Specular Reflectance vs Cone Angle for Aluminized Melinex 'O' Coated by Martin Processing*

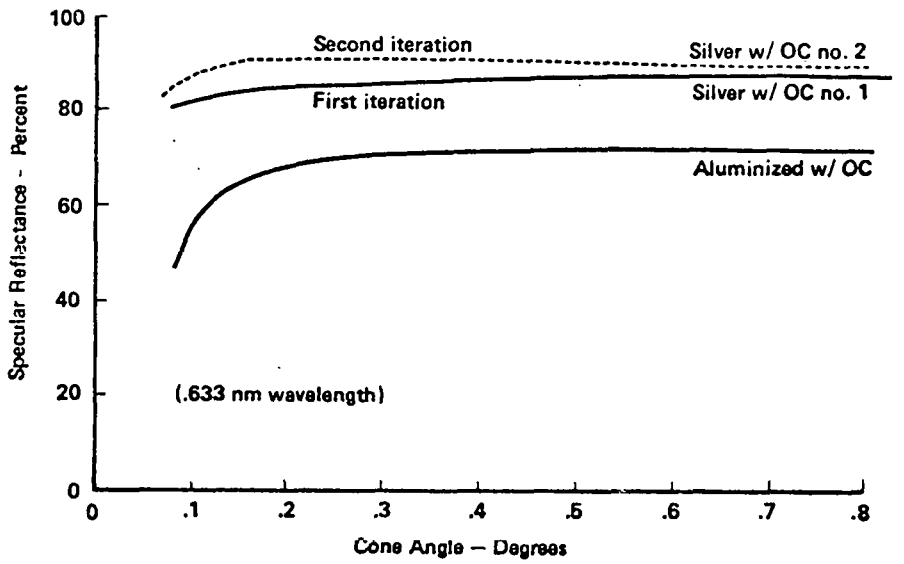

Figure F-12 *Specular Reflectance vs Cone Angle for Aluminized and Silverized Polyester Coated by OCLI*

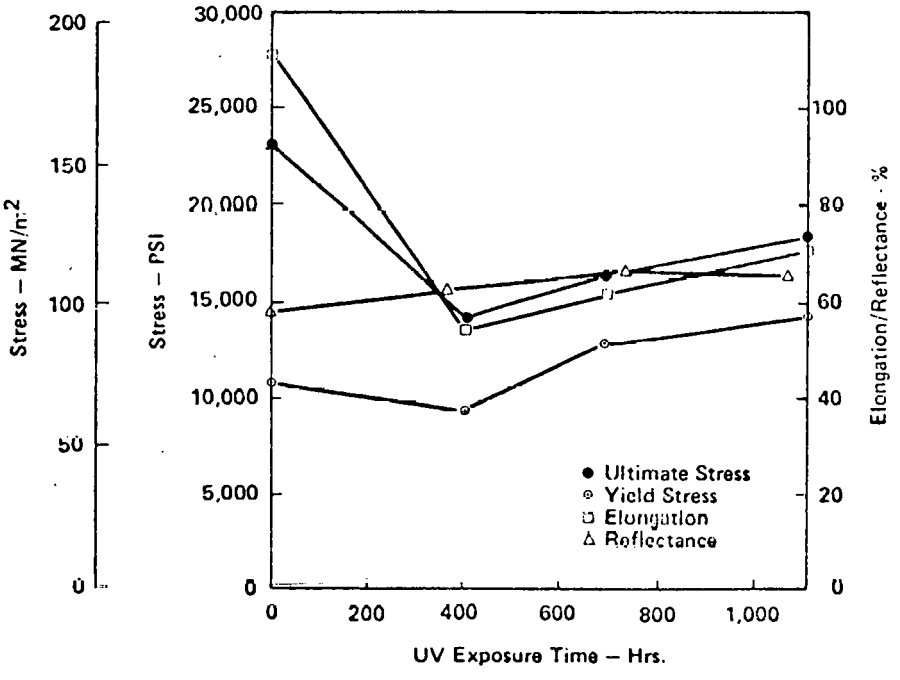

Figure F-13 *U/V Exposure Data for National Metalizing Aluminized Polyester with Overcoat*

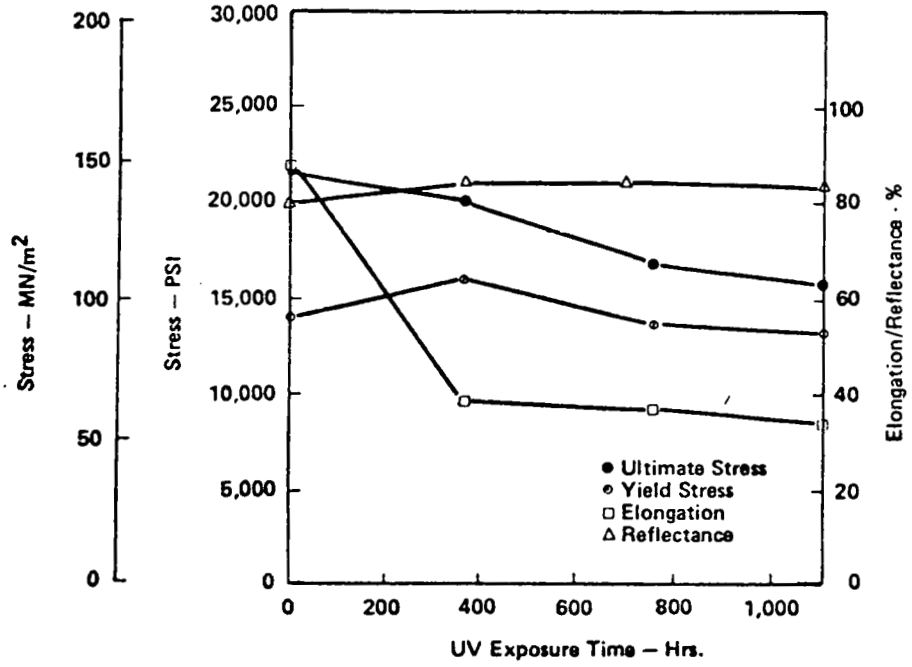

Figure F-14 *U/V Exposure Data for Dunmore Aluminized Polyester w/o Overcoat*

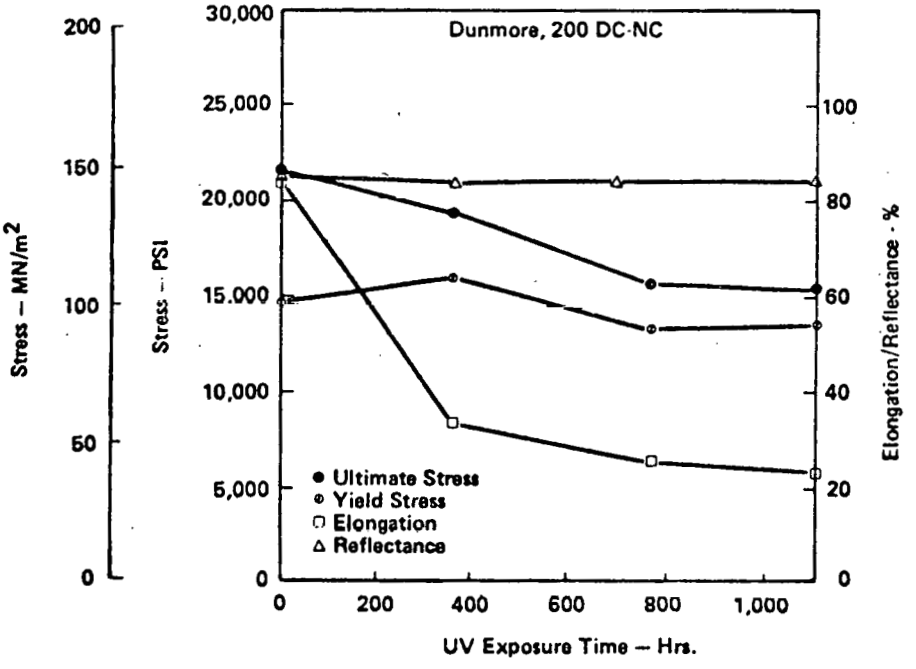

Figure F-15 *U/V Exposure Data for Dunmore Aluminized Polyester with Overcoat*

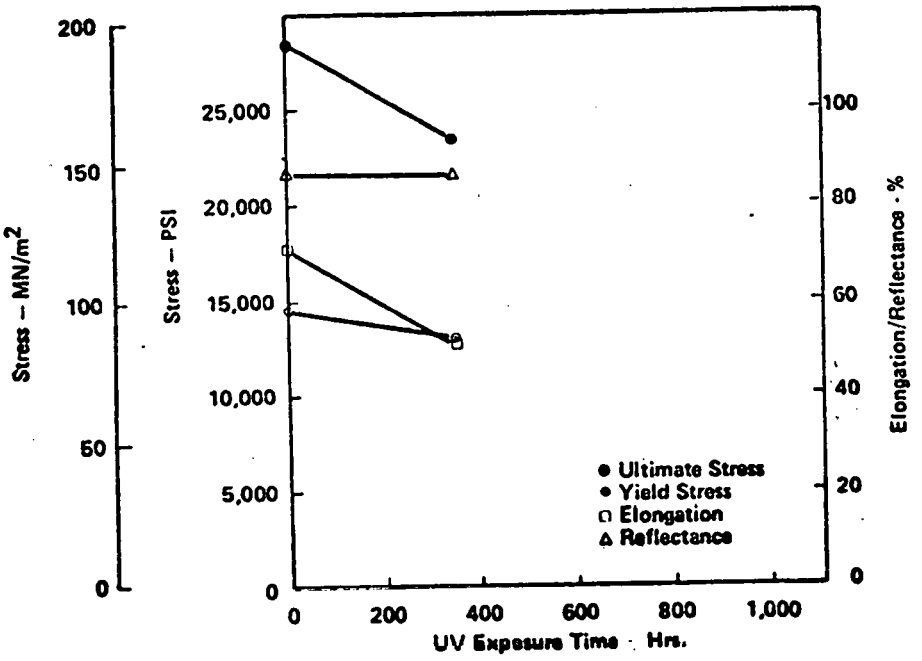

Figure F-16 *U/V Exposure Data for Martin Processing Aluminized Melinex 'O' w/o Overcoat*

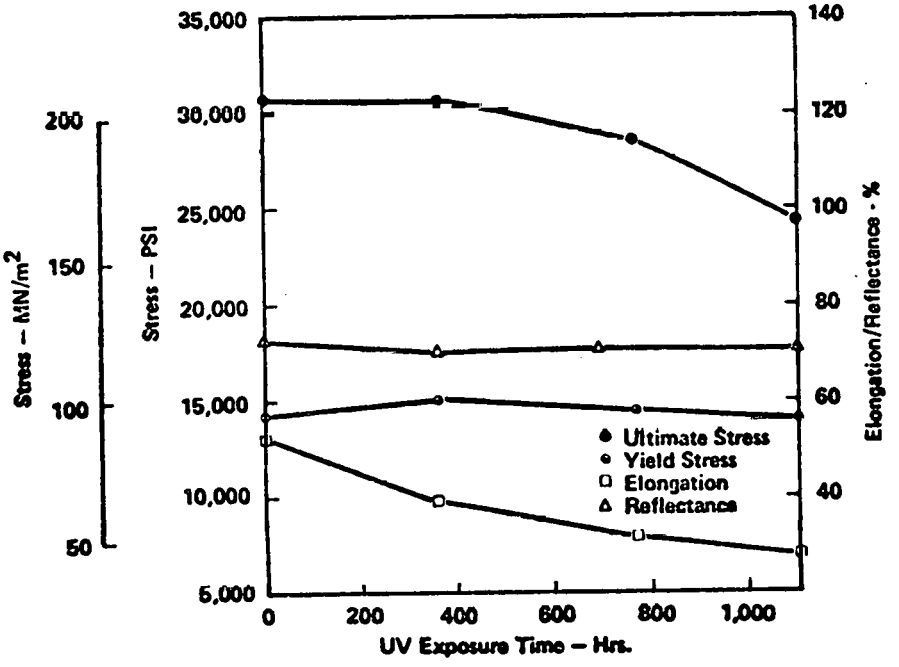

Figure F-17 *U/V Exposure Data for OCLI Aluminized Mylar with Overcoat*

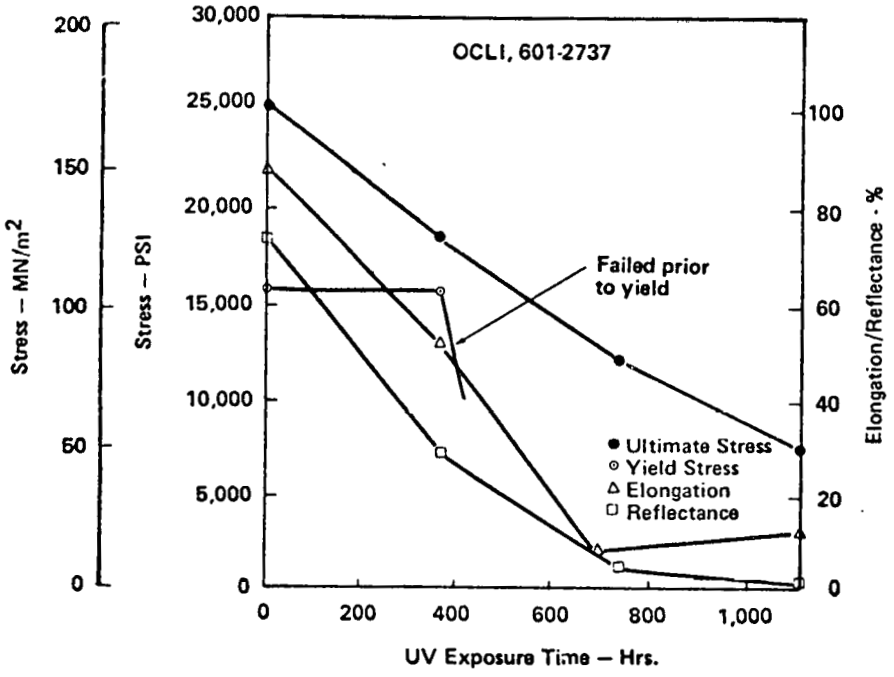

Figure F-18 *U/V Exposure Data for OCLI Silvered Mylar w/o Overcoat*

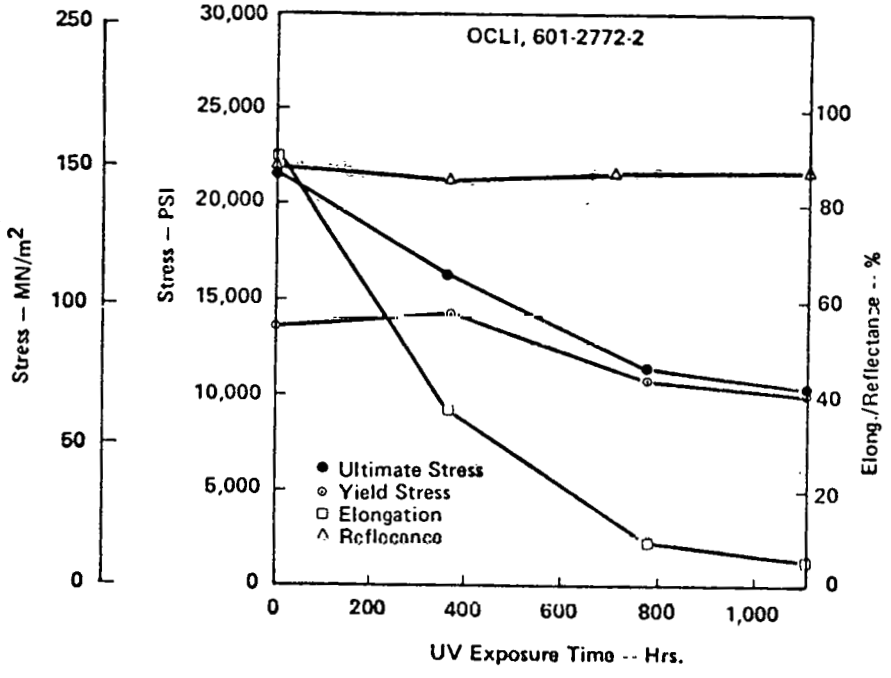

Figure F-19 *OCLI Silverized Mylar with Overcoat U/V Exposure Data*

U.S. GOVERNMENT PRINTING OFFICE: 1979—640-092/ 1140